AD-A111 568 LOCKHEED MISSILES AND SPACE CO INC PALO ALTO CA PALO --ETC F/G 13/13
NUMERICAL PROCEDURES FOR ANALYSIS OF STRUCTURAL SHELLS.(U)
MAR 81 B O ALMROTH, F A BROGAN F33615-76-C-3105
UNCLASSIFIED AFWAL-TR-80-3129 NL

1 OF 2
AD A
111 568

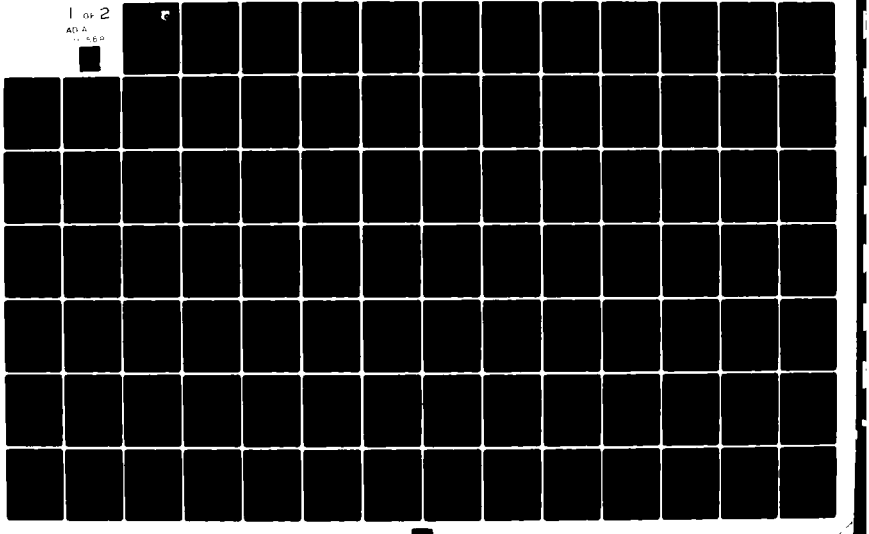

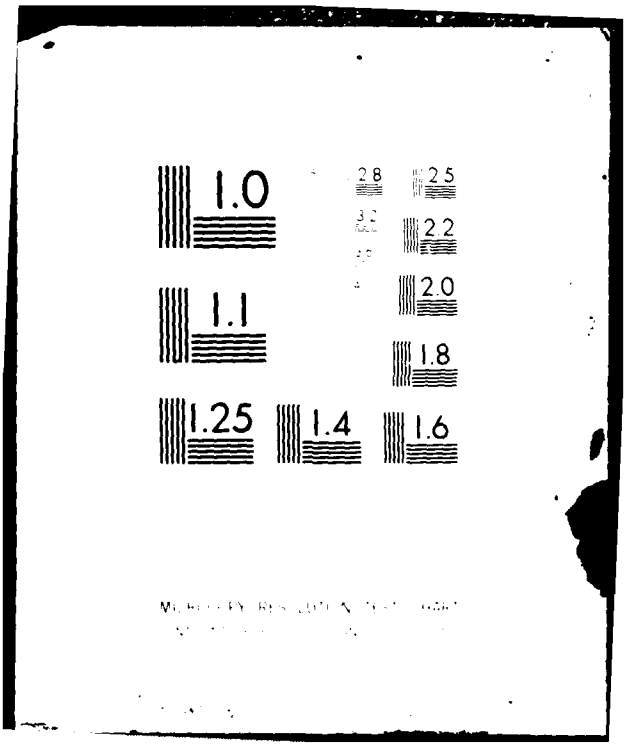
1.0
2.8
2.5
3.2
2.2
2.0
1.1
1.8
1.25
1.4
1.6

AFWAL-TR-80-3129

NUMERICAL PROCEDURES FOR ANALYSIS OF STRUCTURAL SHELLS

B. O. ALMROTH
F. A. BROGAN

LOCKHEED PALO ALTO RESEARCH LABORATORY
3251 HANOVER STREET
PALO ALTO, CALIFORNIA 94304

MARCH 1981

TECHNICAL REPORT AFWAL-TR-80-3129
Final Report for Period June 1976 - October 1980

Approved for public release; distribution unlimited.

FLIGHT DYNAMICS LABORATORY
AIR FORCE WRIGHT AERONAUTICAL LABORATORIES
AIR FORCE SYSTEMS COMMAND
WRIGHT-PATTERSON AIR FORCE BASE, OHIO 45433

NOTICE

When Government drawings, specifications, or other data are used for any purpose other than in connection with a definitely related Government procurement operation, the United States Government thereby incurs no responsibility nor any obligation whatsoever; and the fact that the government may have formulated, furnished, or in any way supplied the said drawings, specifications, or other data, is not to be regarded by implication or otherwise as in any manner licensing the holder or any other person or corporation, or conveying any rights or permission to manufacture use, or sell any patented invention that may in any way be related thereto.

This report has been reviewed by the Office of Public Affairs (ASD/PA) and is releasable to the National Technical Information Service (NTIS). At NTIS, it will be available to the general public, including foreign nations.

This technical report has been reviewed and is approved for publication.

Narendra S Khot

NARENDRA S. KHOT,
Project Engineer

Fred A. Picchioni

FREDERICK A. PICCHIONI, Lt Col, USAF
Chief, Analysis & Optimization Branch

FOR THE COMMANDER

Ralph L. Kuster Jr.

RALPH L. KUSTER, JR., Col, USAF
Chief, Structures & Dynamics Div.

"If your address has changed, if you wish to be removed from our mailing list, or if the addressee is no longer employed by your organization please notify AFWAL/FIBR, W-PAFB, OH 45433 to help us maintain a current mailing list".

Copies of this report should not be returned unless return is required by security considerations, contractual obligations, or notice on a specific document.

UNCLASSIFIED

SECURITY CLASSIFICATION OF THIS PAGE (When Data Entered)

REPORT DOCUMENTATION PAGE		READ INSTRUCTIONS BEFORE COMPLETING FORM
1. REPORT NUMBER AFWAL-TR-80-3129	2. GOVT ACCESSION NO.	3. RECIPIENT'S CATALOG NUMBER
4. TITLE (and Subtitle) Numerical Procedures for Analysis of Structural Shells		5. TYPE OF REPORT & PERIOD COVERED Final June 1976 - October 1980
		6. PERFORMING ORG. REPORT NUMBER
7. AUTHOR(s) B. O. Almroth, F. A. Brogan		8. CONTRACT OR GRANT NUMBER(s) F33615-76-C-3105
9. PERFORMING ORGANIZATION NAME AND ADDRESS Lockheed Missiles and Space Company, Inc. 3251 Hanover Street Palo Alto, California 94304		10. PROGRAM ELEMENT, PROJECT, TASK AREA & WORK UNIT NUMBERS 61102F 2307N102
11. CONTROLLING OFFICE NAME AND ADDRESS Flight Dynamics Laboratory (AFWAL/FIBRA) Air Force Wright Aeronautical Laboratories (AFSC) Wright-Patterson AFB, Ohio 45433		12. REPORT DATE March 1981 13. NUMBER OF PAGES 120
14. MONITORING AGENCY NAME & ADDRESS(if different from Controlling Office)		15. SECURITY CLASS. (of this report) Unclassified 15a. DECLASSIFICATION DOWNGRADING SCHEDULE

16. DISTRIBUTION STATEMENT (of this Report)

Approved for public release; distribution unlimited

17. DISTRIBUTION STATEMENT (of the abstract entered in Block 20, if different from Report)

18. SUPPLEMENTARY NOTES

19. KEY WORDS (Continue on reverse side if necessary and identify by block number)

Finite Elements, Finite Differences, Nonlinear Analysis, Shell Structures

20. ABSTRACT (Continue on reverse side if necessary and identify by block number)

An evaluation is undertaken of currently used discretization procedures in numerical analysis of structures. Emphasis is on the nonlinear behavior of thin shells and plates. It is found that the computer economy is extremely sensitive to the choice of element configuration. A proper balance between the order of the approximations of inplane and lateral displacements is important. The best finite element procedures are superior to finite differences for bifurcation buckling and for moderate nonlinearity. However, for shell collapse analysis the finite difference approach is quite superior to the finite elements.

DD FORM 1 JAN 73 1473 EDITION OF 1 NOV 65 IS OBSOLETE

UNCLASSIFIED

SECURITY CLASSIFICATION OF THIS PAGE (When Data Entered)

BLOCK 20 - CONTINUED

Suggestions are made for improvement of finite element technology for structures undergoing large rotations.

FOREWORD

This report was prepared by Lockheed Missiles and Space Company, Inc., Palo Alto Research Laboratories, 3251 Hanover Street, Palo Alto, California, in partial fulfillment of the requirements under Contract F33615-76-C-3105. The effort was initiated under Project 2307, "Research in Flight Vehicle Structures," Task 2307N102, "Research in the Behavior of Metallic and Composite Components of Air Frame Structures." The project monitor for the contract was Dr. Narendra S. Khot of the Structures and Dynamics Division (AFWAL/FIBRA).

The report covers work under the contract concerned with the efficiency of different discretization procedures. The technical work under the contract was performed during the period June 1976 through October 1980. Review reports were submitted in October 1980 and the final report in March 1981. Results from separate but related efforts are included for completeness. These include the description of an element configuration developed under the LMSC independent research program and a summary of the state-of-the-art performed under contract with AFOSR.

The other reports published under this contract are "Imperfection Sensitivity of Optimized Structures," (AFWAL-TR-80-3128), "Panel Optimization with Integrated Software (POIS)," (AFWAL-TR-80-3073, Vol I and II), "Design of Composite Material Structures for Buckling, An Evaluation of State-of-the-Art," (AFWAL-TR-81-3102), "Supplementary Studies on the Sensitivity of Optimized Structures," (AFWAL-TR-81-3013).

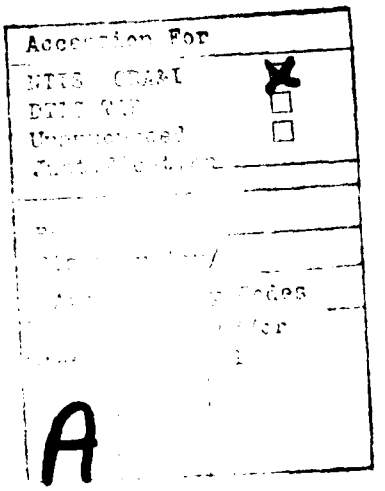

TABLE OF CONTENTS

SECTION		PAGE
	Foreword	iii
	List of Figures	vi
	List of Tables	viii
I	Introduction	1
II	Numerical Differentiation	2
III	Numerical Integration	10
IV	Energy Methods	14
V	Global Function Approach	18
VI	Finite Difference Methods	21
VII	Finite Element Analysis	29
VIII	One-Dimensional Problems	32
IX	Plane Stress Problems	41
X	Plate and Shell Elements	51
XI	Quadrilateral Bending Elements	56
XII	Hybrid Methods	59
XIII	Use of Nonconforming Elements	62
XIV	Ahmad-Type Elements	69
XV	Flat Elements for Curved Shell Analysis	74
XVI	Inextensional Deformation	85
XVII	Shell Collapse Analysis	92
XVIII	Conclusions and Recommendations	97
	References	
	Appendix	

LIST OF FIGURES

Figure	Caption	Page
1	Two-D Finite Difference Grid	4
2	One-D Finite Difference Grid	6
3	Error Function	7
4	Two Finite Difference Schemes	8
5	Numerical Integration Schemes	10
6	Finite Difference Scheme for Column Buckling Analysis	23
7	Two-D Finite Difference Schemes	26
8	A Finite Difference Scheme with Third Order Accuracy	30
9	Linear Basis Function ϕ_n	33
10	Cubic Basis Function	36
11	Rigid Displacement of Curved Element	38
12	Ring with Variable Mesh	40
13	Area Coordinates for Triangular Elements	42
14	Linear Strain Triangle	43
15	Deformation of Annular Plate	46
16	Isoparametric Mapping	49
17	Constant Curvature Triangular Element	52
18	Triangular Elements with Nine (a) and Twelve (b) Degrees of Freedom	53
19	The Clough-Tocher Triangular Bending Element	55
20	Rectangular Bending Element with 12 Degrees of Freedom (QB12)	56
21	Error Versus Gridsize in Plate Bending with QB12 Elements	67
22	Isoparametric Brick Element with 20 Nodes	69
23	Freedom Patterns in an Ahmad Type Element	70
24	Ahmad Type Beam Element with Linearly Varying Bending Moment	72
25	Flat Element for Curved Shell Analysis	75
26	Freedom Pattern in SH411	78
27	Nonlinear Bending of Beam	86
28	Load Displacement Curves for Arch, SH411 Elements	88
29	Load Displacement Curves for Arch, SH410 Elements	89

LIST OF FIGURES (continued)

Figure	Caption	Page
30	Deformed Shape at the Limit Point	91
31	Load Displacement Curves for "Pear-Shaped" Cylinder with SH411	93
32	Load Displacement Curves for "Pear-Shaped" Cylinder with SH440	94
33	Load Displacement Curves for Cylinder with Cutout with SH411	96
A1	The Degrees of Freedom	A-1
A2	The Flat Element	A-2
A3	Inplane Rotation of x-Coordinate Line	A-4
A4	Inplane Rotation of y-Coordinate Line	A-5

LIST OF TABLES

Table	Title	Page
1	COLUMN BUCKLING LOADS	24
2	BUCKLING LOADS VERSUS GRID SIZE FOR AXIALLY LOADED CYLINDRICAL SHELLS	27
3	COLUMN BUCKLING RESULTS	37
4	RING BUCKLING RESULTS	39
5	BUCKLING OF RINGS WITH VARIABLE MESH	40
6	BENDING OF SQUARE PLATE	58
7	BUCKLING OF SQUARE PLATE	65
8	BUCKLING OF SPHERICAL SHELL SEGMENT	66
9	BUCKLING OF FLAT PLATE IN COMPRESSION	79
10	BUCKLING OF FLAT PLATE IN SHEAR	81
11	BUCKLING OF CYLINDRICAL SHELL SEGMENT IN COMPRESSION	82
12	BUCKLING OF IMPERFECT CYLINDRICAL SHELL	84
A1	SHAPE FUNCTIONS AND DERIVATIVES EVALUATED AT NODES AND MID NODES	A-15

Section I

INTRODUCTION

The structural response to a given environment is determined by the differential equations of motion of deformable bodies. Numerical solutions of such equations are discussed in the following for the case in which all derivatives with respect to time can be discarded so that the equations degenerate into a set of static equilibrium equations. Additional questions that may arise in a dynamic environment are not considered. We pay special attention to the behavior of shell structures. For such structures, the mathematical problem is defined by a set of non-linear partial differential equations of elliptic type or by an equivalent energy principle. Analytic solutions of such problems for a reasonably large class of structural configurations are not within the realm of the possible. Consequently, the mathematical problem is recast into a numerical problem for solution on the computer. This transformation can be applied to the equilibrium equations or directly to some energy expression.

The output from the computer consists of a sequence of numbers, in some way representing the functions satisfying equilibrium equations and boundary conditions. If the solution is represented by a linear superposition of a set of "basis functions", then the components of the output vector consist of the coefficients in this series. This is the case if we use the Galerkin or Rayleigh-Ritz procedures. If we use the finite difference or finite element procedures, the solution function is represented by its values at a number of discrete locations within the structure. Because these discretized methods are readily applied in a computer program for a general type of structure, they have been gaining popularity. This applies in particular to the finite element method. The discretized methods make use of numerical differentiation and numerical integration. A review of these operations here is intended to serve as a background to a discussion of the different options that are availble for numerical analysis of shell structures.

Section II

NUMERICAL DIFFERENTIATION

Numerical differentiation consists of the replacement of the derivatives of a function by difference quotients (or finite difference expressions). Such expressions are generally based on local polynomial approximations. A truncated Taylor series can be used for this purpose. In the one-dimensional case (one space variable) the series is of the form

$$f(x) = f(0) + xf'(0) + \frac{x^2}{2} f''(0) + \ldots \frac{x^n}{n!} f^{(n)}(0) + R \qquad (1)$$

where the prime denotes differentiation with respect to x. The remainder R represents the sum of the terms that were excluded when the series was truncated after the $(n+1)$th term. It can be shown that (see Reference 1, for example) that

$$R \leq \frac{x^{n+1}}{(n+1)!} F \qquad (2)$$

where

$$F = \text{Max } [f^{(n+1)}(\xi)]; \; 0 \leq \xi \leq x$$

This bound on the truncation error is useful for estimates of the accuracy of the output vector.

Finite difference expressions may be derived at a number of control points. First, the function values at a number of discrete node points are expressed in terms of the derivatives at the control points by use of a suitably truncated Taylor series. In Equation (1), it is assumed that $x = 0$ at the control point. The procedure leads to a set of linear equations and through solution of this system, expressions for the derivatives at the control point are obtained in terms of the function values at the selected node points. The number of node point values included must be equal to the number of terms of the Taylor series. In the general case the highest order derivative so determined will

be of first order accuracy, i.e., the error $E = O(h)$. If expansion is complete through derivatives of nth order, the kth derivative ($k<n$) will be of order $(n - k + 1)$.

Figure 1 illustrates how finite difference expressions can be derived in a two-dimensional space. A Taylor series approach gives us

$$f_{(\text{at } N_i)} = (f + \alpha_{ij} f' + \beta_{ij} f^{\cdot} + \tfrac{1}{2}\alpha_{ij}^2 f'' + \alpha_{ij}\beta_{ij} f'^{\cdot} + \tfrac{1}{2}\beta_{ij}^2 f^{\cdot\cdot} + \cdots)_{(\text{at } P_j)} \quad (3)$$

where a prime indicates differentiation with respect to the x_1 coordinate, and a dot differentiation with respect to the x_2 coordinate.

If derivatives up to the second order are to be determined, it is sufficient to specify for each control point a set of six neighboring node points (N_i to N_{i+5}). By applying Equation (3) at each of the six node points, we obtain the equation system

$$\begin{Bmatrix} f_1 \\ f_2 \\ f_3 \\ f_4 \\ f_5 \\ f_6 \end{Bmatrix} = \begin{bmatrix} 1 & \alpha_{1j} & \beta_{1j} & \frac{1}{2}\alpha_{1j}^2 & \alpha_{1j}\beta_{1j} & \frac{1}{2}\beta_{1j}^2 \\ 1 & \alpha_{2j} & \beta_{2j} & \frac{1}{2}\alpha_{2j}^2 & \alpha_{2j}\beta_{2j} & \frac{1}{2}\beta_{2j}^2 \\ 1 & \alpha_{3j} & \beta_{3j} & \frac{1}{2}\alpha_{3j}^2 & \alpha_{3j}\beta_{3j} & \frac{1}{2}\beta_{3j}^2 \\ 1 & \alpha_{4j} & \beta_{4j} & \frac{1}{2}\alpha_{4j}^2 & \alpha_{4j}\beta_{4j} & \frac{1}{2}\beta_{4j}^2 \\ 1 & \alpha_{5j} & \beta_{5j} & \frac{1}{2}\alpha_{5j}^2 & \alpha_{5j}\beta_{5j} & \frac{1}{2}\beta_{5j}^2 \\ 1 & \alpha_{6j} & \beta_{6j} & \frac{1}{2}\alpha_{6j}^2 & \alpha_{6j}\beta_{6j} & \frac{1}{2}\beta_{6j}^2 \end{bmatrix} \begin{Bmatrix} f_j \\ f_j' \\ f_j^{\cdot} \\ f_j'' \\ f_j'^{\cdot} \\ f_j^{\cdot\cdot} \end{Bmatrix} \quad (4)$$

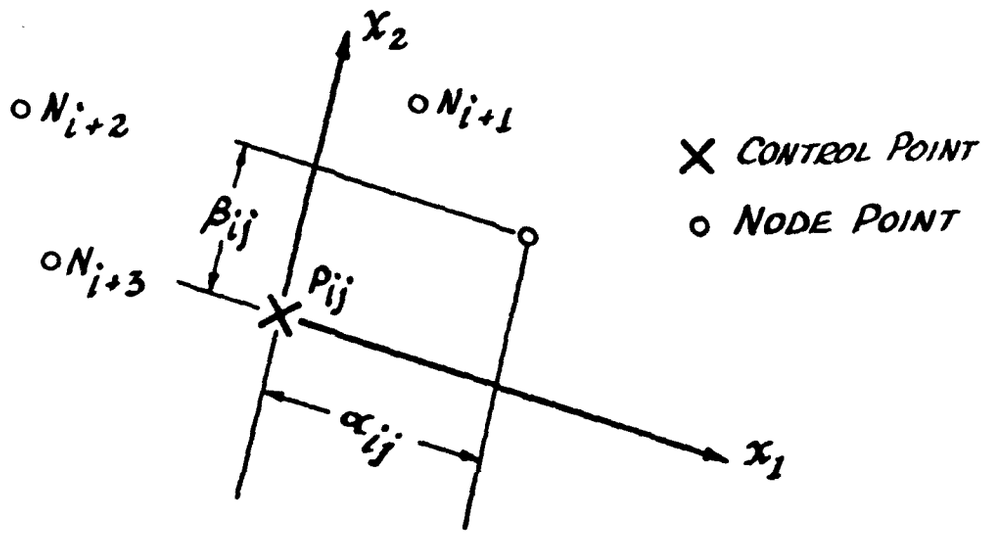

Figure 1 Two-D Finite Difference Grid

The solution of the equation system yields a set of finite difference expressions for the derivatives at control point j. The error bound for the second order derivatives are $E = O(h)$. The first order derivatives are of second order accuracy. If one or more of the second order derivatives is left out, the remaining derivatives may be expressed in terms of five nodal values. Then the first order derivatives are only of first order accuracy and the expressions for the second order derivatives may be meaningless, $E = O(h^0)$. Since there are four different third order derivatives, we must include ten nodal function values in order to raise the accuracy by one order [$E = O(h^3)$ for the first and $E = O(h^2)$ for second order derivaties].

Linear, quadratic or cubic expansions are obtained if all derivatives up to first, second or third order are retained. Bilinear, biquadratic or bicubic are expansions including all derivatives that are at most of first, second or third order with respect to any one of the two space variables. It may be noticed that the order of accuracy of bilinear expansion remains the same as that of the linear expansion and a similar statement holds for higher order expansions.

The nodal values (degrees of freedom) need not be restricted to function values. A higher order derivative at a control point can be expressed in terms of lower order derivatives at the nodal points. These lower order derivatives are then included as support for the local approximation of the solution. Such procedures are discussed in Reference 2, for example.

The location of the control points in relation to the node points can be chosen so that the coefficient becomes zero for the lowest order terms among those that are discarded. In that case the accuracy of the approximation is raised by one order. For demonstration we consider the configuration in Figure 2.

The degrees of freedom of the system are the function values f_1 and f_2 and the first order derivatives β_1 and β_2 at the node points. The finite difference equivalent of the second order derivative at some point in the interval is

determined from a one-dimensional Taylor series

$$f(x) = f_o + xf_o' + \frac{x^2}{2} f_o'' + \frac{x^3}{6} f_o''' + \frac{x^4}{24} f_o^{iv} + \ldots \tag{5}$$

It follows that

$$f'(x) = f_o' + xf_o'' + \frac{x^2}{2} f_o''' + \frac{x^3}{6} f_o^{iv} + \ldots \tag{6}$$

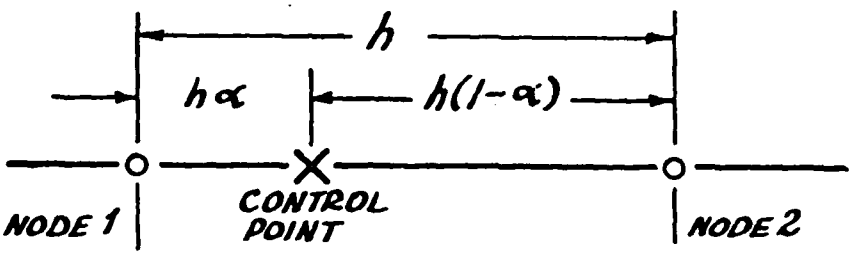

Figure 2. One-D Finite Difference Grid

For simplicity we drop the subscript zero referring to the control point. The finite difference expressions are obtained from the equation system

$$\begin{aligned}
&f + h(1-\alpha)f' + \frac{h^2}{2}(1-\alpha)^2 f'' + \frac{h^3}{6}(1-\alpha)^3 f''' + \frac{h^4}{24}(1-\alpha)^4 f^{iv} = f_2 \\
&f - h\alpha f' + \frac{h^2\alpha^2}{2} f'' - \frac{h^3\alpha^3}{6} f''' + \frac{h^4\alpha^4}{24} f^{iv} = f_1 \\
&f' + h(1-\alpha)f'' + \frac{h^2}{2}(1-\alpha)^2 f''' + \frac{h^3}{6}(1-\alpha)^3 f^{iv} = \beta_2 \\
&f' - h\alpha f'' + \frac{h^2\alpha^2}{2} f''' - \frac{h^3\alpha^3}{6} f^{iv} = \beta_1
\end{aligned} \tag{7}$$

The solution of this equation system includes

$$f'' = \frac{1}{h^2}\left[6(1-2\alpha)(f_2 - f_1) - 2h(2-3\alpha)f_2 + (1-3\alpha)f_1 - \frac{h^2}{12}(6\alpha^2 - 6\alpha + 1)\, f^{iv} + O(h^3)\right] \tag{8}$$

If α is chosen so that the coefficient for f^{iv} vanishes, i.e.,

$$6\alpha^2 - 6\alpha + 1 = 0 \text{ or } \alpha = (1 \pm 1/\sqrt{3})/2$$

then the relative error in the second order derivative (Equation 8) is of third order. The function $y = 6\alpha^2 - 6\alpha + 1$ is shown in Figure 3. Points at which the first term in the error vanishes are sometimes referred to as stress windows.

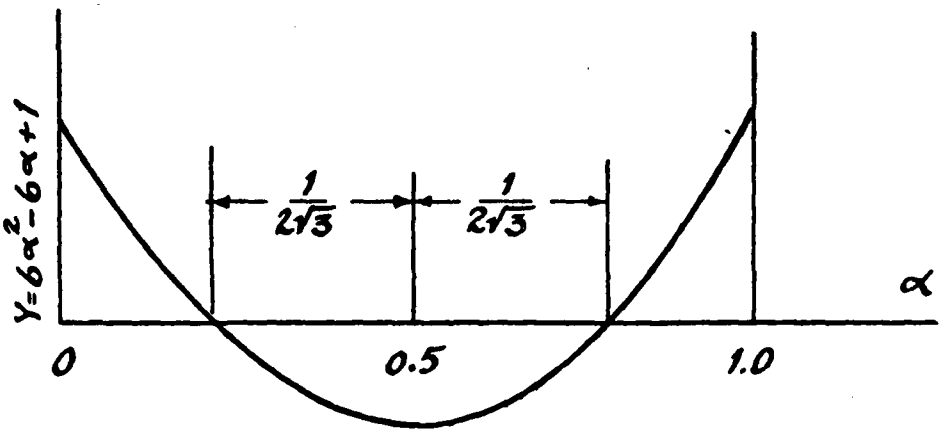

Figure 3. Error Function

The possible advantage of strategic positioning of the control points is further illustrated by the two finite difference schemes shown in Figure 4.

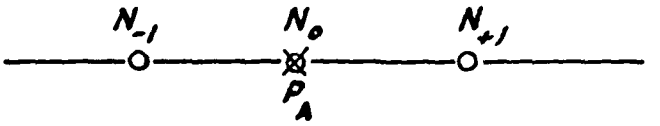

Scheme A

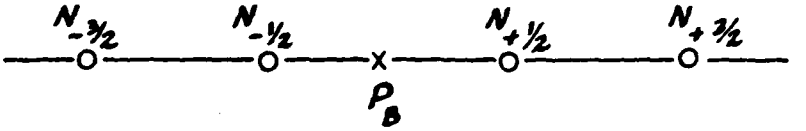

Scheme B

Figure 4. Two Finite Difference Schemes

If function values only are used as freedoms and the nodal spacing is uniform, the stress windows are located at the node points for even order derivatives and halfway between them for odd order derivatives. With Scheme A we find

$$f' = \frac{1}{2h}(f_{+1} - f_{-1}) - \frac{1}{6}h^2 f'''$$
$$f'' = \frac{1}{2h^2}(f_{+1} - 2f_o + f_{-1}) - \frac{1}{12}h^2 f^{iv} \qquad (9)$$

and with Scheme B

$$f' = \frac{1}{h}(f_{+1/2} - f_{-1/2}) - \frac{1}{24}h^2 f'''$$
$$f'' = \frac{1}{2h^2}(f_{+3/2} - f_{+1/2} - f_{-1/2} + f_{-3/2}) - \frac{5}{24}h^2 f^{iv} \qquad (10)$$

For a first order derivative of first order accuracy we need (in the one-dimensional case) two node point values. The first of Equations (10) gives the derivative of second order accuracy at the stress window, halfway

between two nodes. On the other hand, if we derive a formula for the first derivative at a node point from two function values (forward or backward differences) we find that the expression is of first order accuracy, i.e.,

$$f' = \frac{f_2 - f_1}{h} - \frac{h}{2} f'' + \ldots \tag{11}$$

By use of three node points we can define the first order derivative with second order accuracy at any point. If the control point is placed at the node point in the middle the derivative is defined by the first of Equations (9). That is, the error is four times larger than it is in the derivative at the stress window in the two point scheme. On the other hand, the forward and backward difference expressions are still of second order accuracy

$$f' = \frac{1}{2h} (4f_1 - f_2) + \frac{1}{3} h^2 f''' + \ldots \tag{12}$$

It can be shown that first order derivatives determined from a uniform three point scheme are most accurate (of third order) at stress windows, located symmetrically at a distance of $h/2\sqrt{3}$ from the midpoint node.

A comparison of second order derivatives from three- and four-point schemes gives similar results. Even order derivatives in a uniform grid are most accurately computed if one node coincides with the control point and the remaining nodes are placed symmetrically around this point. The location of stress windows in the case of nonuniform spacing is discussed in Reference 3.

Section III

NUMERICAL INTEGRATION

The purpose of numerical integration is to compute an approximate value of $\int_a^b f(x)\,dx$.

In order to achieve this we divide the range of the integral a,b into a number of small subintervals. If the function values are determined at the midpoints of intervals (see Figure 5a), the integral can be obtained by use of the so-called rectangle rule, i.e.,

$$\int_a^b f(x)\,dx = h \sum_{i=1}^{N} f_i \qquad (13)$$

where N is the number of intervals. If the function values are determined at points of division between the intervals (including the end points a,b), then we can use the trapezoidal rule illustrated in Figure 5b.

$$\int_a^b f(x)\,dx = h(1/2\ f_0 + f_1 + f_2 \ldots f_{n-1} + 1/2\ f_n) \qquad (14)$$

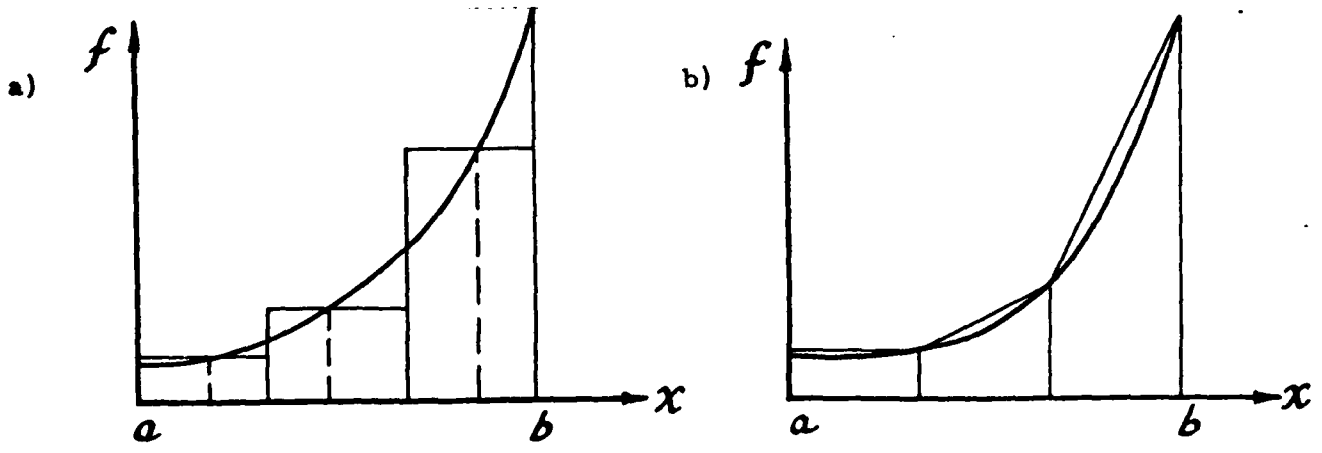

Figure 5. Numerical Integration Schemes

It is shown in Reference 1 that both these methods are of second order accuracy. The rectangle rule is somewhat more accurate with the error bound

$$E \leq \frac{|b - a|h^2}{24}|f''(\xi)|; \; a \leq \xi \leq b. \tag{15}$$

while the error bound for the trapezoidal rule is

$$E \leq \frac{|b - a|h^2}{12}|f''(\xi)|; \; a \leq \xi \leq b. \tag{16}$$

A number of procedures of higher accuracy have been proposed (Euler-McLaurin, Stirling). The Newton-Cotes series of integration formulas are based upon the passing of a polynomial through a sequence of function values and integration of this polynomial over the subintervals. Since the trapezoidal rule is based on a linear approximation over the subintervals, it may be considered as the lowest order method in the Newton-Cotes series. A Newton-Cotes formula of third order accuracy is obtained if we use second order polynomials for interpolation between node points. With uniform spacing, this member of the Newton-Cotes family is well known as Simpson's formula

$$\int_a^b f(x)\,dx = \frac{h}{3}(f_0 + 4f_1 + 2f_2 + \ldots 4f_{n-1} + f_n) \tag{17}$$

We notice that use of Simpson's formula requires that the number of subintervals is even. Higher order Newton-Cotes formulas are increasingly restrictive with regard to the permissible number of subintervals.

A method of special importance in finite element analysis is the Gaussian Quadrature. In this procedure strategic positions are established for the points at which the function is to be determined. As an example we will show here how a two-point integration scheme is derived. If the function values at $x = \pm\alpha\ell$ are f_1 and f_2 with $x = 0$ at the midpoint of the interval, we can approximate the function by

$$f = \frac{f_1 + f_2}{2} + \frac{f_2 - f_1}{2\alpha\ell}\,x + F_2(x) + R \tag{18}$$

where $F_2(x)$ is a function of second degree in x and vanishes at $x = \pm \alpha\ell$ and R is a power series beginning with the third order term.

Due to the symmetry, the integral of odd power terms vanishes and consequently we can write

$$f = \frac{f_1 + f_2}{2} + C_1 \ (\alpha^2\ell^2 - x^2) + C_2(\alpha)x^4 + \ldots \tag{19}$$

and

$$\int_{-\ell/2}^{\ell/2} f(x)\ dx = \frac{\ell}{2}\ (f_1 + f_2) + C_1\ell^3\ (\alpha^2 - \frac{1}{12}) + C_2\ (\alpha)\ \ell^5/5 + \ldots \tag{20}$$

Choosing to determine the function values at the coordinates corresponding to $\alpha = \pm\ 1/2\sqrt{3}$ we obtain

$$\int_{-\ell/2}^{\ell/2} f(x)\ dx = \ell(0.5f_1 + 0.5f_2)\ (1 + E). \tag{21}$$

The relative error $E = C\ell^4/(f_1 + f_2)$ where C is a constant. The method integrates any polynomial up to the third order exactly. The points corresponding to $\alpha = \pm 1/2\sqrt{3}$ are referred to as the Gaussian points. Integration schemes of higher order are obtained by inclusion of additional Gaussian points. Tables are available that give the location of the Gaussian points and corresponding weighting factors for the function value. For exact integration of a jth order polynomial where j is odd we need $(j + 1)/2$ integration points. Sometimes polynomials are integrated with fewer points although this permits the existence of positive definite functions whose integral over the domain vanishes. The procedure is then referred to as reduced integration.

We notice that the position of the "Gaussian points" coincides with the stress windows for the second order derivative in the case with displacements and rotations defined at the end points of the interval (Figure 2). The rectangle

rule, identical to the use of a Gaussian Quadrature over the individual intervals with only one integration point in each, integrates only first order functions exactly.

Section IV

ENERGY METHODS

The equations of equilibrium of a deformable body can be derived by consideration of the balance between elastic forces, body forces and possible surface tractions in an infinitesimal volume element. By use of the constitutive equations, relating strains to stresses, and the kinematic relations, defining strains in terms of displacement components, the equilibrium equations can be expressed in terms of the displacements.

If the loading is conservative and if only elastic deformation is considered, the condition stated by the equilibrium equations is equivalent to the requirement that the sum of the stored strain energy and the potential energy of the applied force system equals zero during a small virtual displacement. Based on this theorem of virtual work we can derive the theorem of minimum potential energy. According to this theorem:

> Among admissible displacements, the configuration corresponding to equilibrium is such that the total potential energy is stationary; for stable equilibrium it is at a minimum.

That is

$$\delta\ (U + W) = 0 \tag{22}$$

where U represents the strain energy and W the potential energy of the external forces, i.e. the negative of the work done by these forces during deformation. Admissible are all displacements that satisfy continuity and essential boundary conditions. The strain energy U can be written

$$U = 1/2 \int_V \varepsilon\ [E]\ \varepsilon\ dV \tag{23}$$

where ε represents a vector of strains and [E] is the (3 x 3) matrix of coefficients in the constitutive relations. The potential energy of the external forces is represented by

$$W = - \int_{S_T} U \cdot T \, dS \tag{24}$$

where T represents the components of surface traction and S_T the part of the structure on which such tractions (external forces) are defined.

The theorem of minimum complementary energy is an alternative formulation also derivable from the principle of virtual work. This theorem states that:

> Among all admissible states of stress the configuration corresponding to equilibrium is such that the complementary energy is stationary; for stable equilibrium it is at a minimum.

That is

$$\delta(U^* + W^*) = 0 \tag{25}$$

where

$$U^* = 1/2 \int_V \sigma [E]^{-1} \sigma \, dV$$

and

$$W^* = - \int_{S_U} T \cdot u \, dS \tag{26}$$

where S_U is the surface upon which displacements are defined and T the corresponding tractions (reactions). Admissible are stress states that satisfy continuity and boundary conditions on surface tractions.

Multifield energy principles including both stresses and strains as free variables can be derived based on the relation

$$\int_V \sigma \, \varepsilon \, dV = U + U^* \tag{27}$$

The expression for the energy is in mathematical terms referred to as a functional. That is, it defines a scalar value U corresponding to a given function. In analysis of plane stress in plates or in a three dimensional analysis, the functional contains derivatives up to the first order only.

In beam analysis or in analysis of plates and shells certain approximations result in the introduction of second order derivatives into the energy functional. Displacements at any point in the structure are expressed in terms of displacements and displacement derivatives at a reference surface. As a consequence, the problem is reduced to be one-dimensional (response quantities are functions of one spatial coordinate only) for the case of beams and two-dimensional for plates and shells. For beams then, the equations of equilibrium become ordinary differential equations, while for plates and shells they remain partial differential equations. The reduction of the number of spatial coordinates can be obtained because the structure is thin, allowing the approximations:

(1) normals to the reference surface remain straight and normal during deformation, and
(2) the transverse normal stress is negligibly small.

In a second order theory, approximately accounting for transverse shear deformation, the normals remain straight but are allowed to rotate in relation to the reference surface.

The assumptions on which a shell theory is based allows the integration through the thickness so that the strain energy is represented by a surface integral. The strain energy is expressed in terms of a six-component vector of reference

surface strains and changes of curvature and the (6 x 6) matrix of coefficients in the equations relating those to the vector of force and moment resultants.

Solutions to the equilibrium problem are obtained by application of one of the energy theorems after numerical analysis procedures has been used to express the corresponding functional in terms of a finite number of degrees of freedom. Another possibility is to seek numerical solutions to the equivalent differential equations of equilibrium.

Section V

GLOBAL FUNCTION APPROACH

In this section we briefly discuss the methods in which the solution function is represented by a linear superposition of basis functions. These are generally allowed to assume nonzero values over the entire domain (except as restricted by boundary conditions). We refer to such a procedure as a global function approach in order to emphasize its distinction from the finite element method to be discussed later.

The Galerkin Method has been widely used to yield approximate solutions to differential equations in structural analysis as well as in many other applications. The method is applicable to partial as well as to ordinary differential equations. For simplicity, we write the equation in the form

$$L(u) = 0 \tag{28}$$

where L is a differential operator and u represents the displacement field. We seek a solution in the space of all trial functions defined by

$$u_N = \sum_{n=1}^{N} a_n \phi_n \tag{29}$$

where the basis functions, ϕ_n, represent kinematically admissible functions (i.e., they are continuous and satisfy given boundary conditions). The components of the output vector are the a_n. Applying Galerkin's method, we determine the a_n through solution of the equation system:

$$\begin{aligned} &\int_V L(u)\,\phi_m dV = 0 \\ &\text{i.e. } \int_V L\left(\sum_{n=1}^{N} a_n \phi_n\right) \phi_m \, dV = 0 \text{ for } m = 1,N. \end{aligned} \tag{30}$$

If $u = U^N$ represents the solution of this system with N basis functions, convergence to the correct solution is implied if the norm

$$||U^N - u^*|| \to 0 \text{ as } N \to \infty \tag{31}$$

where u^* is the solution of the mathematical problem $L(u) = 0$. The norm of a function defined on the domain V can be chosen as

$$||u|| = \int_V u^2 \, dV \tag{32}$$

We will return below to the requirements for convergence with increasing value of N.

The energy methods can also be used directly for construction of a solution to the euqilibrium problem in terms of a linear combination of global functions. One such procedure is the Rayleigh-Ritz Method in which the trial functions

$$U^N = \sum_{n=1}^{N} a_n \phi_n \tag{33}$$

are substituted into the expression for the total potential energy. The basis functions ϕ_n are required to satisfy essential (displacement) boundary conditions. The unknown coefficients a_n are determined through minimization of the total potential energy. Natural boundary conditions are automatically satisfied through the minimization.

A proof for convergence of the method is provided in Reference 4. The conditions for convergence to the correct solution are

(1) For functionals containing derivatives up to the nth order it is required that derivatives of the trial functions up to the (n-1)th order are continuous. This is a sufficient, but as we will see later, not always necessary continuity condition.

(2) The set of trial functions must be complete. That is, the set of trial functions must contain a sequence of functions that in the limit approaches any admissible function arbitrarily close.

(3) Essential (displacement) boundary conditions are satisfied.

The Galerkin method discussed above is in one respect an extension of the Rayleigh-Ritz method. It is applied also to differential equations that cannot be derived through a variational approach. It is shown in Reference 4 that the Galerkin method when applied to variational problems with quadratic functionals is identical to the Rayleigh-Ritz method. This establishes convergence of the Galerkin method within that range. For other cases, it appears that the assumption of convergence is based on conjecture.

Before the introduction of the digital computer, the Rayleigh-Ritz and Galerkin procedures were frequently applied with trial functions chosen on an intuitive basis. Very few terms were included. The use of complete sequences and convergence control became popular with the arrival of high-speed computers. With the demand for programs of general-purpose type, these methods were gradually abandoned in favor of finite difference and finite element methods.

Section VI

FINITE DIFFERENCE METHODS

The finite difference methods are based on replacement of derivatives by finite difference expressions as discussed above. The different expressions can be introduced into the equilibrium equations or in some energy expression. In the former case an algebraic equation system is directly obtained, in which the node point displacements and possibly rotations are the unknowns and each equation expresses equilibrium at one of the control points. The number of equations must be equal to the number of degrees of freedom of the system. Many examples of application of this procedure are given in the literature. In Reference 5, it is applied in an analysis of column buckling.

The problems involved in practical finite difference analysis are much the same if finite difference expressions are used in combination with the energy approach. Since this approach presently is of more direct interest to us, the discussion of the direct use of the equilibrium equations will be restricted to the problem of convergence. Over the years many efforts have been made to show that the method converges with decreasing node point spacing to the solution of the differential equation, i.e.,

$$||U^h - u^*|| \to 0 \text{ as } h \to 0 \tag{34}$$

where U^h is the finite difference solution corresponding to a node point spacing of h.

Rigorous mathematical proofs have been presented for special cases, but due to the diversity of differential equation forms, boundary conditions and shapes of the domain, it appears to be difficult to establish convergence in the general case. However, mathematical rigor has never been the trademark of engineering analysis. Often the assumptions and simplifications in modeling the structure are of such a nature as to make the quest for mathematical rigor rather extravagant. If the application of apparently reasonable methods had been deferred in anticipation of rigorous proofs of uniqueness

and convergence, progress in engineering science would have been considerably retarded.

The finite difference approach appears reasonable from the point of view of an engineering analyst. One difficulty related to the convergence proof is that the error term in the Taylor series expansion contains a derivative $[f^{n+1}]$ (ξ) in Equation 2 of the solution function itself. With some feeling for the physical behavior of the system, the analyst may assume that the solution vector varies continuously with the input data ($|f^{n+1}(\xi)| < C ||T||$) so that the truncation error can be expressed in terms of the loading function rather than in terms of the solution. Whenever the assumption that the solution varies continuously with the input data is violated, finite difference formulations may lead to spurious results. Consider, for example, the case of a beam in bending. We substitute the second order derivative by a three-point central finite difference expression except at one internal point where we use either a backward or a forward difference expression. The beam so defined has a link at the point in question.

It appears reasonable to accept the proposition in Reference 6 that the finite difference approach in solution of differential equations converges toward the correct solution if:

(1) the local truncation error vanishes with the grid size
(2) for small values of h the solution varies continuously with the input data (loads).

The second requirement will exclude a spurious solution such as the one for the beam discussed above.

The use of finite differences in a variational approach is discussed in Reference 7 on page 182. The finite difference expressions are introduced directly into the energy expression and the potential energy is minimized with respect to the values of nodal displacement components. The convergence of the procedure is not discussed in Reference 7. We may appeal to equivalence with finite difference solution of the Euler equations discussed above.

A rigorous and general proof of convergence does not appear to be available. It will suffice for us that whenever the procedure has been applied to a case with a known solution, it has been found to converge toward that solution.

The advantages of introducing the difference quotients into the potential energy expression rather than into the equilibrium equations are that the coefficient matrix becomes symmetric and that the natural boundary conditions are automatically satisfied. For a simple demonstration of the method, we will consider the buckling of a column with uniform cross-section (compare Reference 5, page 283). The buckling load is defined as the load level at which the second variation of the total potential energy vanishes. Hence,

$$2\delta^2 V = \delta^2 \left\{ \int_0^L [EI(w_{,xx})^2 - P(w_{,x})^2] \, dx = 0 \right\} \tag{35}$$

In order to take advantage of the stress windows as discussed above [see Equations (9) and (10)], we will determine $w_{,x}$ at midnodes and $w_{,xx}$ at node points as shown in Figure 6.

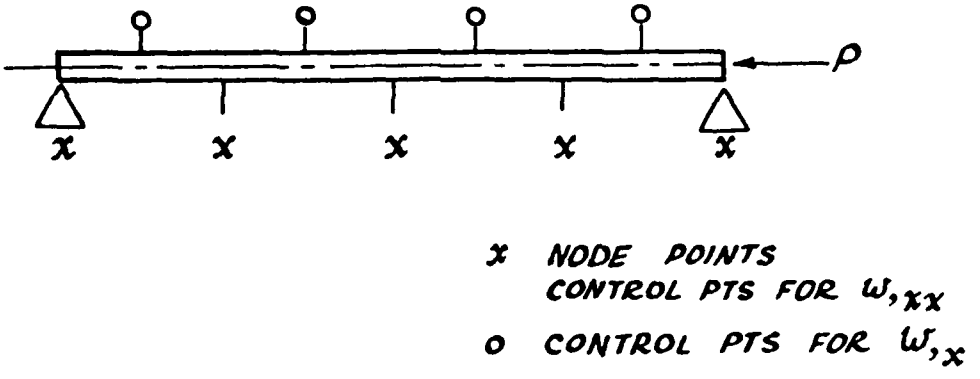

Figure 6. Finite Difference Scheme for Column Buckling Analysis

Then $(w_{,x})^2$ can be integrated by use of the rectangle rule, and $(w_{,xx})^2$ by use of the trapezoidal rule. We have

$$\int (w_{,x})^2 dx = h \sum_{i=1}^{N-1} \frac{1}{h}(w_{i+1} - w_i) \tag{36}$$

and

$$\int (w_{,xx})^2 dx = \frac{1}{2h} (w_2 - 2w_1 + w_0)^2 + h \sum_{i=2}^{N-1} \frac{1}{2} (w_{i+1} - 2w_i + w_{i-1})^2 + \frac{1}{2h} (w_{N-1} - 2w_N + w_{N+1})^2 \tag{37}$$

Fictitious points (corresponding to w_0 and w_{N+1}) have been introduced so that the second order derivatives can be determined at the end points. We could instead introduce forward and backward derivatives at these points or add the rotation at the end points as a freedom. Whenever energy methods are used, the control points at which derivatives are required coincide with the integration points at which the energy density is defined.

After the number of uniformly spaced node points have been chosen, we can form a homogeneous equation system in which P appears as the eigenvalue parameter. Solutions, given in Reference 5, are shown in Table 1.

TABLE 1

COLUMN BUCKLING LOADS

Number of Nodes on Half Column (i)	$\overline{P}_{CR}$ Critical Load / $[EI(\pi/L)^2]$
3	0.9495
4	0.9774
5	0.9872
7	0.9943
9	0.9968
11	0.9979
∞	1.0000

Since the finite difference expressions as well as the numerical integrations are of second order accuracy, we expect the error in the solution to be proportional to the square of the spacing between node points if the grid is fine enough so that fourth order terms in the error are insignificant. (We have omitted the step showing that natural boundary conditions are satisfied to the same degree of accuracy.) As the grid spacing equals L/2(i-1), we obtain from the first two results in the table above

$$E_3 = c\left[\frac{L}{2(3-1)}\right]^2 = \bar{P}_{CR} - 0.9495$$
$$E_4 = c\left[\frac{L}{2(4-1)}\right]^2 = \bar{P}_{CR} - 0.9774 \qquad (38)$$

Dividing the first of Eqations (38) by the second, we obtain an equation from which we determine $\bar{P}_{CR} = 0.9997$. In view of the fact that the values of $\bar{P}_{CR}$ for 3 or 4 points were rounded to four figures, this is as close to the exact solution as we possibly can expect and thus verifies the assumption of second order convergence. First order derivatives from two nodal points and second order derivatives from three are generally of first order accuracy. A second order accuracy is obtained by a favorable choice of nodes and integration points. This type of phenomenon is referred to as superconvergence in Reference 8. By use of two solutions corresponding to very coarse nodal spacing, and the assumption of second order accuracy, we are in this case able to predict a very accurate result through extrapolation. This method is referred to as Richardson's extrapolation.

In the two-dimensional case, it is more difficult to utilize stress windows in order to obtain superconvergence. We will briefly discuss the problems involved in the definition of efficient finite difference schemes for rectangular nets with uniform spacing. (In the case of nonuniform spacing, it is possible to make use of the same expressions by mapping the shell upon a domain with a suitable definition of a distance.) Examples of two-dimensional finite difference schemes are shown in Figure 7. The scheme used in Figure 7a defines the inplane displacements at half-stations. A rectangular integration scheme is used, and the strain energy is defined at the w-node at the center

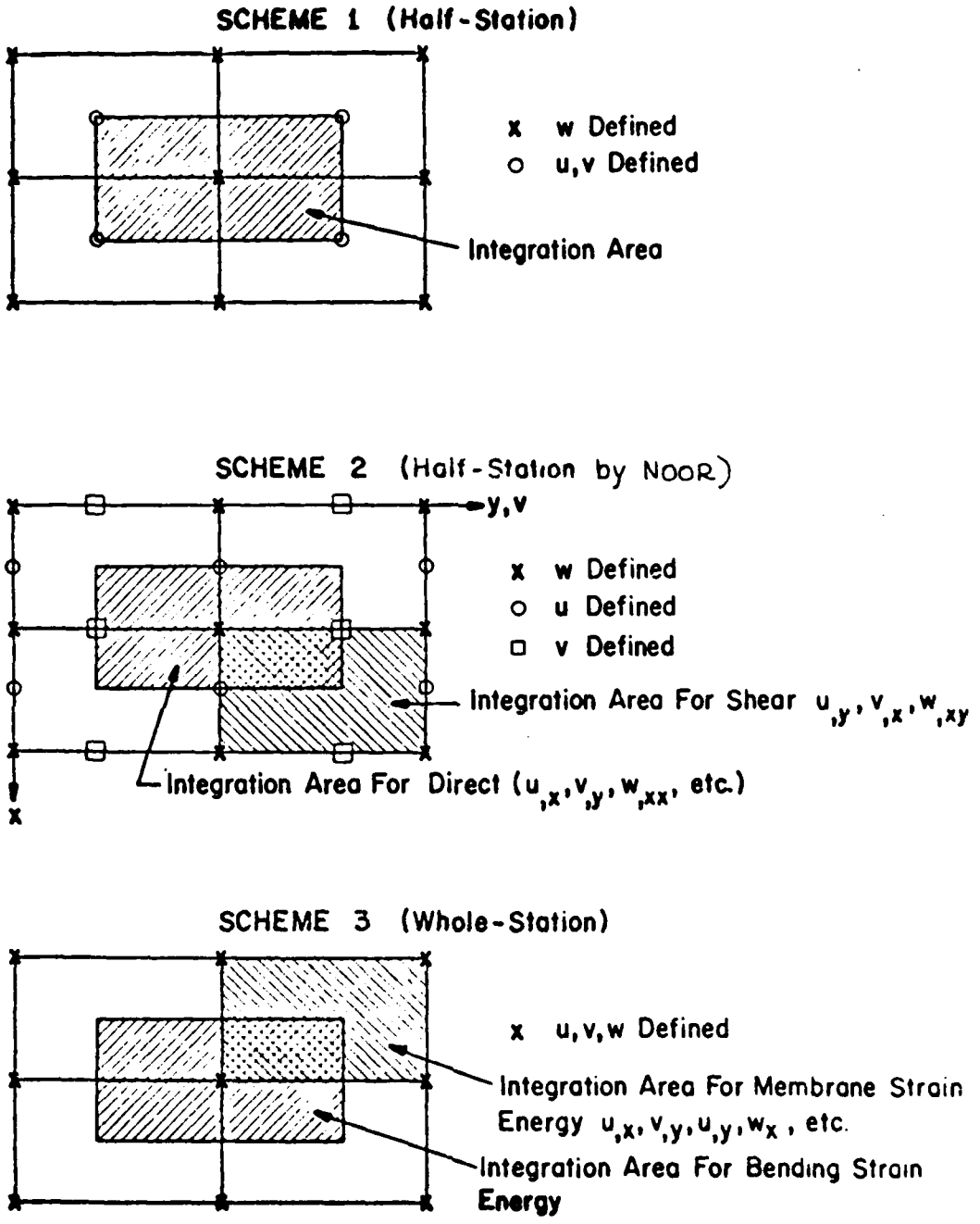

Figure 7. Two-D Finite Difference Schemes

of the figure. This point then represents a stress window for bending as well as membrane strains. There is one obvious weakness in this scheme. The membrane strain ε_x, for example, at the integration point must be obtained as an average of its values at points A and B. While this operation is still of second order accuracy the coefficient of the error term is increased.

This problem is eliminated in the modified half-station scheme introduced in Reference 9 by Noor (Figure 7b). However, both the half-station schemes shown here are somewhat inefficient for nonlinear or stability analysis. It is sufficient for illustration of this problem to consider a straight beam element with

$$\varepsilon_x = u_{,x} + 1/2(u_{,x}^2 + w_{,x}^2) \tag{39}$$

For definition of the membrane strain ε_x, we need to express both the spatial derivatives $u_{,x}$ and $w_{,x}$ at the same integration points. If w is defined at the node points and u at half-stations, it is not possible to use the most favorable expression for $u_{,x}$ as well as for $w_{,x}$.

By introduction of the whole-station, illustrated in Figure 7c, both these problems are eliminated. With the membrane and bending energies integrated over different sets of integration points, it is possible to make use of the stress window for $u_{,x}$ as well as for $w_{,x}$. This results in much better convergence for the buckling load as illustrated in Table 2.

TABLE 2

BUCKLING LOADS VERSUS GRID SIZE FOR
AXIALLY LOADED CYLINDRICAL PANELS

Grid Axial x Circumf.	Half-Station Figure 7a	Whole Station Figure 7c
10 x 5	350	825
12 x 6	525	875
16 x 8	770	925
20 x 10	865	945
32 x 16	960	960

We conclude from the results in Table 2 that for similar accuracy we can use almost twice as large grid spacing with the whole-station scheme. Also, it appears that the error in both cases varies quadratically with the grid spacing. However, the eigenvalues were not computed with sufficient accuracy to give reliable information about the rate of convergence.

Unfortunately, the whole-station scheme becomes less efficient if the constitutive relations contain terms that couple force and moment resultants (such as eccentrically stiffened shells). This problem occurs because the strain energy then includes products of first order derivatives of in-plane and normal displacements. It appears possible to circumvent this problem, but since the interest largely has shifted to finite element formulations, this search has not been vigorously pursued.

Another problem is related to the integration of the membrane strain energy by use of the rectangle rule, or as observed above, by Gaussian integration with only one point. A polynomial that matches the function values at all four corners must include at least one second order term. Therefore, this is a case of reduced integration allowing a nonzero deformation pattern with vanishing strain energy. This pattern is defined by $u = c_1xy$ and $v = c_2xy$, where x and y are space coordinates with $x=y=0$ at the integration point. Such a deformation is referred to as a mechanism, and if allowed, sometimes leads to spurious solutions. The deformation pattern is usually prevented by displacement constraints on shell boundaries and therefore it is somewhat questionable whether it is worthwhile to remedy the situation by use of integration with four Gaussian points.

Section VII

FINITE ELEMENT ANALYSIS

In the previous paragraph it is demonstrated that for maximum efficiency in a finite difference discretization it is important to choose the position of each control point (or integration point) judiciously. It is important also that the functions and their derivatives are expressed in terms of the function values at a suitable set of neighboring nodes. The major flaw in the whole-station scheme of the previous section was that both factors in terms representing coupling between bending and membrane action cannot be represented by the most efficient expression at the same integration points.

Continuing the search for a better formulation we may consider the scheme illustrated in the one dimensional case in Figure 8. One integration interval is shown in the figure. According to Equation (8) the second order derivative of the lateral displacement is of third order accuracy at the integration points. The first order derivative of the lateral displacement based on the same four freedoms is at least of third order accuracy anywhere in the interval. Based on three function values, at the midpoint and at the end points of the interval, first order derivatives (of inplane displacements) are of third order accuracy at the Gaussian points for two-point integration [compare the discussion following Equation (11)]. As a consequence all quantities included in the strain energy are of third order accuracy at the two Gaussian points.

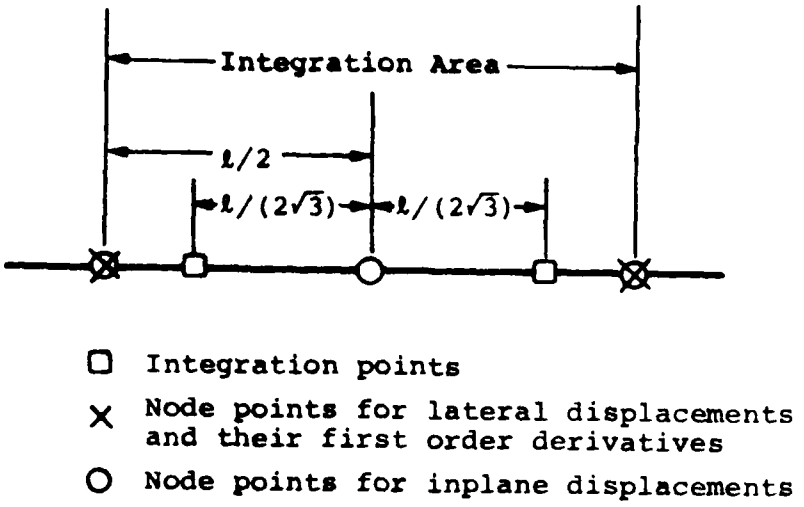

Figure 8. A Finite Difference Scheme with Third Order Accuracy

Characteristic for the scheme in Figure 8 is that the derivatives at all integration points within any integration interval are based on the same system of neighboring nodal values, and that no nodal values outside of the integration area are engaged in the formulation. Due to these properties the formulation adheres in the strictest sense to the rules that define a finite element procedure. However, these rules are somewhat artificial and there appears to be no meaningful distinction between the finite element and the energy based finite difference analyses. In Reference 10 Felippa refers to this finite difference procedure as finite elements with extended support because the energy density at the integration points is expressed in terms of nodal displacement freedomes outside of the closed domain of the element. We may refer to configurations that satisfy the stricter rule as self-contained elements.

It may be noticed at this point that the finite difference formulation for the membrane energy in the two-dimensional scheme is a self-contained finite element. In the bending part on the other hand the energy expression is based on freedoms at nodes outside the element boundaries.

It is clear then, that the finite element method could have been derived through a specialization or refinement of the finite difference energy method. As will be seen in the following it could also have been the result of a specialization of the Rayleigh-Ritz method. In either case, it would have been directly applicable for solution of any set of ordinary or partial differential equations derivable from a potential. However, in contrast to the Rayleigh-Ritz procedure and the finite difference method the finite element method was originally derived by means of physical and largely heuristic considerations in the field of structural mechanics rather than in the field of applied mathematics. As an afterthought the method was given a mathematical interpretation (Reference 11). This led to considerable refinement of the method and made possible the extension to problems outside of the field of structural mechanics.

The mathematical interpretation of the finite element method is based on the Ritz principle. While the heuristic mechanical approach may have great appeal to many engineers, the best understanding of the method, its scope and its convergence properties is obtained if it is presented as a special form of the Rayleigh-Ritz method, much in the same way as in the book by Strang and Fix (Reference 6). From this point of view, the finite element method entails the definition of a set of trial functions, complete in the sense that it contains at least one function arbitrarily close to any admissible solution (displacement field). The solution of the problem is represented by that member of the set of trial functions which renders the functional (energy expression) stationary. Typical for the finite element method is that the trial functions are obtained as a linear combination of <u>locally defined basis functions</u>. That is, each basis function is zero over the major part of the domain. The advantage with this arrangement is that most of the basis functions are uncoupled, and thus, the coefficient matrix of the final equation system has a relatively narrow bandwidth. Also, the system is generally well conditioned.

Section VIII

ONE-DIMENSIONAL PROBLEMS

For the purpose of defining local basis functions, the domain is subdivided into a number of intervals or subdomains called finite elements. Once the domain has been so divided, the unknown function within each element can be expressed, for example, in terms of local power series with unknown coefficients. Each local power series is constrained by the condition that at the endpoint of the interval its sum equals the discrete value of the solution functions f_i at corresponding node point. The nodal values of the function and the free coefficients in the power series are the degrees of freedom of the system with respect to which the functional is minimized. If additional constraints on these freedom are introduced as dictated by boundary conditions, the trial functions so obtained form a complete set of admissible functions. With a fixed subdivision, a mesh, the finite element method properly applied would converge with increasing order of the local approximations. In such a case we have p-convergence. If the mesh is coarse, a large number of terms may be needed in the power series, then the band width of the equation system becomes large and also the system may become ill-conditioned.

A more common practice is to use a fixed form of the local shape functions. In that case h-convergence is obtained with gradually refined mesh spacing. Or rather, the mesh is made fine enough so the analyst feels reasonably certain of obtaining a solution of satisfactory accuracy.

In the simple one-dimensional case with only first order derivatives the basis functions may be linear as shown in Figure 9. The value of ϕ_n is equal to unity at node n and zero at all other nodes.

It is clear then, that the finite element method could have been derived through a specialization or refinement of the finite difference energy method. As will be seen in the following it could also have been the result of a specialization of the Rayleigh-Ritz method. In either case, it would have been directly applicable for solution of any set of ordinary or partial differential equations derivable from a potential. However, in contrast to the Rayleigh-Ritz procedure and the finite difference method the finite element method was originally derived by means of physical and largely heuristic considerations in the field of structural mechanics rather than in the field of applied mathematics. As an afterthought the method was given a mathematical interpretation (Reference 11). This led to considerable refinement of the method and made possible the extension to problems outside of the field of structural mechanics.

The mathematical interpretation of the finite element method is based on the Ritz principle. While the heuristic mechanical approach may have great appeal to many engineers, the best understanding of the method, its scope and its convergence properties is obtained if it is presented as a special form of the Rayleigh-Ritz method, much in the same way as in the book by Strang and Fix (Reference 6). From this point of view, the finite element method entails the definition of a set of trial functions, complete in the sense that it contains at least one function arbitrarily close to any admissible solution (displacement field). The solution of the problem is represented by that member of the set of trial functions which renders the functional (energy expression) stationary. Typical for the finite element method is that the trial functions are obtained as a linear combination of <u>locally defined basis functions</u>. That is, each basis function is zero over the major part of the domain. The advantage with this arrangement is that most of the basis functions are uncoupled, and thus, the coefficient matrix of the final equation system has a relatively narrow bandwidth. Also, the system is generally well conditioned.

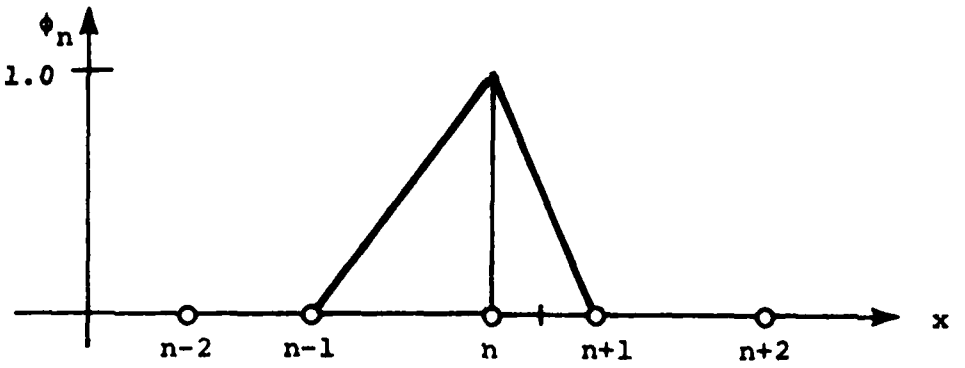

Figure 9. Linear Basis Function ϕ_n

The trial functions (with $f_1 = f_N = 0$) have the form

$$f^N = \sum_{n=2}^{N-1} a_n \phi_n \quad \text{where} \tag{40}$$

$$\phi_n = \begin{cases} (x - x_{n-1})/(x_n - x_{n-1}) & \text{for } x_{n-1} \leq x \leq x_n \\ (x_n + 1 - x)/(x_{n+1} - x_n) & \text{for } x_n < x \leq x_n + 1 \\ 0 \text{ elsewhere} \end{cases}$$

This set consists of all piecewise linear functions. It is complete since, with decreasing mesh spacing (increasing N) any continuous function can be arbitrarily closely approximated. The trial functions (but not its first derivatives) are continuous over the domain as required by the Ritz theory. The local power series are of the form

$$f = f_i + \frac{f_{i+1} - f_i}{x_{i+1} - x_i} (x - x_i) \tag{41}$$

That is they are of first order in x.

The trial functions defined in Eq. (40) may be used to determine arbitrarily closely the function f(x) that minimizes the functional

$$U = \int_L F(x) f'^2_x + G(x) f \, dx \tag{42}$$

Where L is the total length of the domain on which f is defined and F(x), G(x) are known functions x. After substitution of Equation (40) into Equation (42) the integral is evaluated over each interval and summed over the domain. Due to the local characters of the basis functions, the products $\phi_m \phi_n$ are zero everywhere if $|n-m| < 1$. Consequently the terms $C_{mn} a_m a_n$ in the functional corresponding to $F(x) f'^2_x$ will vanish if $|n - m| > 1$, i.e., the equation system obtained through minimization ($\partial U / \partial a_n = 0$, n = 2, N - 1) will be narrowly banded (tridiagonal).

In analysis of beams, plates and shells the strain energy functional includes second order derivatives of the lateral displacements. For such problems the Ritz theory requires that the trial functions belong to the functior space C^1. That is, it is required that the trial functions, as well as their first order derivatives, are continuous over the domain. In the one dimensional case (beam analysis) this is readily achieved if the function value as well as its first order derivative (rotation in beam analysis) are considered as nodal freedoms. A cubic representation of the lateral displacement field can be obtained by use of the Taylor series approach [compare Equations (6) and (7)]. Continuity requirements are satisfied since the values of the functions and their first order derivatives at any node are common to the two elements connected at the node.

An equivalent representation can be obtained by use of a set of four shape functions defined (Figure 10) such that in each function one nodal freedom equals unity and the other three are zero. The basis function corresponding to the nth node is

$$f_n = \sum (a_n \phi_n + b_n \psi_n) \tag{43}$$

where a_n is the function value and b_n its first order derivative at node n.

Here a_n and b_n represent the degrees of freedom of the system. The bending moments and the rotations at each of the integration points can be expressed in terms of these freedoms. The total bending strain energy is then readily expressed in the form

$$V_e = \{g\}^T [K]_e \{g\} \tag{44}$$

where

$$\{g\}^T = [(a_n)_1 , (a_n)_2 , (b_n)_1 , (b_n)_2] \tag{45}$$

and K is referred to as the element stiffness matrix. Summation over all elements gives an assembled or global stiffness matrix (see Reference 12, for example).

Column buckling analysis includes such terms as $w,_x^2$ [see Equation (35)]. With a cubic representation of w this term is a fourth order polynomial, accurately integrated by use of a Gaussian scheme with three integration points.

The critical load for a cantilevered column is $1/4\ EI\ (\pi/L)^2$. A finite element buckling analysis of a column with $(EI)/(4L^2) = 1.0$ based on cubic representation of the lateral displacement and three Gaussian points gives the results shown in Table 3.

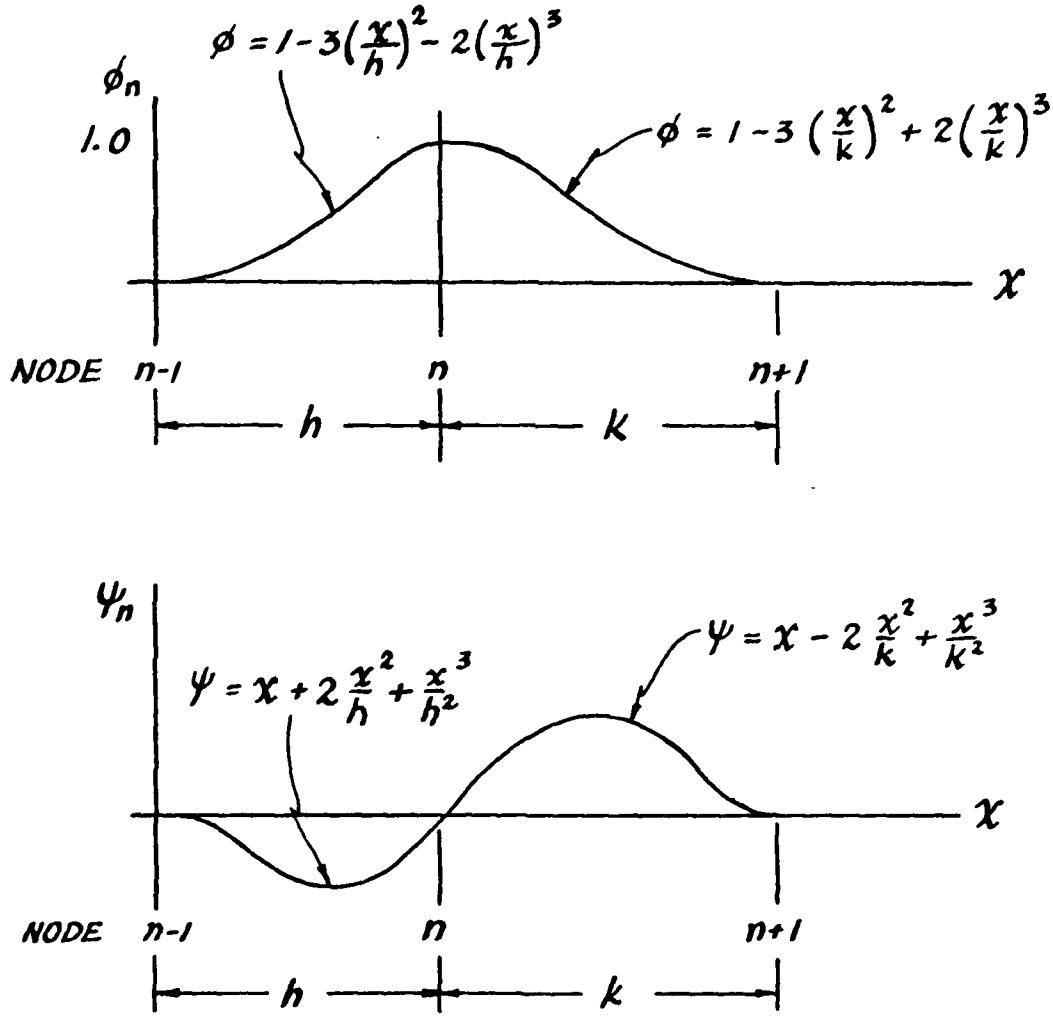

Figure 10. Cubic Basis Function

TABLE 3

COLUMN BUCKLING RESULTS

Number of Elements, i	P_{CR}	ERROR E	Ei^4
1	9.943847	.07424	.0742
2	9.874659	.005055	.0809
3	9.870620	.001016	.0823
4	9.869928	.000323	.0827
9	9.869617	.000013	.0853

With increasing number of elements the accurate solution, $P_{CR} = \pi^2 = 9.869604$ is rapidly approached. It appears that the error times the fourth power of the number of elements is almost a constant. This would indicate that the error is of the fourth order rather than third as expected, may be somewhat fortuitously. With very coarse spacing the lowest order term is not the dominating error and with very fine spacing the accuracy may be governed by round off errors. As a compromise, we base an extrapolation on the values corresponding to 3 and 4 elements. The assumption of fourth order accuracy then leads to a value of 9.869612 for the critical load, i.e., the relative error is less than 10^{-6}.

With only one element, corresponding to two elements per half-wave in the buckling pattern, the error is still less than one percent. In engineering analysis such accuracy is generally quite acceptable. However, with a solution available only for one grid size the analyst does not know whether it is within the range of acceptable accuracy. Unless a sequence of gradually refined solutions is available he is not on firm ground.

For analysis of rings or arches it seems natural to develop curved beam elements. In that case, the special problem of strain energy due to a rigid body displacement, self-straining, must be considered. For illustration, an element of a circular arch is shown in Figure 11.

If the circular arch is rigidly displaced a distance δ in the x-direction, the displacement components are defined by

$$\begin{aligned} w &= \delta \sin \theta \\ v &= \delta \cos \theta \end{aligned} \tag{46}$$

It is not possible with a truncated power series to represent this displacement pattern exactly. As a consequence a rigid body displacement introduces some strain energy in the element. This situation occurs whenever the geometry of the element cannot be exactly represented by use of the functions (usually polynomials) representing the displacement components.

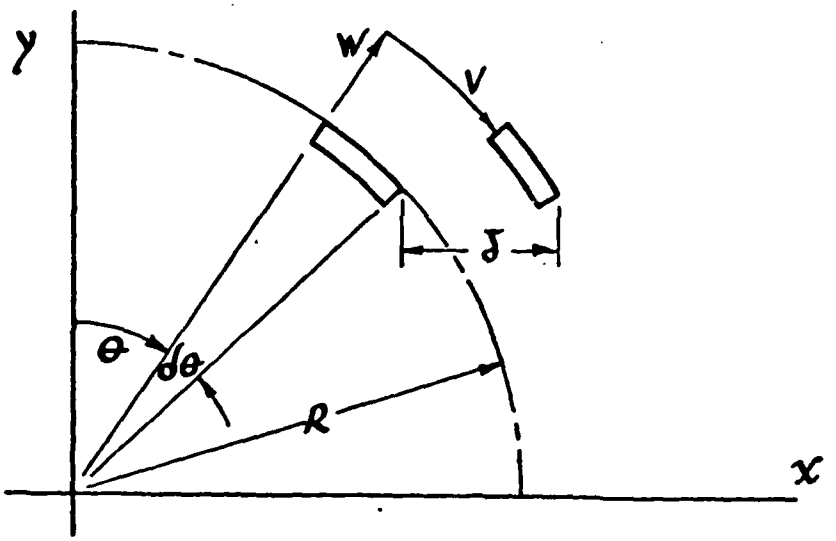

Figure 11. Rigid Displacement of Curved Element

Elements with the strain energy for rigid body displacements proportional to some power of h may still give good convergence in most applications. However, there are cases in which the rigid body displacement of an element is very large in comparison to the displacements corresponding to element distortion. In such cases, h-convergence may be very slow for elements in which the rigid body energy is not exactly zero but proportional to some power of the nodal spacing.

Flat elements are often used to represent curved beams or surfaces. The reason for this approach is that it simplifies the formulation and also that it eliminates problems with strain energy under rigid body displacement. Table 4 shows some results from a buckling analysis with cubic straight beam elements of a ring under constant direction pressure. The critical pressure is

$$p_{CR} = \frac{4EI}{R^3} \tag{47}$$

The results in Table 4 correspond to a ring with $EI/R^3 = 0.25$ lbs/in, i.e., the exact solution is $p_{CR} = 1.0$.

TABLE 4

RING BUCKLING RESULTS

Number of elements, i (Over 90° arc)	p_{CR}	Error E	Ei^2
4	1.006970	.006970	.1015
6	1.002965	.002968	.1067
8	1.001641	.001641	.1050
10	1.001042	.001042	.1042

We notice that the method now is of second accuracy (Ei^2 is constant) and that to achieve somewhat less than one percent error it is necessary to use four elements per half-wave in the buckle pattern. Use of Richardson's extrapolation based on second order accuracy with 8 and 10 elements leads $p_{CR} = 1.00002$ lbs/in.

As long as each element is self-contained, the order of the accuracy is not changed if the mesh has a variable spacing. For buckling of a ring under uniform pressure there is no reason to use a finer spacing in any local region. A constant mesh spacing gives the more efficient model and the results for rings with the mesh indicated in Figure 12 are shown only for demonstration of the effect of variable spacing.

Some computed buckling loads are shown in Table 5. The second order accuracy is maintained. A Richardson extrapolation based on the results for 9 and 12 elements over the 90° arch leads to $P_{CR} = 0.99997$. Comparison with the results in Table 4 indicates that the results are somewhat less accurate than those obtained with the finest of the two spacings used and somewhat better than those obtained with the coarser spacing. The prebuckling solution for the variable mesh with 6 elements shows a rather large error in lateral displacement although the error in the buckling loads is only 0.43%. The computed displacements vary from about 7% above to about 7% below the analytic solution ($w = pR^2/EA$), being too small in the area with coarse spacing.

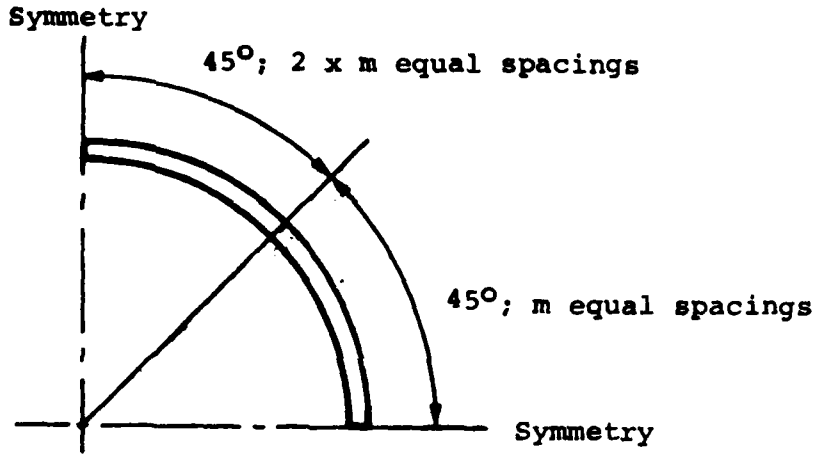

Figure 12. Ring with Variable Mesh

TABLE 5

BUCKLING OF RINGS WITH VARIABLE MESH

Number of Elements, i on 90°	P_{CR}	Error E	Ei^2
6	1.004271	.004271	.1538
9	1.001836	.001836	.1487
12	1.001020	.001020	.1469

Section IX

PLANE STRESS PROBLEMS

In plane stress problems the displacement components u, v are functions of two spatial coordinates x, y. The strain energy is defined in terms of the first order derivatives $u_{,x}$, $u_{,y}$, $v_{,x}$, $v_{,y}$. Consequently, the Ritz theory requires that the functions u and v are continuous over the domain. The simplest element for analysis of plane stress problems is the triangular element. A Taylor series in two dimensions including derivatives up to the first order contains three terms. Consequently, a displacement field in which the first order derivatives are of first order accuracy can be determined from three nodal function values. The obvious choice then is an element in which the degrees of freedom are represented by the values of u and v at the corners. Two adjacent elements have identical values of the displacement components at both ends of the interface and these components vary linearly with the space coordinates. Thus, the values of u and v in the two elements are identical over the entire interface, i.e., u and v are continuous over the domain. Elements that satisfy the continuity requirements of the Ritz theory are referred to as conforming elements.

With linear variation of the displacements all strains (in linear analysis) are constant within an element. The triangular 6-degree-of-freedom element is usually referred to as the "Constant Strain Triangle" or the CST-element. As the strain is constant throughout the element it is obviously sufficient to use integration with one Gaussian point, i.e., the c.g. of the triangle. This point is also the stress window where the strain is expressed with a second order accuracy. In a range of sufficiently small elements the error in analysis with CST elements varies with the square of the mesh spacing.

Equivalent to the Taylor series approach is the use of linear shape functions. For triangular elements it is convenient to express these shapefunctions in terms of so called area coordinates as discussed, for example in Reference 12. The definition of such coordinates is illustrated in Figure 13.

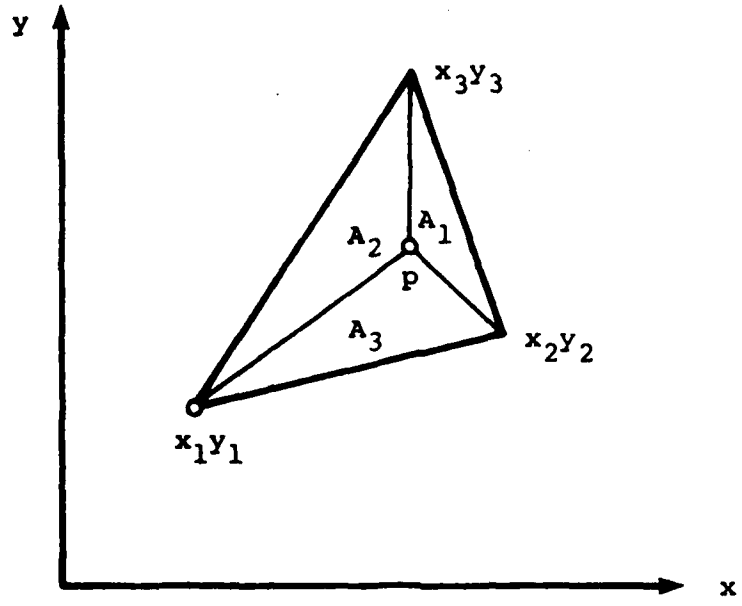

Figure 13. Area Coordinates for Triangular Elements

The location of a point P inside the triangle is uniquely determined if two of the areas of the subtriangles A_i are known. Consequently these areas, or rather the areas normalized with respect to the total area A of the element, can be used as space coordinates.

$$\xi = A_1/A \ , \ \eta = A_2/A \ , \ \zeta = A_3/A \tag{48}$$

As the relation $\xi + \eta + \zeta = 1$ holds, the Cartesian coordinates of point P can be written in the form

$$\begin{Bmatrix} 1 \\ x \\ y \end{Bmatrix} = \begin{bmatrix} 1 & 1 & 1 \\ x_1 & x_2 & x_3 \\ y_1 & y_2 & y_3 \end{bmatrix} \begin{Bmatrix} \xi \\ \eta \\ \zeta \end{Bmatrix} \tag{49}$$

The same interpolation may be used for the displacement components u and v, i.e.,

$$\begin{Bmatrix} 1 \\ u \\ v \end{Bmatrix} = \begin{bmatrix} 1 & 1 & 1 \\ u_1 & u_2 & u_3 \\ v_1 & v_2 & v_3 \end{bmatrix} \begin{Bmatrix} \xi \\ \eta \\ \zeta \end{Bmatrix} \tag{50}$$

where $u_i v_i$ represent the discrete values of the displacement components at corner i. The inversion of Equation (49) is needed for expression of the location of Gaussian integration points in terms of the area coordinates. The inverse is given in Reference 12.

In order to raise the order of accuracy of the triangular plane stress element it is necessary to add another three freedoms for each displacement component (there are three second order derivatives). A natural choice then is to add the displacements at midside nodes on each of the element boundaries. Figure 14 shows a triangular element with midside nodes and indicates nodal values of the area coordinates.

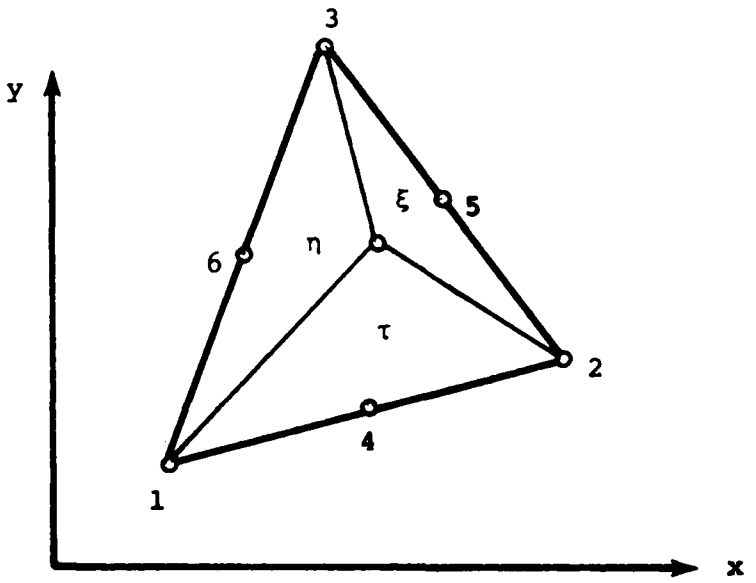

Point	x	y	ξ	η	ζ
1	x_1	y_1	1	0	0
2	x_2	y_2	0	1	0
3	x_3	y_3	0	0	1
4	x_4	y_4	1/2	1/2	0
5	x_5	y_5	0	1/2	1/2
6	x_6	y_6	1/2	0	1/2

Figure 14. Linear Strain Triangle

The relation between Cartesian and area coordinates is given by:

$$\begin{Bmatrix} 1 \\ x \\ y \end{Bmatrix} = \begin{bmatrix} 1 & 1 & 1 & 1 & 1 & 1 \\ x_1 & x_2 & x_3 & x_4 & x_5 & x_6 \\ y_1 & y_2 & y_3 & y_4 & y_5 & y_6 \end{bmatrix} \begin{Bmatrix} \xi\ (1 - 2\xi) \\ \eta\ (1 - 2\eta) \\ \zeta\ (1 - 2\zeta) \\ 4\xi\eta \\ 4\eta\zeta \\ 4\zeta\xi \end{Bmatrix} \tag{51}$$

Using the corresponding interpolation for the displacement components we obtain a simple expansion, equivalent to the result of a quadratic Taylor series approach.

That is

$$\left.\begin{aligned} u &= \sum_1^6 u_i P_i \\ v &= \sum_1^6 v_i P_i \end{aligned}\right\} \tag{52}$$

where each of the six shape functions

$$P_i = \{\xi(1 - 2\xi)\ ,\ \eta(1 - 2\eta)\ ,\ \zeta(1 - 2\eta)\ ,\ 4\xi\eta\ ,\ 4\eta\zeta\ ,\ 4\zeta\xi\} \tag{53}$$

are equal to unity at one of the six nodes and zero at the others.

From Equations (52) and (53) it follows that the displacement components are quadratic with respect to the spatial coordinates. Since two adjacent elements have three freedoms (for each displacement component) in common the linear strain triangle (LST element) is conforming and the convergence requirements of the Ritz procedure are satisfied.

With the same nodal pattern we can define the displacements inside the element by use of four constant strain triangles. Clearly this gives a less accurate representation of the strain than the linear variation obtained by use of the shape functions in Equation (51). We would expect therefore that the higher order representation (the linear strain triangle) should lead to a more efficient analysis.

Triangular plane strain elements with fourth order accuracy require at least a displacement field based on ten degrees of freedom (there are four third order derivatives). Such elements can be derived (see Reference 12, for example) by introduction of a node internal to the triangle and use of two midside nodes on each side. Alternatively freedoms at midside nodes can be substituted by displacement derivatives at the corner nodes. This seems to be undesirable because it involves use of normal strains $u_{,x}$ and $v_{,y}$ as freedoms. These are generally not defined on boundaries.

Three sided elements with curved boundaries can be defined in the same way as the triangular elements. Generally such elements will not be free from strain energy due to a rigid body displacement (compare the discussion of curved beam elements above). If the element is rigidly displaced in its plane a strain free configuration is possible only if the shape functions used for displacement can exactly represent the initial shape of the element boundary. In other cases an error is introduced which disappears with diminishing gridsize. The order of the error depends on the order of the power series representing the displacements. One way to avoid self-straining is referred to as isoparametric representation. In this procedure the same shape functions are employed to describe (approximately) the element boundaries as well as the inplane displacement configuration. For example, with LST elements the element boundaries can be approximated by polynomials up to the second order.

The relative efficiency of linear strain triangles versus constant strain triangles is illustrated in Figure 15. A section of an annular plate as shown in the figure is clamped at Side 1. The curved sides are free and Side 3

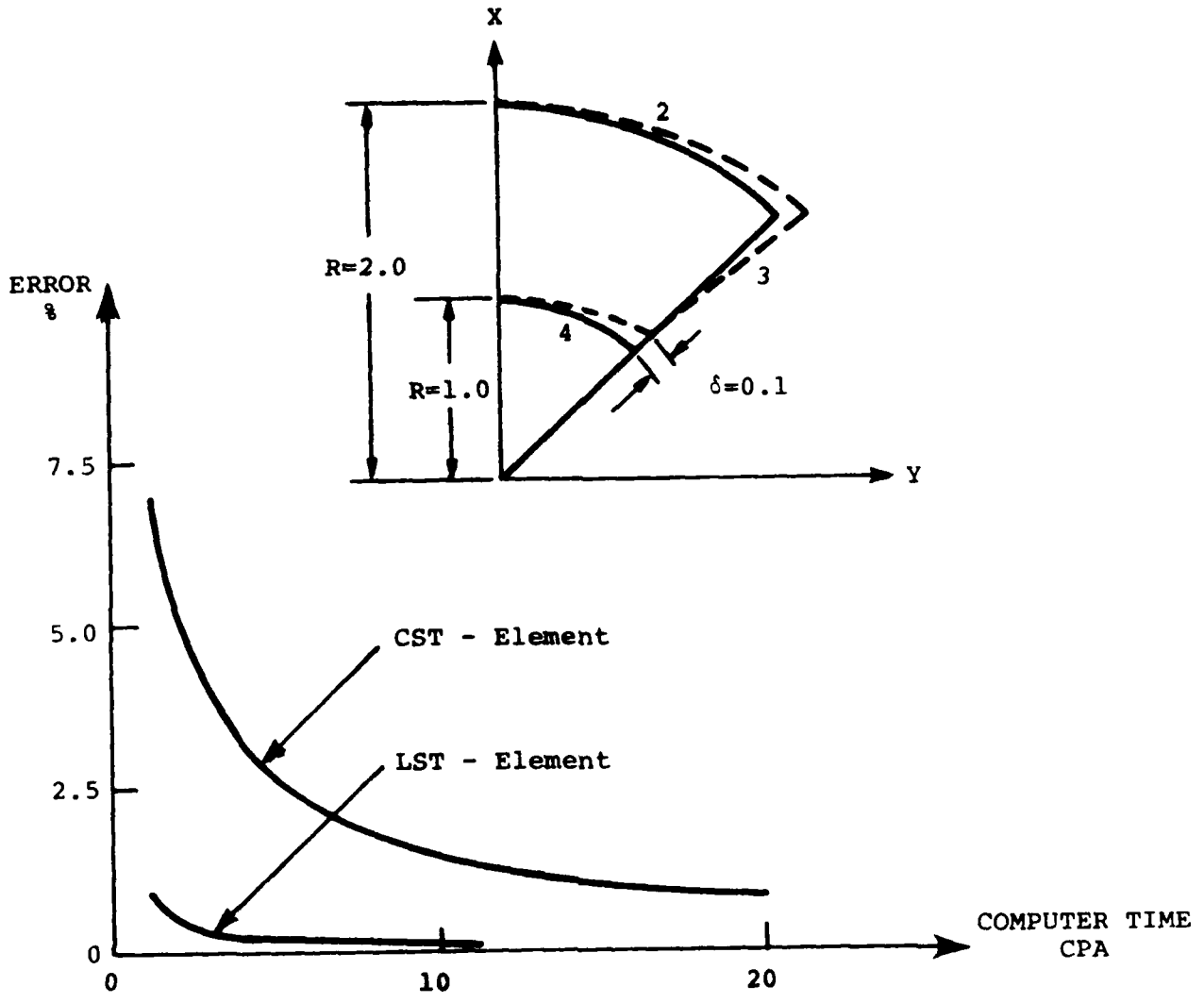

Figure 15. Deformation of Annular Plate

is subjected to a displacement of 0.1 in. and a rotation of 0.01 radians as shown. The figure shows the error in the total reaction force, normal to Side 1. It appears that for the same accuracy in the results the analysis with constant strain triangles leads to computer cost that is some twenty times higher than it is with linear strain triangles. With $E = 10^7$ psi, $\nu = 0.3$ and the plate thickness 0.1 in. and a 17 by 17 grid the total reaction is 52905 lbs. The linear strain triangle (or quadrilateral) should only be used as the membrane part of a plate element and its use should be restricted to situations in which accurate representation of the bending behavior requires a grid fine enough for analysis of the membrane behavior with constant strain elements.

Quadrilateral plane stress elements can conveniently be defined by combination of two or more triangular elements. In case of a linear analysis the freedoms corresponding to nodes that become internal to the element can then be eliminated by condensation. That is, they can be eliminated through energy minimization on the element level and do not appear as freedoms in the final trial functions.

It is, of course, also possible to derive quadrilateral elements directly in the same way as was done for triangular elements. In order that the displacements at nodes be compatible with that of adjacent elements it is necessary that the displacements at all four corners be included as degrees of freedom. Consequently, it is generally not possible to restrict the displacement pattern to one that represents constant strain. Using the Taylor series approach we must include the function itself, the two first order derivatives and at least one of the second order derivatives. To avoid directional bias we must choose the mixed derivative on the right hand side of Equation (4), i.e., the bilinear expansion. For convenience we introduce the coordinate system ξ, η with the property that ξ equals -1 and +1 respectively on two opposite sides and η similarly equals -1 and +1 on the other two sides as shown in Figure 16. The coordinates ξ and η are expressed in terms of the x and y coordinates at the element corners by

$$x = \sum_{i=1}^{4} x_i P_i \; ; \; y = \sum_{i=1}^{4} y_i P_i \tag{54}$$

where

$$P_1 = \frac{1}{4}(1 - \xi)\ (1 - \eta) \qquad P_3 = \frac{1}{4}(1 + \xi)\ (1 - \eta)$$

$$P_2 = \frac{1}{4}(1 + \xi)\ (1 - \eta) \qquad P_4 = \frac{1}{4}(1 - \xi)\ (1 - \eta)$$

Similarly a displacement component can be defined by

$$u = \sum_{i=1}^{4} u_i P_i \tag{55}$$

where the u_i are the nodal values of the displacement u. In this case identical interpolating polynomials are used for displacements and coordinates (isoparametric representation). The mapping (Figure 16) from the x,y to the ξ,η space is referred to as isoparametric mapping. Two adjacent element have common displacements at the endpoints of the interface. Since either ξ or η is constant along any element boundary the displacement field is linear along boundaries and an element based on these shape functions is conforming.

In order to achieve second order accuracy in the definition of the first order derivatives anywhere inside the element we must include at least six degrees of freedom. Directional bias will result unless the number of nodes is divisible by four, a possible node at the element midpoint not counted. Consequently the higher order element should have 8 (or 9) nodes. It seems logical to add a node at the middle of each side.

The higher order representation of the displacements allows parabolic approximation of curved element boundaries without self-straining.

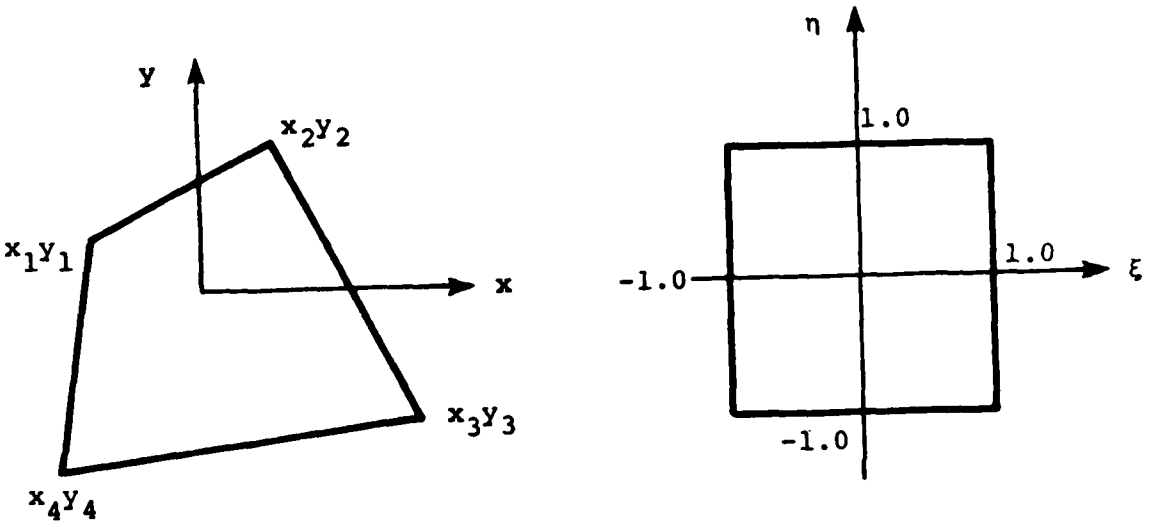

Figure 16. Isoparametric Mapping

In general, third order accuracy in the first order derivatives requires that at least ten degrees of freedom are utilized in the definition of the displacement field. However, in the one-dimensional case, the three point scheme for inplane displacements shown in Figure 8 results in an expression for the first order derivative with a third order error at the two Gaussian point. Therefore, we can expect a third order accuracy in the element with nine nodes. These linear strain quadrilateral elements are referred to as the LSQ8 and LSQ9 elements. With two inplane displacement components these elements have 16 and 18 degrees of freedoms, respectively.

Section X

PLATE AND SHELL ELEMENTS

The energy functional based on plate or shell theory contains changes of curvature of the reference surface, i.e. second order derivatives of the lateral displacements. Consequently, the trial functions as well as their first order spatial derivatives must be continuous across element boundaries in order that convergence with decreasing grid size to the correct solution will follow from the Ritz theory. Efforts to define efficient and conforming plate or shell elements has led to a great proliferation of bending element configurations.

In linear analysis of flat homogenous plates, with the midsurface as reference surface, membrane and bending behavior are uncoupled. The bending energy in the plate depends exclusively on the lateral displacement w and the membrane energy exclusively on the inplane displacements u and v. In that case it is possible to superimpose bending elements onto the membrane (plane stress) elements discussed in the preceding paragraphs. In nonlinear analysis the membrane energy, due to stretching of the middle surface, depends on the lateral displacement pattern and in analysis of curved elements the bending energy is a function of inplane as well as lateral displacements.

Bending and membrane elements then have common degrees of freedom but as long as the constitutive equations for the shell wall do not introduce membrane-bending coupling it is still possible to superimpose independent bending and membrane elements. Most problems involved in the development of finite element configurations for shell or plate analysis are independent of this coupling. Therefore, it is helpful to discuss some aspects of these configurations in the less comple framework of pure bending analysis.

Plate bending elements generally include as degrees of freedom rotations (displacement derivatives) as well as lateral displacements. In a triangular element the number of degrees of freedom, must be divisible by three, those at a possible node at the midpoint of the element not counted, as otherwise

directional bias would occur. Second order-derivatives must be determined at least to a first order accuracy. As a consequence the lowest possible number of degrees of freedom is six.

The element in Figure 17 shown in a Cartesian system x, y, z then represents the simplest possible triangular bending element. Use of a Taylor series approach leads to a uniquely determined complete quadratic representation of the lateral displacement field, that is

$$w = a + b_1 x + b_2 y + c_{11} x^2 + c_{12} xy + c_{22} y^2 \tag{56}$$

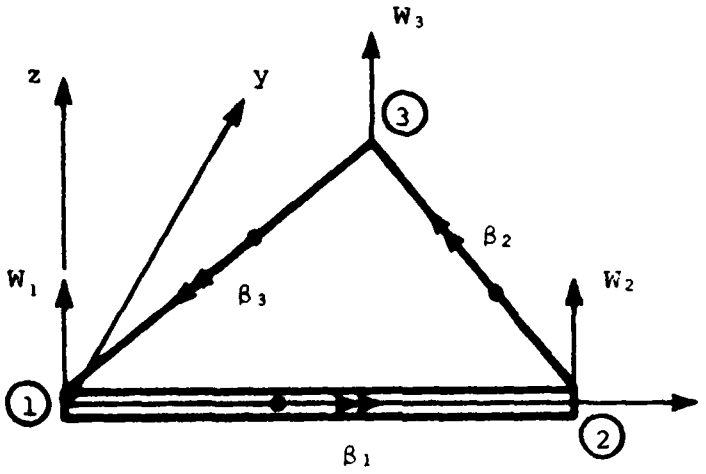

Figure 17. Constant Curvature Triangular Element

The changes of curvatures as second order spatial derivaties of w are all constant over the element surface. Along a side, between nodes 1 and 2 (y = 0) for example, the rotation around the element boundary is of the form

$$w_{,y} = b_1 + c_{12} x \tag{57}$$

That is, the slope varies linearly. However, two adjacent element have only one rotational freedom in common. Therefore, the constant bending element is nonconforming. Similar problems are encountered when triangular bending elements of higher order are developed. Elements with nine and twelve freedoms are shown in Figure 18.

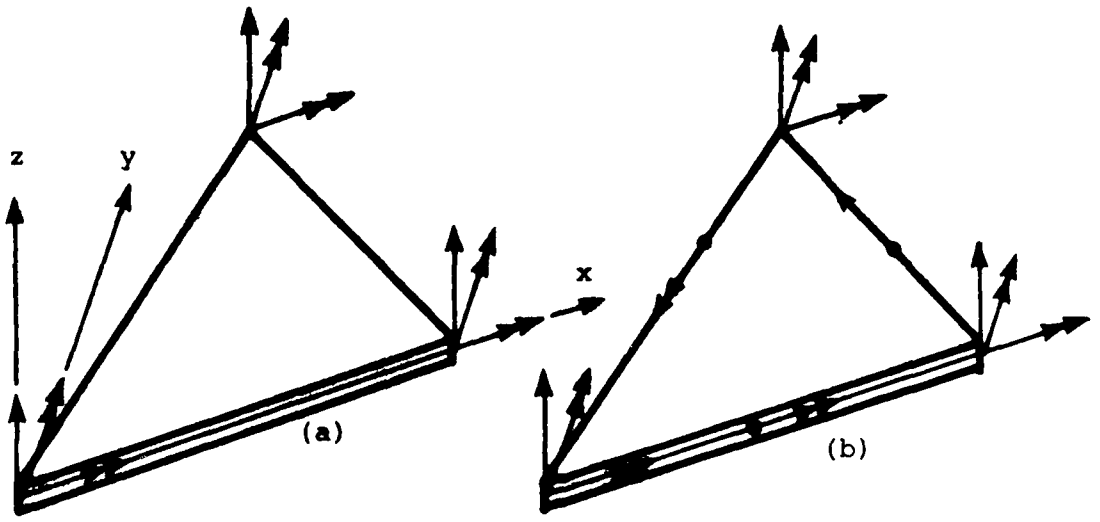

Figure 18. Triangular Elements with Nine (a) and Twelve (b) Degrees of Freedom

A complete cubic can be determined by use of ten degrees of freedom. Thus the displacement field in the nine degrees of freedom element, can be determined by use of a cubic Taylor series only after a constraint is introduced. For example, the coefficients for the x^2y or xy^2 terms may be required to be identical. In that case the expression for the rotation around the element boundary contains terms which are second order in a coordinate along the boundary. As only two rotational freedoms are common between adjacent elements rotational nonconformity is allowed.

With twelve degree of freedom element two quartic terms are included. Either of the pairs x^4, y^4 or x^3y, xy^3 can be included but in any case the edge rotation becomes cubic in terms of the spatial coordinate along the boundary. As four coefficients are required to determine uniquely a cubic and adjacent elements only have three rotational freedoms in common, the element is non-conforming.

It is possible to eliminate slope nonconformity through introduction of displacement constraints or to minimize its effect through introduction of penalty functions. The latter approach can be applied to the twelve degrees of freedom element. A fictitious term

$$\Delta U = C_1 a_{31}^2 + C_2 a_{13}^2 \tag{58}$$

is added to the energy, where a_{31} and a_{13} are the coefficients in the x^3y and xy^3 terms while C_1 and C_2 are constants chosen large enough to provide a sufficient penalty on the strain energy due to the quartic terms.

Introduction of constraints (or penalty functions) to achieve conformity lowers the order of the accuracy of the local approximation. Since the six degree of freedom bending triangle is of first order accuracy only it cannot be made conforming by introduction of constraints.

A conforming triangular bending element, introduced by Clough and Tocher in Reference 13, is based on partition into three subtriangles. This element is discussed in some detail in Reference 12. Each subtriangle has 10 degrees of freedom as shown in Figure 19 allowing a complete cubic representation. The directional bias in the subtriangles is eliminated when they are combined into one element. Since the internal subtriangle boundaries do not include midpoint rotations as freedoms it is necessary for rotational compatibility to constrain the element so that the rotation varies linearly along these boundaries. The combined element has 3 freedoms at each corner, 3 freedoms at the element midpoint and 3 midside rotational freedoms for a total of 15 freedoms. For linear analysis the freedoms at the element midpoint can be eliminated on the element level through condensation. While the introduction of contraints reduces the order of accuracy, condensation does not have any effect on the final solution.

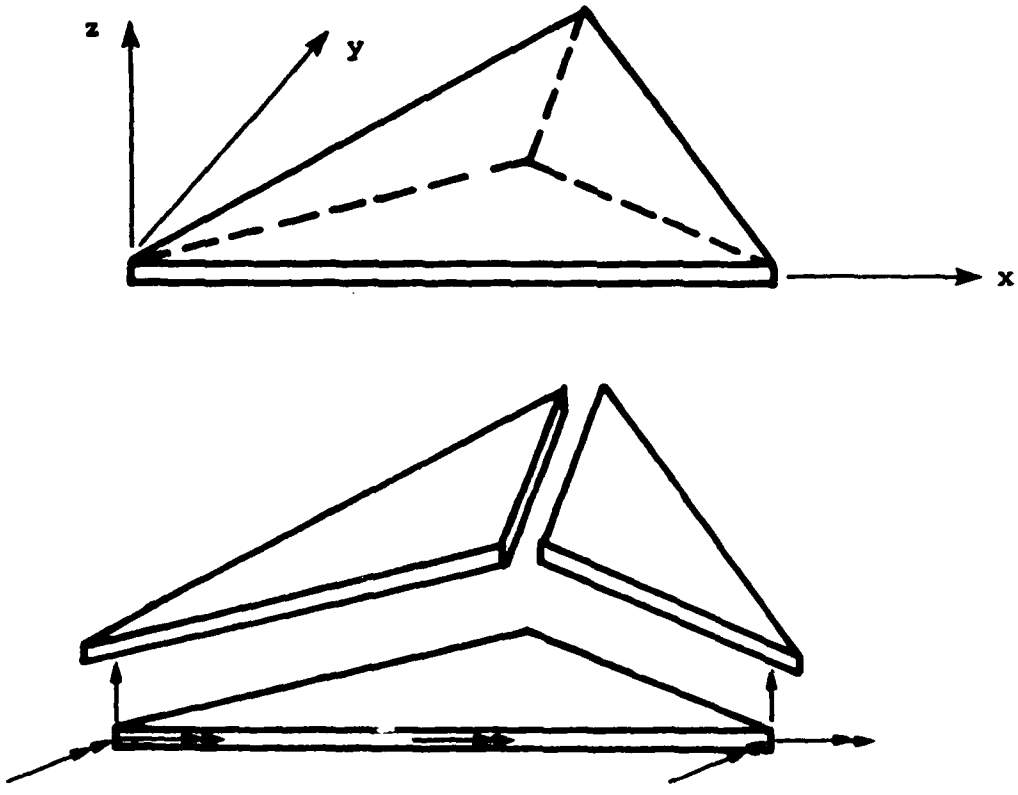

Figure 19. The Clough-Tocher Triangular Bending Element

Section XI

QUADRILATERAL BENDING ELEMENTS

The number of freedoms in a quadrilateral element must be divisible by four in order that directional bias be avoided (possible freedoms at an element midpoint node discarded). A bending element must as a minimum include all six terms up to the second order. Consequently the simplest possible quadrilateral element would have 8 degrees of freedoms. Experience with constant strain elements for plane stress analysis indicates that such an element is not likely to be very efficient.

The first element for analysis of the bending of flat plates was a rectangular element with the freedom pattern illustrated in Figure 20. As the element has 12 degrees of freedom, the displacement pattern can, as in the triangular element with the same number of freedoms be represented by a complete cubic and two quartic terms, for example, x^3y and yx^3. Such an element was introduced (Reference 14) and successfully applied in plate bending analysis before the finite element method was established as a form of the Ritz procedure. We refer to this element with the notation QB12 (quadrilateral bending, 12 freedoms). Shape functions for this element equivalent to the Taylor series solution are presented in Reference 15.

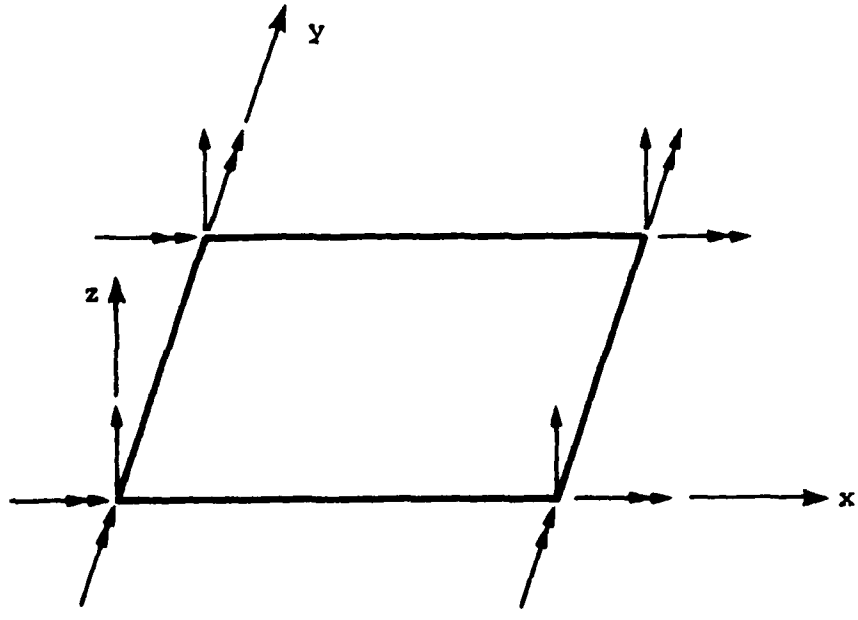

Figure 20. Rectangular Bending Element with 12 Degrees of Freedom (QB12)

After the finite element method was given a solid theoretical foundation, the wisdom in the use of nonconforming element was questioned. Efforts were made to improve the performance of the bending elements through introduction of displacement constraints. As the order of accuracy of the local approximations thus was reduced these efforts were not particularly successful. Generally the nonconforming elements led to better results within the range of engineering accuracy.

In the pursuit of more efficient conforming bending elements Clough and Felippa derived quadrilateral elements through the combination of the Clough-Tocher triangular elements. Either two or four triangles are combined to form quadrilateral elements and for linear analysis internal freedoms are eliminated through condensation. After condensation the elements have 12 degrees of freedom and we refer to them as the CF12,2 or CF12,4 elements depending on the number of subtriangles used. With three rotational freedoms along each side and only quadratic representation of the rotations(cubic in the displacements) the element is conforming. The disadvantage with the element is that the subtriangle approach makes it necessary to use a large number of integration points resulting in excessive computer time.

A conforming bending element was presented by Bogner, Fox and Schmit in Reference 16. A theory for curved shells is utilized in the derivation of the stiffness matrix. The strain energy due to rigid body displacement is exactly zero (independent of grid size) only for flat rectangular elements. Shape functions are used for interpolation to ensure conformity. The only version of the element that can be seriously considered is one BFS16 with 16 degrees of freedom in which the twist, $w_{,xy}$, has been added as a freedom at each node. While the interpolating polynomials contain terms up to the sixth order the rotation along the shell boundary is cubic.

Some results obtained with this element are presented in Reference 16. A flat plate 20 x 20 in 0.1 in. thick with clamped edges is loaded by a uniform normal pressure of 0.2 psi. The material is characterized by $E = 10^7$ psi,

$\nu = 0.3$. The results are shown in Table 6 together with corresponding results based on analysis with the CF12,2 element.

Table 6
BENDING OF SQUARE PLATE

Number of Elements (on one quarter of the plate)	Midpoint Displacement (in) CF12,2	BFS 16
2 x 2	.035592	.040475
3 x 3	.039713	.040482
4 x 4	.040274	.040487
5 x 5	.040409	
6 x 6	.040453	
10 x 10	.040485	

The convergence with the BFS16 element is exceptionally good. For example, the solution based on 16 such elements is as good as one based on 100 CF12,2 elements. Still it appears that the BSF16 element has seen little use. One reason may be that it is self-straining unless flat and rectangular. A more important disadvantage is that the twist w_{xy} is used as a degree of freedom. This displacement parameter cannot readily be defined on shell boundaries.

Section XII

HYBRID METHODS

The finite element method was originally developed as a direct extension of the methods for analysis of statically determined structures. In these methods internal forces were introduced as unknowns rather than displacements (Reference 17, for example). The derivation of equilibrium equations was based on the principle of minimum complementary energy. While the displacement method has become the dominant procedure in finite element analysis the so called force method still shows some signs of life. A plate element based on the principle was recently presented in Reference 18.

The difficulties encountered in satisfying continuity conditions at boundaries between adjacent elements for shell or plate bending elements has motivated the pursuit of other avenues, such as the development of mixed or hybrid methods in which both displacement and force fields are assumed. The hybrid method developed by Pian and Tong (Reference 19) represents an important contribution in finite element technology. In this method the displacement freedoms are not directly used for definition of the displacements inside the element. A stress field with undetermined coefficients is assumed in addition to the nodal displacements on the element boundary. The unknown coefficients in the stress field are determined through energy minimization on the element level with the nodal displacements defining the boundary conditions. The element stiffness matrix so obtained is based on the nodal displacement freedoms.

As the principle of complementary strain energy is to be applied the strain energy is written in terms of stresses, i.e.,

$$U = \frac{1}{2} \int_v \{\sigma\}^T [N] \{\sigma\} \, dv \tag{59}$$

where [N] is the matrix of compliance. That is the inverse of the stiffness matrix.

$$\{\sigma\} = [C] \{\epsilon\} , \quad N = [C]^{-1} \tag{60}$$

The stress vector is defined in terms or a number of undetermined coefficients $\{\beta\}$ (stress freedoms)

$$\{\sigma\} = [P]\ \{\beta\} \tag{61}$$

where the elements of the matrix [P] are functions (polynomials) of the spatial coordinates similar to the displacement shape functions discussed above. The strain energy in terms of stresses then can be written in the form

$$U = \frac{1}{2}\ \{\beta\}^T\ [H]\ \{\beta\} \tag{62}$$

where

$$H = \int_V [P]^T\ [N]\ [P]\ dV \tag{63}$$

The displacements along element boundaries are expressed in terms of the nodal displacement freedoms. Forces along the boundaries are obtained by substitution of the appropriate values of the spatial coordinates in the expression for the stress field,Equation (61). After integration along element boundaries the work done by these boundary forces is readily obtained

$$\Omega = \{\beta\}^T\ [T]\ \{q\} \tag{64}$$

where $T\{q\}$ represents an interpolation of the displacements along element boundaries in terms of the vector of nodal freedoms $\{q\}$.

Minimization of the complementary energy

$$V = U - \Omega \tag{65}$$

leads to

$$\{\beta\} = [H]^{-1} [T] \{q\} \tag{66}$$

and the total strain energy can be written as

$$U = \frac{1}{2} \{q\}^T [K] \{q\} \tag{67}$$

where

$$K = [T]^T [H]^{-1} [T] \tag{68}$$

is the element stiffness matrix corresponding to the displacement freedoms q.

While the use of forces as freedoms leads to an underestimate of the strain energy, the displacement method, provided the rules of the Ritz theory are followed, overestimates the strain energy. The hybrid method as presented above gives results that are bracketed by those obtained from force and displacement methods. Consequently, the convergence in many cases is very good. A rectangular bending element of this type was presented in Reference 19. This element has 12 displacement freedoms and up to 23 coefficients in the stress field. A general quadrilateral version of the element is used in the SPAR computer program (Reference 20). We refer to this element by the notation QH12 (quadrilateral hybrid, 12 freedoms).

Section XIII

USE OF NONCONFORMING ELEMENTS

After the finite element analysis was given a firm theoretical foundation as a form of the Ritz procedure, the question of possible convergence of nonconforming elements has been a subject of considerable interest (References 6 and 21, for example). The process of integration of the energy over the individual elements followed by a summation over all elements leaves out possible work done by forces on the element boundaries. For conforming elements this work vanishes because contributions from adjacent elements cancel one another. If the elements are nonconforming the work corresponding to the forces on the boundary and the discontinuity in displacement (or rotation) is left out of the energy balance. The procedure can converge to the correct solution only if this work vanishes with diminishing grid size.

In Reference 22 Irons and his coworkers suggested a simple test to be applied to nonconforming elements. This test has later become known as the patch test and it appears that the passing of this test is a sufficient but not always necessary convergence requirement. As first presented the patch test required that for any patch of elements subjected to displacements corresponding to constant strain (constant curvature for bending elements) on its boundary, the solution everywhere in the interior should be accurate, i.e., the strain is constant throughout the patch.

In Reference 6 Strang and Fix show that the patch test is equivalent to the requirement that the work corresponding to displacement discontinuities along element boundaries vanishes. A rectangular element developed by Wilson (Reference 23) is used for demonstration. Wilson raises the order of the bilinear plane stress elements (Figure 16) by addition of the two so called bubble modes

$$P_5 = (1 - \xi^2) \quad \text{and} \quad P_6 = (1 - \eta^2) \tag{69}$$

These are clearly nonconforming modes, independent on the nodal displacement components. The formulation was suggested for rectangular elements only and for such elements it is shown in Reference 6 that the addition of the nonconforming bubble modes results in a considerable improvement in the convergence rate.

It is shown in Reference 6 that "the energy of the discontinuity" vanishes identically when the integration is carried over the entire boundary. For a general quadrilateral element on the other hand, the integral over the boundary can be represented as a constant times the difference in the lengths of opposite sides.

Consequently, the contribution to the energy from one element is proportional to the grid spacing. However, the total length of all element boundaries is proportional to $1/h^2$. Therefore, it does not seem likely in any given case that analysis based on nonrectangular elements with bubble modes will converge to the correct solution. A modification of this approach presented in Reference 24 makes it possible to use the bubble modes also with nonrectangular elements.

A relatively simple and often used nonconforming bending element is the quadrilateral 12 degree of freedom element QB12 (see Figure 20). For this element the lateral displacement component can be expressed in the form

$$\begin{aligned} w = {} & C_o + C_1x + C_2y + C_3x^2 + C_4xy + C_5y^2 \\ & + C_6x^3 + C_7x^2y + C_8xy^2 + C_9y^3 \\ & + C_{10}x^3y + C_{11}xy^3 \end{aligned} \tag{70}$$

The element edge rotation is represented by the normal derivative, that is, if the side makes an angle α with the y-axis

$$\partial w/\partial n = \partial w/\partial x \cos \alpha + \partial w/\partial y \sin \alpha \tag{71}$$

Two adjacent elements have matching slopes at the end points of the common boundary. Consequently terms of lower than second order in the coordinate along the boundary do not cause any slope discontinuity. The mismatch in

slope between adjacent elements is of the form

$$\Delta\frac{\partial w}{\partial n} = C\xi^2 + \text{higher order terms} \tag{72}$$

To obtain the energy of the discontinuity we multiply the slope discontinuity by the average bending moment M_o (higher order terms are irrelevant) and integrate the product over the length h of the interface. The result is of the form $CM_o h^3$. As the total length of element boundaries is proportional to $1/h^2$, the total energy of the discontinuity is proportional to the grid spacing. We expect therefore that the use of the QB12 element will lead to convergence of first order, i.e., $E = O(h)$.

If the element is rectangular it passes the patch test as posed in Reference 6. Consequently, any displacement pattern with constant curvature is exactly represented, independently of grid size, i.e., the accuracy is at least of second order. The general quadrilateral element passes a milder form of the test, requiring that the error in energy introduced by the nonconforming modes is proportional to some power $n>0$ of the gridsize.

The performance of the QB12 element is illustrated here in a few examples. A simply supported square plate 5 x 5 in. and 0.1 in. thick is made of a material with $E = 10^7$ psi and $\nu = 0.3$. The plate is subjected to unidirectional compression. In that case (see Reference 25 for example) the critical load is

$$N_{CR} = 4\,\frac{\pi^2 Eh^3}{12(1-\nu^2)b^2} = 1446.0958 \text{ lb/in.} \tag{73}$$

The buckling mode may be assumed symmetric about two planes. Hence, in the finite element analysis it is sufficient to consider a quarter model of the plate. Some results are shown in Table 7, where N represents the number of elements, in each direction, on this quarter model.

TABLE 7

BUCKLING OF SQUARE PLATE

No. of Elements	QB12			QH12		
N x N	Critical Load	Error E	EN^2	Critical Load	Error E	EN^4
2 x 2	1391.19	54.91	220	1451.04	4.94	79
4 x 4	1431.44	14.66	235	1446.41	.31	79
6 x 6	1439.50	6.60	238	1446.16	.06	78
8 x 8	1442.37	3.73	239			
10 x 10	1443.71	2.39	239			

Richardson's extrapolation based on the results for N = 8 and N = 10 with the assumption of second order convergence leads to N_{CR} = 1446.100, i.e., to an error of 0.00028 percent. It can be little doubt then that the use of this nonconforming element leads to a second order convergence. For a one percent error we need four elements per quarter wave. Four elements per half wave gives a barely acceptable 3.8 percent error.

Table 7 shows also results obtained with the hybrid element QH12. In this case convergence is from above and clearly a fourth order accuracy is obtained. With four elements per halfwave the error is as small as 0.34 percent. For the same grid the runtime with the QS12 element is only slightly larger than with QB12.

The problem of buckling of a spherical shell under uniform external pressure was considered in a study of the convergence behavior of the nonrectangular QB12 element. In order that effects of approximations in the inplane displacement field be eliminated, such displacements were suppressed in the buckling mode. The computed buckling loads, then are physically meaningless but this does not mar the conclusions about the numerical behavior of the bending element. A spherical segment with radius 10 in., thickness 0.1 in., Young's modulus 10^7 psi and Poisson's ratio 0.3 was analyzed. Circumferentially the segment covers 9 degrees. In the direction of the meridian the segment covers the range 36 to 45 degrees measured from the apex. This segment buckles in a mode with one half wave in the meridional and one quarter wave in the circumferential direction. Therefore, it was assumed that the buckling mode was antisymmetric with respect to one of the sides along a meridian. Symmetry conditions were applied at the other three sides. Buckling loads are shown in Table 8.

TABLE 8

BUCKLING OF SPHERICAL SHELL SEGMENT

Number of Elements N x M	Critical Load	Error %
4 x 2	9034.1	12.82
6 x 3	9704.4	6.35
8 x 4	9965.9	3.83
10 x 5	10091.9	2.61
12 x 6	10161.7	1.94
16 x 8	10232.1	1.26
20 x 10	10265.0	0.95
24 x 12	10283.3	0.77
28 x 14	10295.0	0.65
32 x 16	10303.5	0.57

It appears that the convergence is of first order and for grids as fine as 24 x 12 or better the first order term dominates the error. In that case the buckling load would be 10362.6 psi. The errors given in the table are based on this value. The convergence in this case is much worse than it is with rectangular elements. Eight elements per halfwave correspond to an error of 3.8%, and for a one percent accuracy we need 20 elements per half wave.

The results from two linear plate bending analyses are shown in Figure 21. In one case a quadratic plate with clamped edges is subjected to uniform lateral pressure. The error in the midpoint displacement is shown as a function of the number of elements along each side on a quarter model of the plate. Despite the nonconformity the displacement is underestimated.

The other case is one with nonrectangular elements. The annular plate is clamped at one of the straight edges and the other three edges are free. The plate is subjected to a uniform pressure. The error in lateral displacement at point A is shown in the figure. As a result of rotational nonconformity, convergence is now from the opposite direction, i.e., the displacements are overestimated. However, the convergence is still relatively good

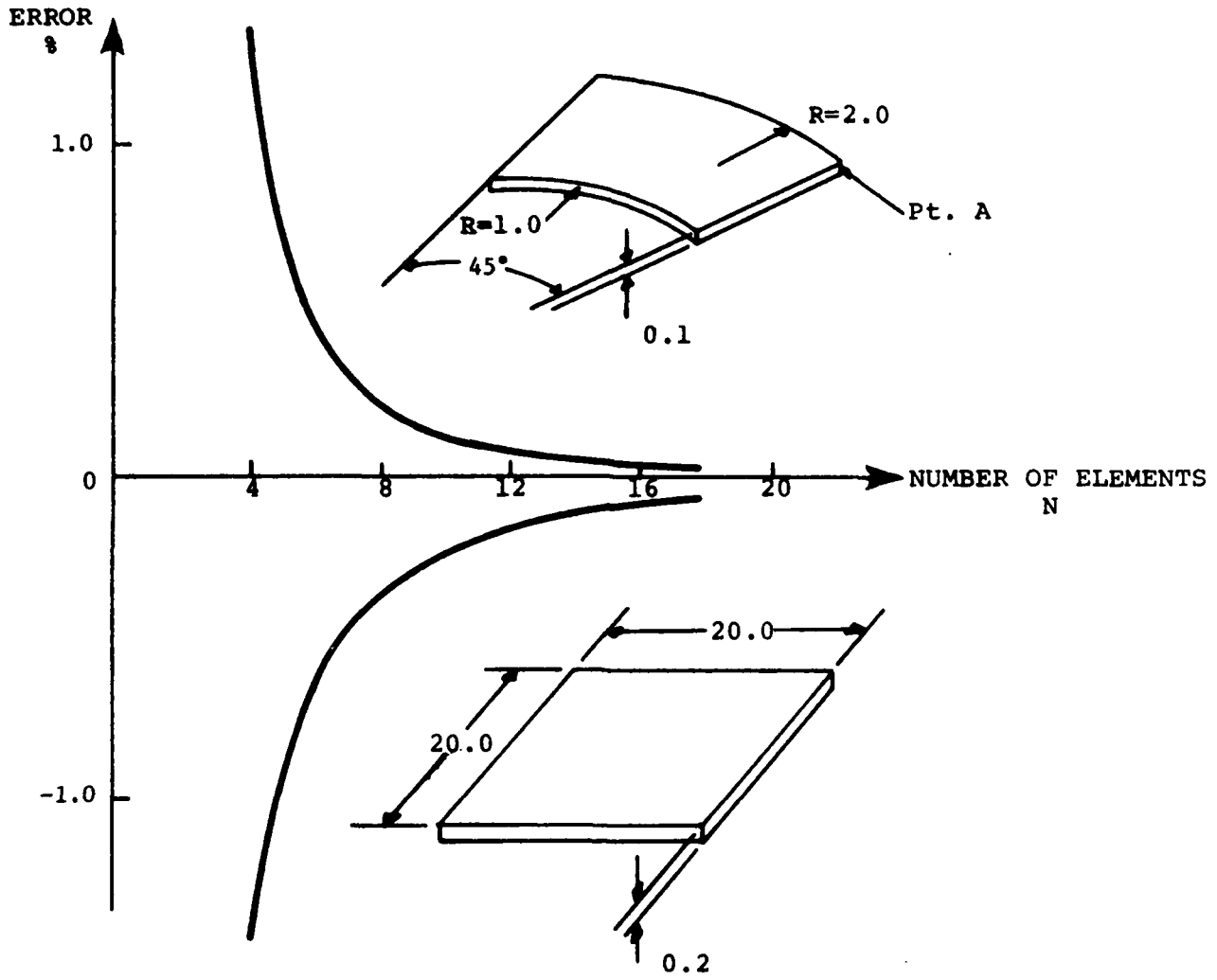

Figure 21. Error Versus Gridsize in Plate Ending with QB12 Elements

presumably because inaccuracies due to the nonconformity and approximation of the deformation mode tend to cancel one another.

For some reason, presently unexplained, the bending analysis of the annular plate leads to an illconditioned equation system. With grids 13 x 13 or finer it was necessary to apply a linear refinement procedure in order to obtain accurate results (on CDC 175). This problem did not occur in the buckling analysis of the spherical shell segment. However, with slow convergence for the spherical shell and conditioning problems in the annular plate analysis it seems advisable to avoid use of QB12 elements that deviate substantially from a rectangular plan form. The rectangular version of the element may often be unsuitable for buckling analysis because the critical load converges from below. This restricts the possibilities to increase the grid spacing in areas with light loading.

Section XIV

AHMAD-TYPE ELEMENTS

Three-dimensional elements can easily be derived by direct extension of the isoparametric representation for the plane stress case discussed above (see Figure 15). Second order derivatives (curvature changes) do not appear in the functional, and therefore it is sufficient for convergence that the displacement components themselves are conforming. There is no requirement of interelement compatibility of displacement derivatives (rotations). In view of the difficulties encountered in the derivation of elements based on the theory of plates and shells, it appears worthwhile to try to represent the shell by a single layer of such brick elements (Figure 22).

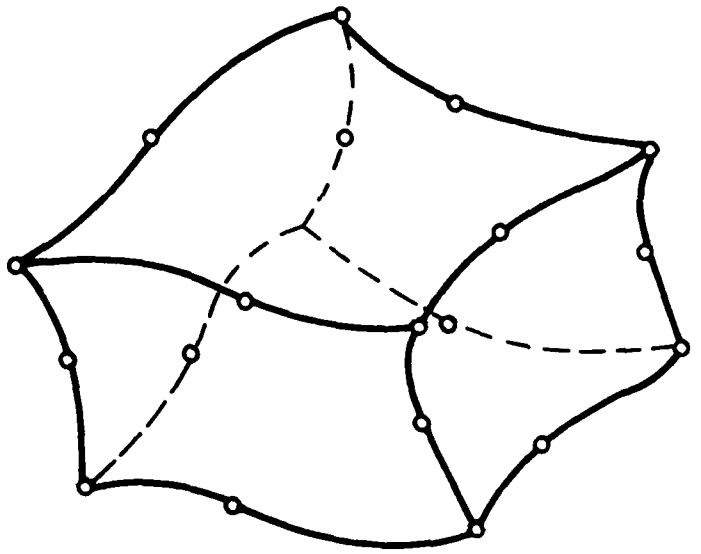

Figure 22. Isoparametric Brick Element with 20 Nodes

Primarily due to the problem with illconditioned matrices this approach did at first not meet with much success. The thinner the shell, the less suitable are the brick elements. This problem was circumvented in a publication by

Ahmad, Zienkiewicz, and Irons (Reference 26) by introduction of the basic assumptions of the shell theory into the formulation of the brick element. First it is assumed that the energy due to stresses in the direction of the shell normal can be disregarded. The assumption that normals to the shell remain straight is also invoked. As a consequence it is possible to express the displacement components at nodes on the shell surface in terms of displacements and rotation components at the shell reference surface by use of simple transformation matrices. The set of freedoms referred to in the interface with a program user is shown in Figure 23a and the equivalent set of basic freedoms on which the energy expression is based is shown in Figure 23b.

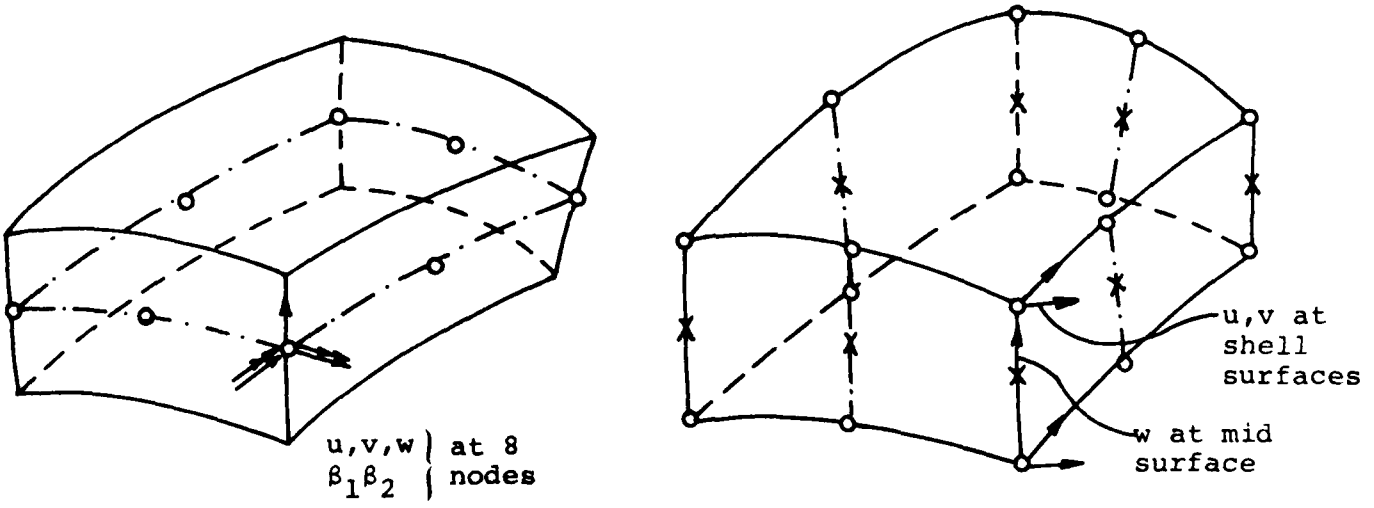

a) "User Freedoms" b) Basic Freedoms

Figure 23. Freedom Patterns in an Ahmad Type Element

The user freedoms are three displacements and two rotations at each of eight reference surface nodes for a total of 40 freedoms. The basic freedom pattern contains two freedoms at each of 16 shell surface nodes and one freedom at each of 8 midsurface nodes, again for a total of 40 freedoms.

In a first order shell theory it is assumed that normals remain straight and normal to the reference surface in the deformed configuration. This means that the theory neglects deformattions due to transverse shear stresses. A second order theory approximately includes transverse shear effects as the normal is assumed to remain straight but is allowed to rotate with respect to the shell reference surface. The shell assumptions introduced in the Ahmad element correspond to those of a second order theory.

A first order shell theory also contains the assumption that the ratio of thickness to shell radius is small so that it can be neglected in comparison to one. This assumption is not introduced in an Ahmad type element. A more accurate description of the shell bending deformation is therefore obtained and together with the inclusion of transverse shear deformation this extends the applicability of an analysis with Ahmad type elements to the range of "moderately thick" shells.

The inclusion of transverse shear deformation introduces a special problem. The description of the deformation pattern must be general enough to inhibit the development of excessive transverse shear strain. The presence of such strains leads to unsatisfactory convergence properties with the early Ahmad type elements. In Reference 27 Pawsey circumvents this problem through introduction of reduced integration. Following Reference 27 we illustrate the problem in the one dimensional case. We consider the case in which the bending moment varies linearly and vanishes at the midpoint of the beam element as illustrated in Figure 24a.

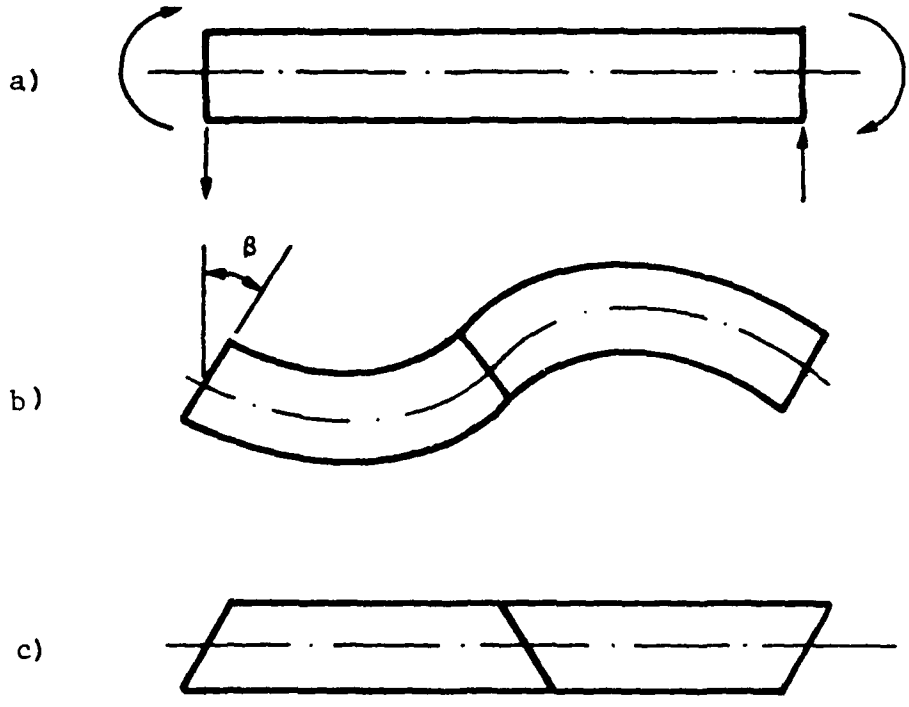

Figure 24. Ahmad Type Beam Element with Linearly Varying Bending Moment

The correct solution with the rotations $+\beta$, $-\beta$, $+\beta$ at the three nodes is shown in Figure 24b. Since the shape functions are not sufficiently general to allow this deformation pattern, the solution represented in Figure 24c is instead obtained. In this deformation pattern the transverse shear contributes a very large part to the strain energy. However, Pawsey shows that the correct value of the shear strain is obtained at the Gaussian points with two-point integration. A similar problem is encountered for curved beam elements subjected to a constant bending moment. For this case Pawsey shows that a spurious normal membrane strain develops, but also that this strain vanishes at the two Gaussian points.

It was established thus in Reference 27 that for the Ahmad type element, convergence with gridsize is considerably better if we use a reduced integration scheme. For the plate bending element this would mean that eight (two sets of four points) integration points are used rather than the eighteen points that would be required for accurate integration of the linear part of the strain energy. As noted above the use of reduced integration can

allow the development of strain-free deformation modes (mechanisms). For the 8-noded Ahmad-Pawsey element these are:

1) A membrane deformation mode with

$$u = \left(\eta^2 - \frac{1}{3}\right) \xi$$
$$v = \left(\frac{1}{3} - \xi^2\right) \eta \tag{74}$$

2) A bending mode with

$$w = \frac{1}{2} (1 - \xi^2) (1 - \eta^2) - \frac{1}{3} (\xi^2 + \eta^2) \tag{75}$$

Here ξ and η are nondimensional space coordinates chosen such that they vanish at the midpoint of the element and equal plus or minus unity on element boundaries. It was shown by Taylor (see Reference 6, p. 189) that the bending mode is not "contagious", i.e. it occurs only for a single element. With more than one element the global stiffness matrix is not singular for any boundary conditions suppressing the membrane mode.

Section XV

FLAT ELEMENTS FOR CURVED SHELL ANALYSIS

Curved shell elements require large amounts of computer time for formulation of the stiffness matrix. Also the use of curved elements introduces the problem with self straining. Therefore, curves shells have most frequently been analyzed by use of flat elements. This results in a conformity problem that seems to be particularly important in nonlinear or stability analysis. Figure 25 shows two flat elements representing a portion of cylindrical surface. Rotational compatibility at the nodes is enforced after the components of rotation are referred to the same set of coordinates, implying that

$$\begin{aligned} \left(\beta_y^{(1)} - \beta_y^{(2)}\right) \cos(\alpha/2) - \left(\beta_z^{(1)} + \beta_z^{(2)}\right) \sin(\alpha/2) = 0 \\ \left(\beta_z^{(1)} - \beta_z^{(2)}\right) \cos(\alpha/2) + \left(\beta_y^{(1)} + \beta_y^{(2)}\right) \sin(\alpha/2) = 0 \end{aligned} \tag{76}$$

where the superscripts (1) and (2) refer to the element number.

When adjacent flat elements meet at an angle, it is necessary to introduce the normal rotation as a freedom of the system. A disadvantage with this is that the normal rotation does not appear in the strain energy expression. As a consequence the resulting linear equation system becomes increasingly ill-conditioned as the angle between the planes of adjacent elements becomes smaller. Generally, finite element computer codes define a small limit α_o and if $\alpha<\alpha_o$, the rotation β_z is ignored and as an approximation the conformity constraint becomes $\beta_y^{(1)} = \beta_y^{(2)}$.

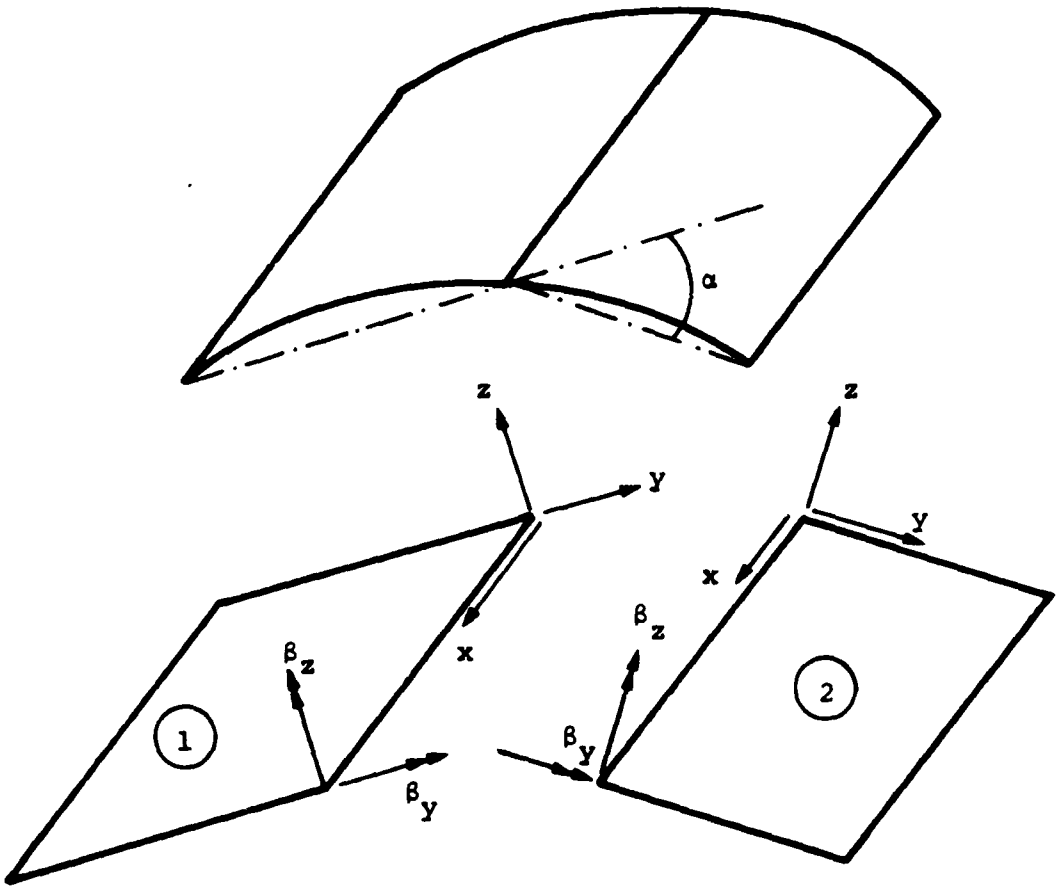

Figure 25. Flat Element for Curved Shell Analysis

A more serious problem caused by the use of flat element for curved surfaces is related to interelement displacement nonconformity. The strain energy expression includes derivatives of the inplane displacements u, v of first order only while the bending strains include second order derivatives of the transverse displacement. Therefore, w is usually represented by polynomials of higher order than those representing u and v . Typically w is cubic and u and v are either linear or quadratic within the element.

For two adjacent flat elements at an angle with one another, complete displacement compatibility requires that along the entire boundary

$$\begin{aligned}\left(v^{(1)} - v^{(2)}\right) \cos(\alpha/2) - \left(w^{(1)} + w^{(2)}\right) \sin(\alpha/2) = 0 \\ \left(w^{(1)} - w^{(2)}\right) \cos(\alpha/2) + \left(v^{(1)} + v^{(2)}\right) \sin(\alpha/2) = 0\end{aligned} \tag{77}$$

Clearly, these conditions cannot be satisfied unless v and w along the interface are represented by polynomials of the same order. Failure to enforce this compatibility allows the individual elements to buckle under axial compression as plates with free edges. Displacement conformity can be restored by introduction of constraints on w. However, this results in a very stiff element and the buckling load shows rather slow convergence from above with decreasing grid size.

On the other hand displacement conformity can be restored by raising the order of the polynomials representing inplane deformation. With a cubic representing w it is necessary that third order polynomials are used to represent u in terms of the y-coordinate and v in terms of the x-coordinate. This can be achieved through inclusion of normal rotation components as supporting freedoms for the inplane displacement field. This approach was used in the development at Lockheed Missiles & Space Company, Inc of a flat element for thin shell analysis. The out of plane deformations (bending element) were defined in the same way as in the QB12 element discussed above. That is, rotational nonconformity is permitted. The accuracy is of second order for rectangular and first order for general quadrilateral elements.

Inplane displacements were defined through an extension of the bilinear plane stress element. The derivatives $u_{,x}$ and $v_{,y}$ represent normal strains and inclusion of these as degrees of freedom would lead to difficulties in the specification of boundary conditions. On the other hand, the derivatives $-v_{,x}$ and $u_{,y}$ represent rotations around the normal of short line segments in the x and y directions, respectively. Unless the shear strain is zero these two rotation components are distinct and independent of one another.

The shear strain is equal to the difference between these rotation components, i.e., $u_{,y} + v_{,x}$. If the shear strain is allowed to be discontinous at the node there can be more than two distinct normal rotation components. Inclusion of those does not seem to be practical as it leads to great complexities in the formulation. After introduction of the normal rotations as freedoms, an inplane displacement field is obtained in which displacements normal to the element boundaries are cubic in the coordinate along the boundary. The detailed derivation of the stiffness matrix for the element is given in the Appendix.

The use of the normal rotations as support freedoms for the inplane displacement field raises the order of the polynomial expressions for these displacements in one of the coordinates only. As the constant strain elements are known to have poor convergence properties, the orders of u in the x-direction and v in the y-direction were raised by addition of tangential displacement freedoms at midside nodes. The element is referred to here as SH411. Its freedom pattern is illustrated in Figure 26.

A somewhat simpler version of this element SH410 excludes the midside nodes and uses only an average normal rotation component at the corner nodes. This means that u is linear in the x-direction and v is linear in the y-direction, and also that the shear strain is suppressed at the nodes. This limits the usefulness of the element to special cases. The SH411 element has nine and the SH410 has five integration points. However, it is also possible to use reduced integration with four points in each of these elements.

The membrane part of these elements has also been combined with the hybrid bending element. We refer to these elements as SH416 with the more refined inplane displacement field and SH415 with the lower approximation.

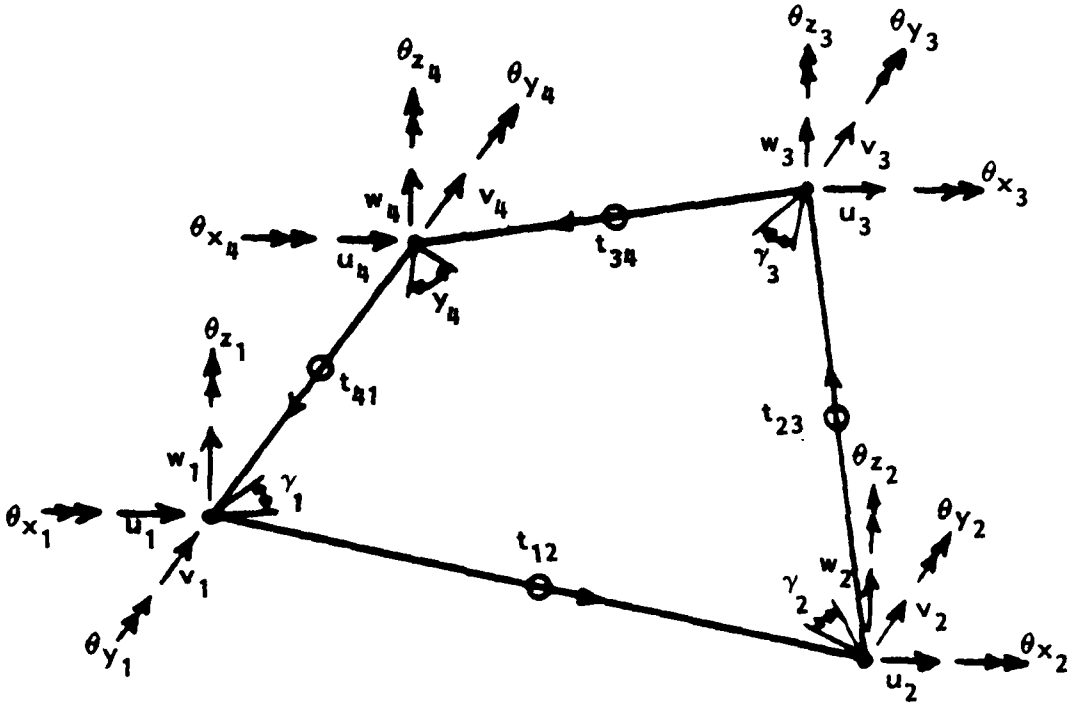

Figure 26. Freedom Pattern in SH411

The problem with displacement nonconformity is illustrated here by use of a study of the convergence with gridsize of the buckling loads for flat and cylindrical panels subjected to axial compression or shear. Results were obtained with the elements SH410 and SH411 and also with flat elements developed through combination of the bending element CF12, discussed above, with quadrilateral membrane elements obtained through combination of LST or CST triangles. We refer to these elements as SH420 (with constant strain triangles) and SH422. For flat panels the buckling mode does not include inplane displacements. Therefore, the results with SH411 and SH422 would be practically the same as those obtained with SH410 and SH420 respectively, and the elements with higher order representation of inplane displacements are not included in this comparison.

Results of an analysis of buckling of a flat plate under axial compression are shown in Table 9.

TABLE 9

BUCKLING OF FLAT PLATE IN COMPRESSION

Grid	Critical Load (lbs/in) with SH410	SH420	SH440
3 x 3	1391.1934 (2.0)	1454.2594 (2.8)	
5 x 5	1431.4386 (4.2)	1446.7181 (7.6)	1449.8566 (8.1)
7 x 7	1439.5026 (8.4)	1446.2242 (16.6)	1442.9518 (14.8)
9 x 9	1442.3723 (20.1)	1446.1372 (29.8)	1442.5526 (25.5)
11 x 11	1443.7136 (32.3)	-	1442.4792 (40.4)
13 x 13	—	-	1442.4565 (58.7)
15 x 15	1444.9247 (69.9)	-	-
19 x 19	1446.5234 (130.3)	-	-
∞	1446.10	-	1442.42

The AHMAD-type element is referred to here as SH440. In the definition of a grid the mid side nodes in that element have been included, i.e., a 3 x 3 grid corresponds to only one SH440 element. The run times (CPH on the CDC175 NOS, BE system) are given in parenthesis after the corresponding buckling load.

The plate dimensions and material properties are the same as those leading to Equation (74), i.e., the critical load is 1446.10 lbs/in. With the SH440 the critical load is somewhat lower since transverse shear deformation is included. Extrapolation from the results in Table 9 indicates that the critical load would be 1442.42. To obtain an accuracy in the buckling load of 0.5 percent the following run times are required

with	SH410	8.4	sec
	SH420	2.8	sec
	SH440	8.1	sec
	SH415	2.0	sec

If a higher accuracy were required analysis with the SH410 element would be considerably more expensive.

Table 10 shows results from buckling analysis of a simply supported flat plate in shear. The plate dimensions are 5 x 5 inches and the thickness 0.1 in. and the material properties are $E = 10^7$ psi, $\nu = 0.3$. The reason that run times are smaller in this case in comparison to those with the same grid in the axial compression case is that the convergence in the eigenvalue analysis is much faster. The results with SH415 indicate fourth order accuracy and extrapolation from these values we determine the critical loads 3371.3 lbs/in. without and 3339 lbs/in. with transverse shear effect (SH440). The figures in the table then show that for 0.5 percent accuracy the required computer time is:

with	SH410	33	sec
	SH420	27	sec
	SH440	100	sec
	SH415	9	sec

If the accuracy requirement is reduced to 2 percent the corresponding times are:

with	SH410	11	sec
	SH420	15	sec
	SH440	40	sec
	SH415	6	sec

TABLE 10

BUCKLING OF FLAT PLATE IN SHEAR

Grid	Critical Load (lbs/in) with SH410	SH420	SH440	SH415
5 x 5	3182.59 (3.6)	3650.60 (7.5)	53063.0 (7.3)	3544.61 (3.9)
7 x 7	3255.39 (6.5)	3423.80 (15.5)	—	3406.72 (7.1)
9 x 9	3301.26 (10.9)	3389.11 (27.5)	4093.58 (19.6)	3382.54 (11.8)
11 x 11	3325.28 (16.6)	3379.00 (44.1)	—	-
13 x 13	3338.92 (24.1)	—	3403.48 (40.2)	-
15 x 15	3347.31 (32.9)	3373.30 (80.9)	3365.06 (82.0)	-
17 x 17	—		3352.20 (100.1)	-
19 x 19	3356.61 (52.7)		3347.25 (170.1)	-

TABLE 11

BUCKLING OF CYLINDRICAL SHELL SEGMENT IN COMPRESSION

Grid	Critical Load lbs/in with SH410	SH411	SH420	SH422	SH440
3 x 5	2502.49 (1.4)	2564.50 (2.4)	2488.89 (3.2)	2846.59 (3.5)	3606.27 (4.2)
4 x 7	2503.78 (4.0)	2525.03 (6.0)	2568.35 (9.1)	2112.98 (10.1)	–
5 x 9	2505.31 (8.1)	2513.63 (13.5)	2538.54 (14.4)	2262.53 (22.4)	2513.58 (13.7)
6 x 11	2506.22 (12.6)	2508.74 (27.5)	2524.83 (23.2)	2345.80 (40.1)	–
7 x 13	–	–	–	–	2501.18 (34.1)
8 x 15	2507.12 (26.2)	2504.67 (47.1)	2513.01 (48.7)	2426.81 (91.4)	–
9 x 17	–	–	–	–	2500.45 (61.5)
11 x 21	2507.75 (71.5)	2502.30 (103.3)	–	–	–
16 x 31	2508.23 (120.1)	2501.66 (227.0)	–	–	2500.18 (100.5)

Results for a cylindrical shell segment under axial compression are shown in Table 11. The segment represents a complete cylinder, simply supported at the edges, with a length of 11.0 in. and a radius of 36 in. The thickness is 0.125 in., Youngs modulus 10^7 psi, and Poisson's ratio 0.3. It is assumed that symmetry conditions prevail at midlength and that the cylinder buckles in 15 circumferential waves. Consequently a 5.5 in. long 12 degrees wide cylindrical segment is considered with symmetry enforced on three sides. The critical load according to an analytical solution (Reference 24) is 2500.69 lbs/in. Since the element SH410 in the limit supresses inplane shear in the buckling mode the critical load converges towards a value that is somewhat too high. However, the results are surprisingly close to the analytical solution for all grid-sizes, the error in no case being above 0.3 percent.

Both for SH420 and SH410 it appears that the relatively good performance is due to a fortuitous and presumably case dependent cancellation of errors in different directions. Thus it makes little sense to include those in a comparison of run times for different elements. For 0.5 percent accuracy in the buckling load the following run times are required.

with	SH411	13 sec
	SH422	not achieved
	SH440	13 sec
	SH416	8 sec

For an accuracy of 2 percent the corresponding results are

with	SH411	3 sec
	SH421	120 sec
	SH416	5 sec

Since the elements SH420 and SH422 give good results only in flat plate analysis and in some cases may perform extremely poorly, they are not included in further considerations. However, the triangular version (the Clough-Tocher triangle) may be useful in shell configurations that cannot easily be represented by quadrilateral elements only.

In order to include effects of a nonuniform strain distribution in the prebuckling range, a case was also considered in which a cylindrical shell with axisymmetric imperfections was subjected to axial compression. The cylinders radius is 36 in. and its thickness 0.125 in. Material data are $E = 10^7$ psi and $\nu = 0_3$. The imperfection is defined by

$$W_o = 0.03125 \sin (\tfrac{3}{4} \pi x/L) \; [\cos (\pi x/L) - 1] \tag{78}$$

Results from analysis with the SH410 and SH411 elements are compared to results with finite differences (STAGSC) in Table 12. The results are not quite accurate since the analysis does not include nonlinearities in the prebuckling range. However, the trend is quite clear. The critical load appears to be about 1255 lbs/in. and with the 5 x 5 grid and SH411 elements a 2 percent accuracy is obtained. Similar accuracy with the other two discretization procedures would require a very fine grid spacing. In comparison to SH410 the SH411 element yields the same accuracy in the final results with about one fifth of the run time. For a fixed grid size the STAGSC program requires much less computer time but still, the run time is SH411 is smaller almost by an order of magnitude.

TABLE 12

BUCKLING OF IMPERFECT CYLINDRICAL SHELL

Grid	Critical Load (lbs/in) with SH410	SH411	Finite Differences
3 x 3	–	1651	–
4 x 4	1931	1299	–
5 x 5	1578	1280	1865
7 x 7	1405	–	1538
8 x 8	1375	–	–
13 x 13	1316	–	1346

Section XVI

INEXTENSIONAL DEFORMATION

Thin shells bend easily but resist stretching. Therefore, deformation modes tend to be inextensional. For a straight beam element the neutral surface strain is

$$\varepsilon_x = u_{,x} + \frac{1}{2}\,(u_{,x}^2 + w_{,x}^2) \tag{79}$$

Unless the rotation of the element is very large, $u_{,x}^2 << w_{,x}^2$. Inextensional deformation then implies that $u_{,x}$ is approximately equal to $-\,1/2\; w_{,x}^2$. With a third order polynomial representing w, $w_{,x}^2$ is of fourth order. In that case the relation $u_{,x} = -1/2\; w_{,x}^2$ can hold everywhere within the element only if u is represented by a polynomial of the fifth order. This problem was first recognized by Haftka et al. in Reference 28. However, accurate integration of the nonlinear terms would require use of 25 integration points on a quadrilateral plate element. This leads to excessive computer time and, since reduced integration with respect to the nonlinear terms does not introduce mechanisms in the system, cubic plate bending elements are usually based on a nine point integration scheme. With a nine point integration scheme it is possible to make the midsurface strain vanish at all integration points if the inplane displacements are represented by cubic shape functions.

The simple case of a cantilever beam subjected to a point load, as shown in Figure 27 can be used for demonstration of the problem. The results shown below are obtained by use of a model with two finite elements. The lateral displacements are represented by a cubic and a three point Gaussian scheme is used for integration. Linear, quadratic or cubic polynomials are used for axial displacements. Within the limitations of the theory (a Lagrangian formulation and the curvature defined as $w_{,xx}$) the case with cubic u gives exact results. The case of linear u gives poor results even at rather moderate values of the rotation at the end point. A two to three degree rotation appears to define the range of applicability of results obtained with such an element.

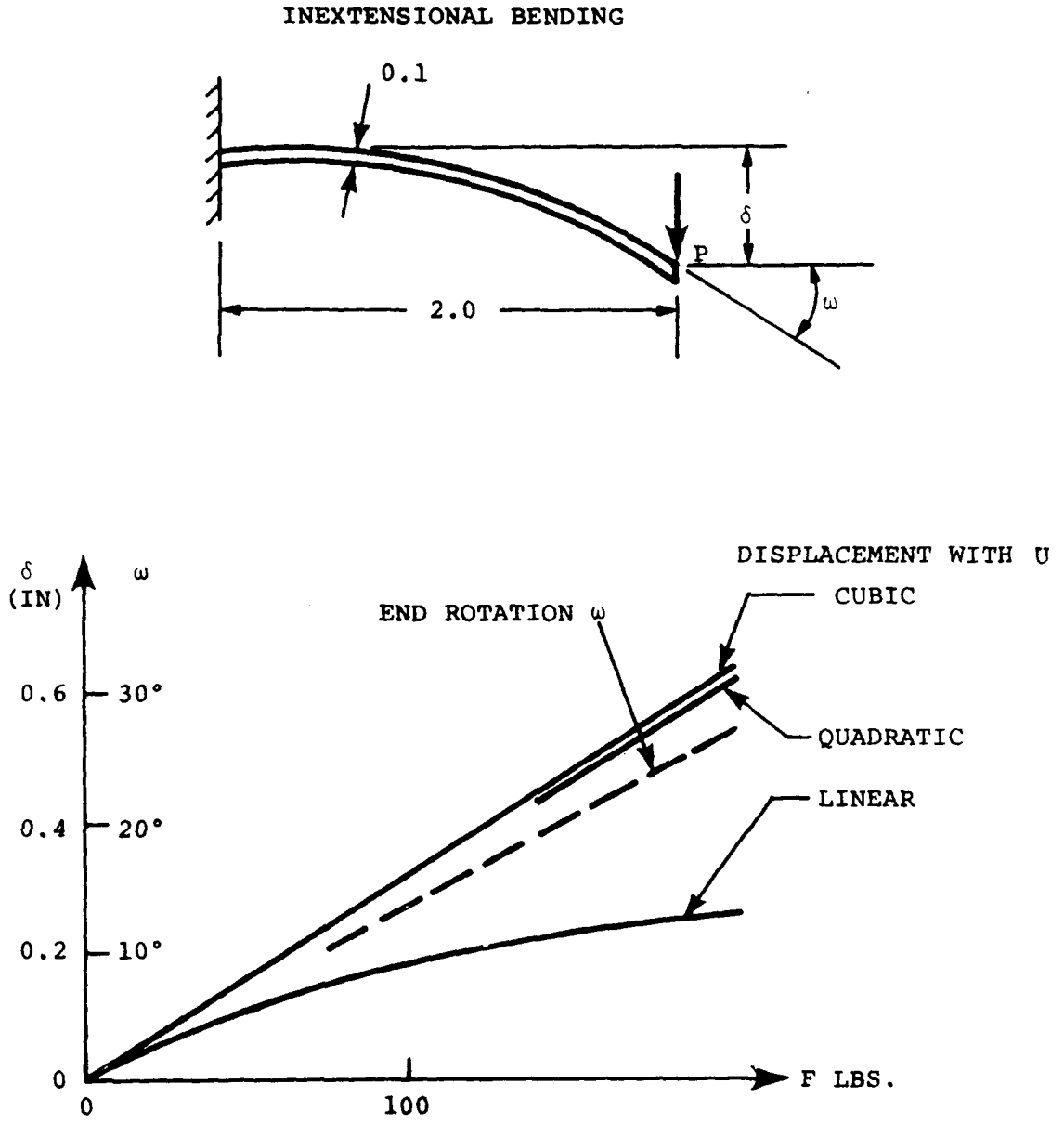

Figure 27. Nonlinear Bending of Beam

AD-A111 568 LOCKHEED MISSILES AND SPACE CO INC PALO ALTO CA PALO --ETC F/G 13/13
NUMERICAL PROCEDURES FOR ANALYSIS OF STRUCTURAL SHELLS.(U)
MAR 81 B O ALMROTH, F A BROGAN F33615-76-C-3105

UNCLASSIFIED AFWAL-TR-80-3129 NL

2 OF 2
AD A
111 568

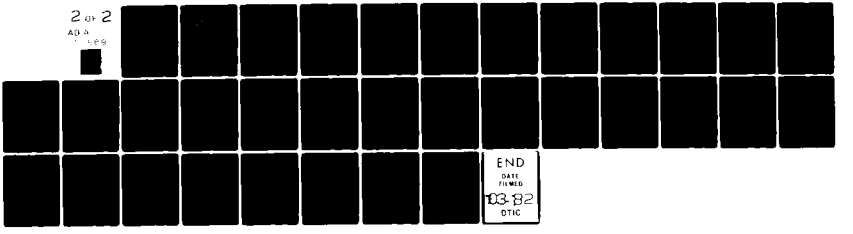

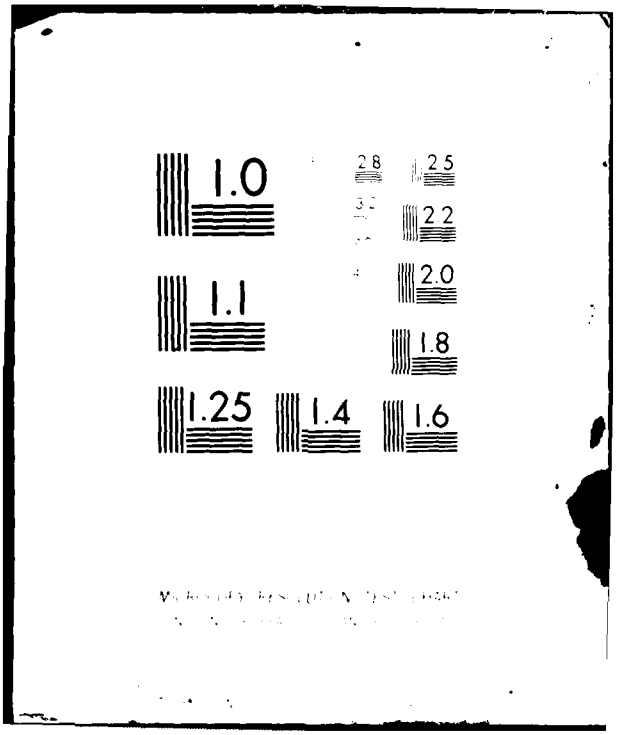
1.0
1.1
1.25
1.4
1.6
2.0
1.8
2.2
2.5

The results for a beam element with quadratic representation of u are close to the accurate solution. However, the simple case considered here is not quite representative and analysis of more complex structures show that even with second order polynomials for u and v , a substantial stiffening due to spurious stretching of the neutral surface can take place even at rather moderate rotations. The element SH411 discussed in the preceding paragraph can be modified to be bicubic in the inplane displacement components by use of two midside nodes. The only freedom at these nodes would be the tangential displacements. This would result in a considerable increase in computer time and it appears that the use of reduced integration may be a more attractive solution.

Reduced integration, with four Gaussian points (i.e., reduction beyond exact integration of the second order terms in the energy) was introduced as an option in the elements SH410 and SH411. Figures 28 and 29 show some results on nonlinear bending of a thin and relatively deep arch. The thickness is 0.125 in. and the width 1.0 in. A solution to this problem, presented in Reference 29, is indicated by the dotted curve. The results with SH411 elements are also shown in Figure 28. Only half the arch is modeled and the analysis was performed with either four or eight elements on this model. Clearly the rate of convergence with grid size is much better if the reduced integration is used, so that spurious stretching of the middle surface is avoided.

Results from analyses with SH410 elements are shown in Figure 29. The difference between use of four or five integration points is surprisingly large but even with four points spurious neutral surface stretching cannot be avoided and the results seem to have little resemblance to actual structural behavior.

Although significantly different the results obtained here as well as those in Reference 29 appear to represent converged solutions (with grid size). Most likely the discrepancy is due to differences in the basic theory. For example the definition of the strain ε_y in Reference 29 does not include

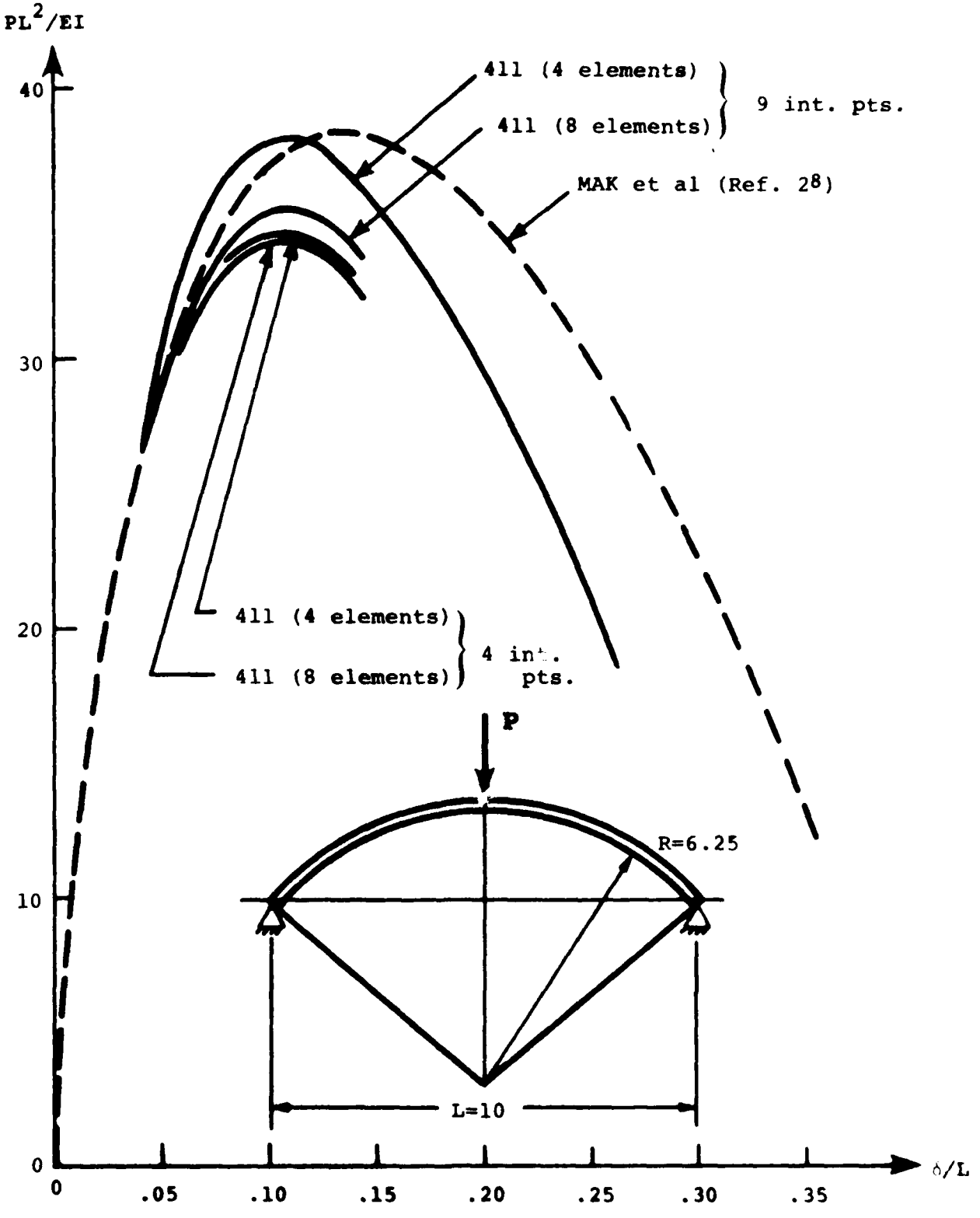

Figure 28. Load Displacement Curves for Arch, SH411 Elements

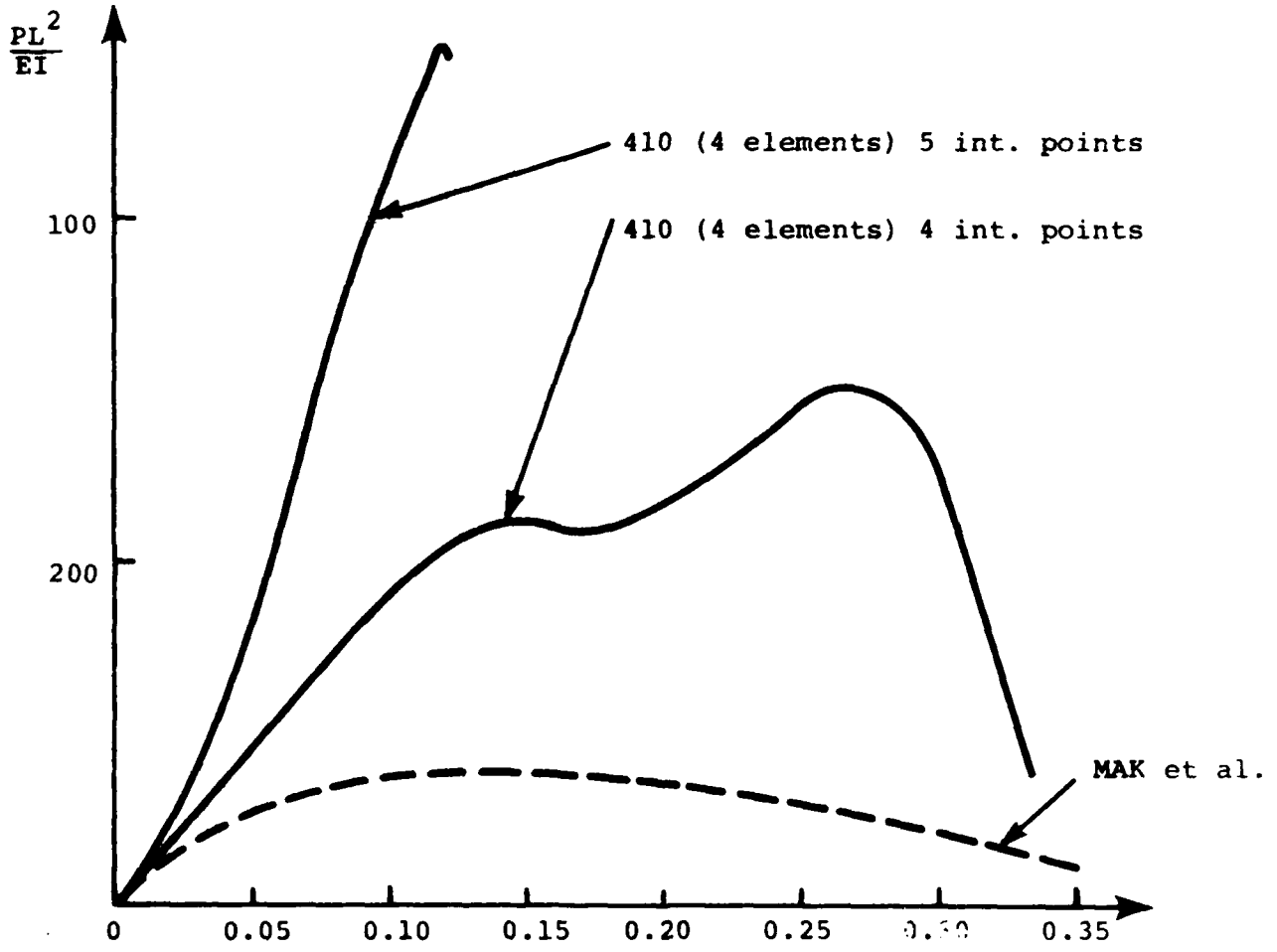

Figure 29. Load Displacement Curves for Arch, SH410 Elements

the term $1/2(v_{,y})^2$. The formulation for SH411 was temporarily modified through exclusion of this term. With the modified elements the computed limit point is only two percent below the one reported in Reference 29. The deformed shape at the limit point as computed with SH411 (4 elements, 4 integration points) is shown in Figure 30.

Further exploration of the use of reduced integration to avoid spurious stretching of the middle surface indicated even greater advantage for more complex cases. For example a good estimate of the collapse load for long cylinders in bending (Brazier effect) can be obtained with a relatively coarse grid (6 x 6 elements for the example used) with SH411 and with four integration points. With nine integration points and the same grid the collapse load is overestimated by a factor of two.

An attempt was also made to solve the arch problem (Figure 30) by use of the Ahmad type element, SH440. However, even with a very fine grid, 21 points over the half arch the load displacement curve does not contain a limit point. It seems that this element has a tendency to "lock" with increasing rotation of structural elements. At the limit point the maximum rotation in the deformation pattern is about 35 degrees. Possibly the locking of the element is due to the fact that the transformation of a vector of rotation components is valid only in the small rotation range. However, displacement configurations with rotations as large as 35 degrees are not within the range of the moderate rotation theory. In that case all elements using rotations as freedom would suffer from this problem in large displacement analysis based on a Lagrangian formulation. It appears that the elements SH410 and SH420 elements are less sensitive to the locking problem. More light is thrown on this problem in the following section.

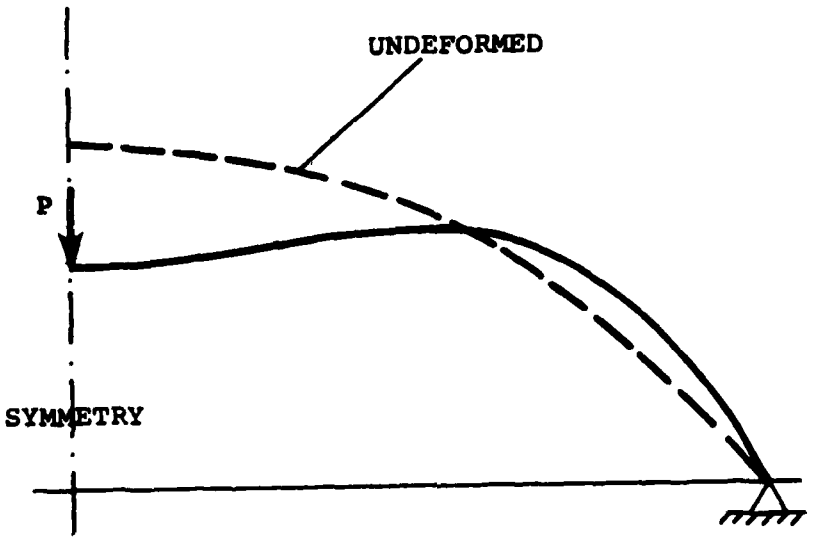

Figure 30. Deformed Shape at the Limit Point

Section XVII

SHELL COLLAPSE ANALYSIS

For a final evaluation of the shell elements, represented by SH411, and the degenerate brick element (SH440) a couple of cases with strongly nonlinear behavior were selected. The first one of these is the so called "pear-shaped" cylinder, first presented as an example case in Reference 30. Load displacement curves (Figure 31) are shown from analysis with the SH411 element for three different grid configurations. The computed failure loads are

with	3 x 27 grid	3586 lbs
	5 x 37 grid	2731 lbs
	7 x 47 grid	2586 lbs

For moderate values of the load there is no significant difference between the results for different grid sizes. The convergence difficulties at higher load levels may be due to the fact that the displacement pattern becomes more complex with higher values of the load. It could also be related to the locking phenomenon discussed in the previous section.

Load displacement curves for the pear-shaped cylinders obtained by use of the SH440 element are shown in Figure 32. The failure loads are

with	5 x 37 grid	2657 lbs
	7 x 47 grid	2530 lbs

Since the elements appear to have a tendency to lock with increasing values of the rotation components, the problem of convergence with grid size becomes complex. It is not possible to relate the error to the grid size alone and extrapolate with confidence. However, it appears that in both cases the collapse load is somewhere around 2300 or 2400 lbs, that is close to the 2340 lbs obtained with a STAGS A analysis based on a 9 x 45 grid reported in Reference 30. With the same grid size the finite difference program gives results that are at least as close as those obtained by use of

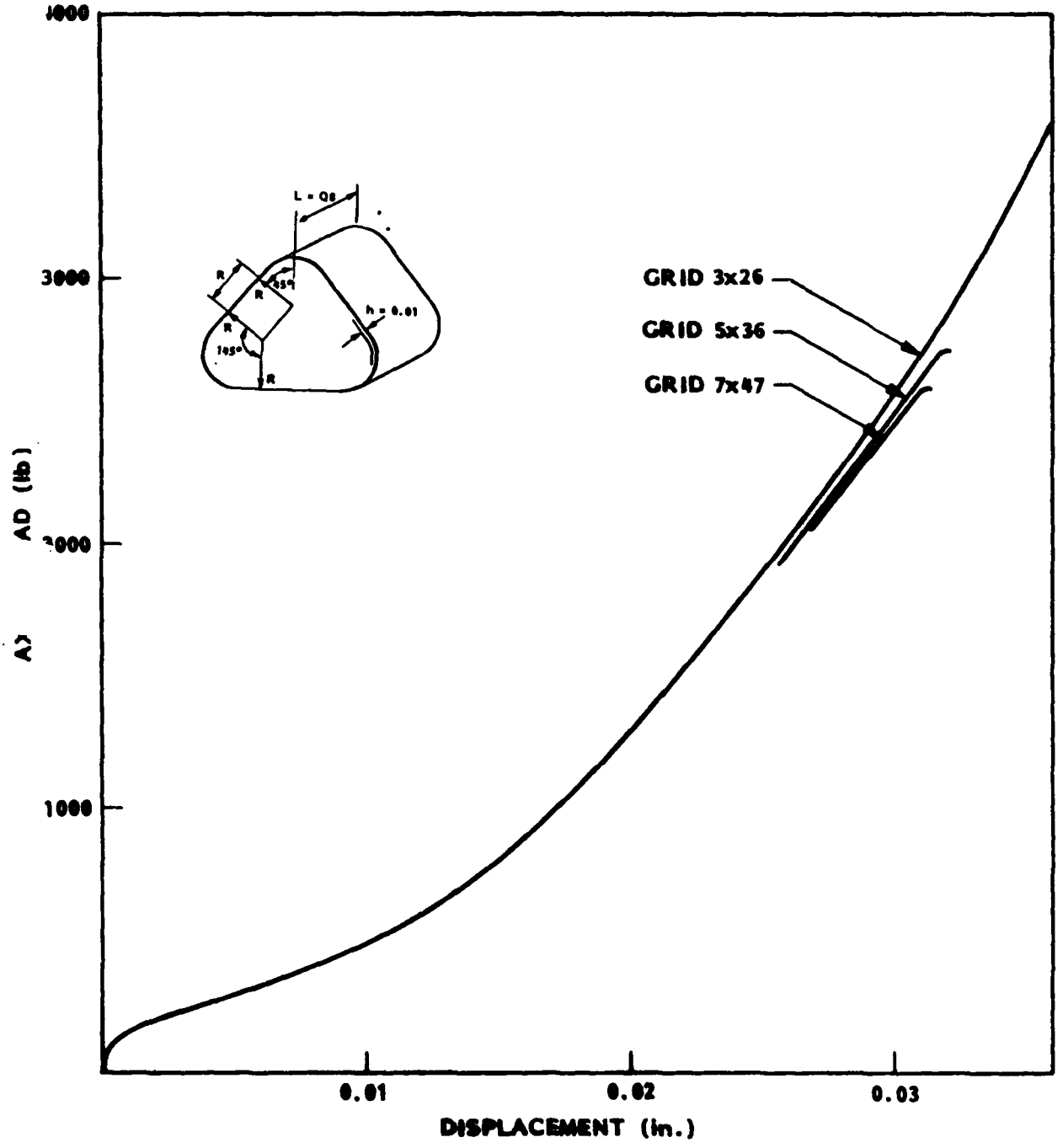

Figure 31. Load Displacement Curves for "Pear-Shaped" Cylinder with SH411

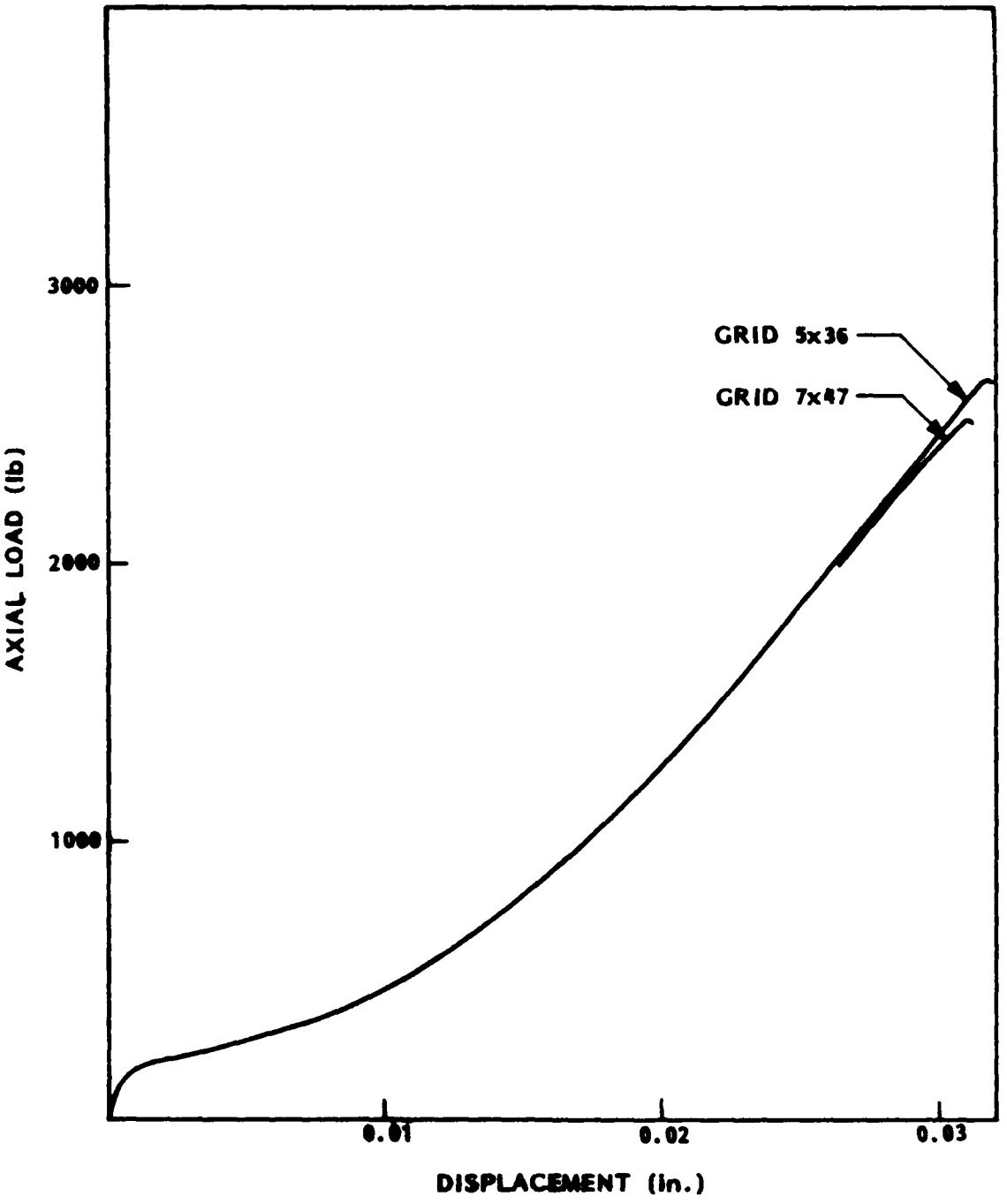

Figure 32. Load Displacement Curves for "Pear-Shaped" Cylinder with SH440

any of the two finite elements, at a cost that is an order of magnitude less.

The second case considered is the cylinder with a rectangular cutout for which analytical as well as experimental results are presented in Reference 31. The dimensions of the cylinder and the results from analysis with the SH411 element are shown in Figure 33.

The computed failure loads are

with	11 x 13 grid	3698 lbs
	17 x 19 grid	3060 lbs
	23 x 27 grid	2922 lbs
	29 x 37 grid	2750 lbs

With SH440 elements the following results were obtained

17 x 19 grid	3733 lbs
23 x 29 grid	3098 lbs

Finite difference solutions and experimental results (Reference 31) are in good agreement. A finite difference analysis with a 21 x 23 grid gives a collapse load of 2250 lbs. in good agreement with experiment. It is not economically feasible to obtain a converged solution in this case with any of the finite elements. The true value of the critical load may be somewhat higher than that obtained in the experiments, but still it appears that the finite difference approach is vastly more efficient for this type of analysis. The maximum rotations at failure for the two cases discussed in this paragraph are rather moderate, about 7 degrees in both cases.

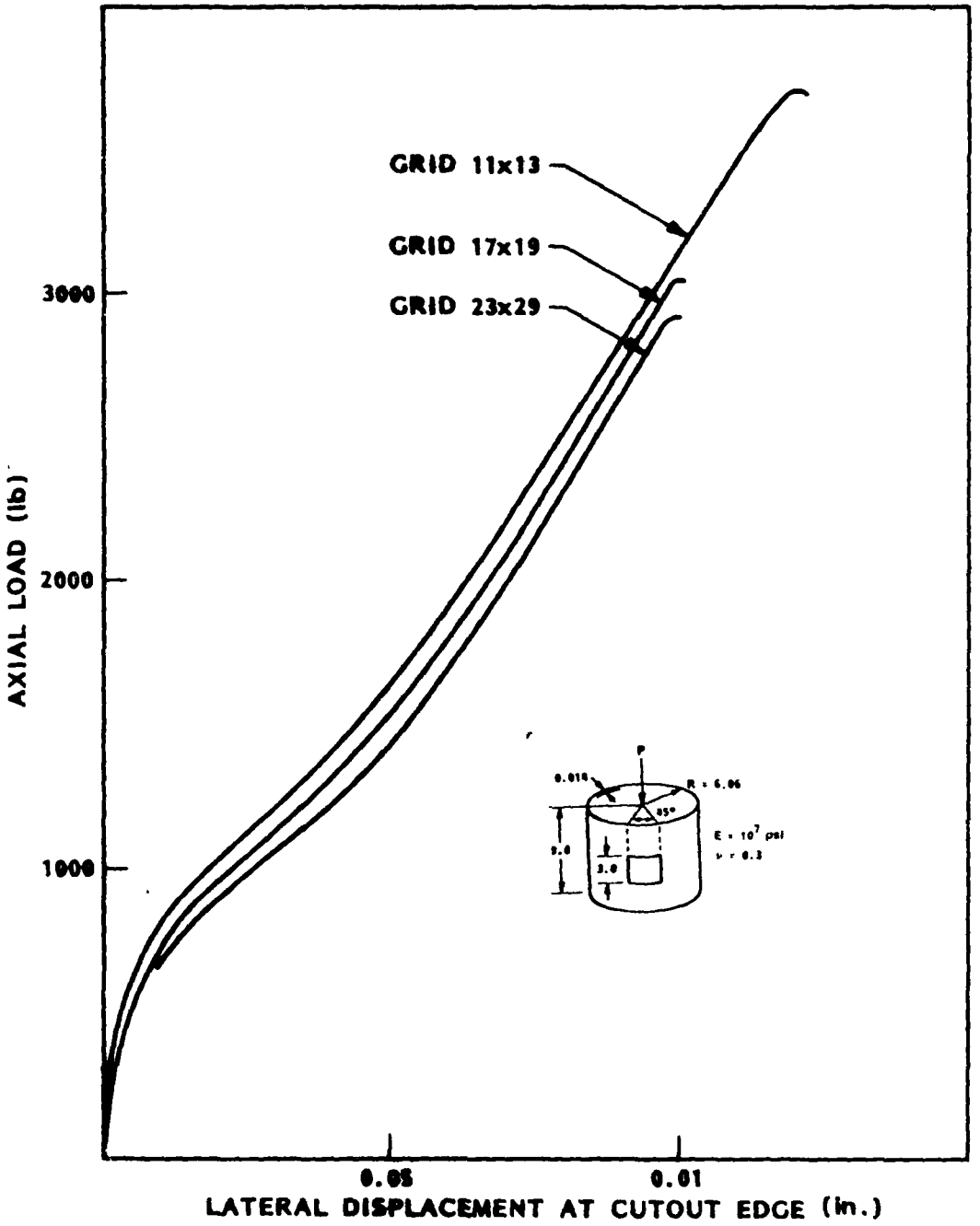

Figure 33. Load Displacement Curves for Cylinder with Cutout with SH411

Section XVIII

CONCLUSIONS AND RECOMMENDATIONS

More than anything else the results presented in the preceding sections tend to stress the importance of the choice of discretization procedure in analysis of shells, particularly when it comes to buckling and collapse analysis. It is shown for example that the price for a buckling analysis with a two percent accuracy of a cylindrical panel may vary by as much as a factor of 40 depending on the choice of element. While analysis with SH410 requires about half the run time in comparison with SH411 for buckling of a panel with uniform prestress, it requires about five times as much if an axially symmetric imperfection is introduced to generate a nonuniform prebuckling stress distribution. Most striking may be is that while the finite element configurations investigated here result in very efficient analysis of bifurcation buckling loads they appear to be hopelessly inferior to the finite difference method (elements with extended support) in nonlinear analysis of shells that undergo relatively large rotations (5 to 10 degrees) before collapse occurs. It seems reasonable to assume that this problem is related to the use of shell equations, based on the moderate rotation assumption together with a Lagrangian formulation. The finite difference procedure does not include rotations as freedoms. This may explain why it is less sensitive to these assumptions.

For bifurcation buckling analysis of thin shells the elements SH415 and SH416 are efficient and reliable (SH416 only if the prebuckling membrane strain is reasonably uniform). While sometimes the elements SH410 and SH411 may lead to somewhat more economic analysis, due to the balance between positive and negative errors, they are for the same reason less reliable. In particular the tendency to converge from below in many cases is undesirable as it can lead to spurious local buckling behavior unless a very fine grid is used. Also SH410 and SH411 are not suitable if the element planform deviates much from a rectangle. On the other hand the hybrid forms SH415 and SH416 can not be used without some penalty on computer time or accuracy for shells exhibiting coupling between membrane and bending behavior. For such cases the elements SH410 and SH411 are recommended if the elements are close to rectangular.

It must be stressed that the investigation reported here, although extensive, is

far from exhaustive. For example Iron's Semi-loof element (Reference 32) and the hierarchy of modified degenerate brick elements recently developed by Hughes and his coworkers (Reference 33) should be considered. No curved elements based on shell theory were included in the study. Except for flat plates then, the analysis based on the shell elements included is reduced to a second order accuracy, that is the same as in the finite difference analysis.

For thicker shells the analysis must be based on a second order theory. For this case the Ahmad type element, SH440, is the only element included in the investigation that will lead to accurate results (for bifurcation buckling as well as nonlinear collapse analysis). Generally, the Ahmad element works well also for thin shells, and the fact that it is the only choice in some shell codes has some justification. It is feasible that the relatively slow convergence in plate shear buckling will be cured by inclusion of the ninth node (at the midpoint). However, with reduced integration this may lead to problems with mechanisms. Also, it may be noted that the Ahmad type elements will be penalized in terms of computer time for shell walls with membrane-bending coupling.

The most disturbing aspect of this investigation is undoubtedly the poor performance of the finite elements included in the collapse analysis of the pear-shaped cylinder and the cylinder with a cutout. Since the finite element formulation with the same grid size gives a more accurate description of the deformation pattern it should not require a finer grid in the collapse analysis. There are good grounds therefore to assume that the apparent stiffening of the structure with increasing rotation can be cured by a nonlinear analysis procedure that includes "updating of the geometry". The so-called "corotational approach" advocated by Horrigmoe and others (Reference 34, for example) appears to be most promising since it allows for such updating without modification (with increasing deformation) of element shape functions.

It is clear that much work remains to be done in the area of discretization procedures for stability and nonlinear collapse analysis of thin shell structures. It is recommended here that flat and curved shell elements as well as degenerate brick elements be introduced in STAGSC-1 for analysis of an extended set of benchmark cases. With the corotational approach the problem with self-straining of curved elements should be essentially eliminated while a third or fourth order accuracy is maintained. If such elements do not prove to be substantially

more economic than the flat elements for curved shell analysis the possibilities of reintroducing finite difference formulations must be seriously considered. However, this alternative seems less attractive because much work would be needed in order to derive formulations that are comparable to finite elements in modeling capability. Particularly, programming procedures involving geometry updating for problems with large rotations will be considerably more complex if the elements are not self-contained.

REFERENCES

1. Dahlquist, G., and Björk, A., "Numerical Methods," Prentice Hall, Englewood Cliffs, N.J., 1974.

2. Noor, A.K., "Improved Multilocal Finite-Difference Variant for the Bending Analysis of Arbitrary Cylindrical Shells," University of South Wales Rept. No. R-63, Australia, March 1971.

3. Brogan, F. A., and Almroth, B.O., "Practical Methods for Elastic Collapse Analysis for Shell Structures," AIAA J., Vol. 9, Dec 1971, pp 2321-2325.

4. Sokolnikoff, I.S., "Mathematical Theory of Elasticity," McGraw Hill, N.Y., 1956.

5. Brush, D. O., and Almroth, B.O., "Buckling of Bars, Plates and Shells," McGraw Hill, N.Y., 1975.

6. Strang, G. and Fix, G.J., "An Analysis of the Finite Element Method," Prentice Hall, Englewood Cliffs, N.J., 1973.

7. Forsythe, G.E., and Wasow, W.R., "Finite Difference Methods for Partial Differential Equations," Wiley, N.Y., 1960.

8. Zlámal, M., "Superconvergence and Reduced Integration in Finite Element Method," Mathematics of Computation, Vol. 23, July 1978, pp 663-685.

9. Noor, A.K. and Schnobrich, W.C., "On Improved Finite Difference Discretization Procedures," Variational Methods in Engineering, Ed. Blebbia and Tottenham, Southampton University Press, Southampton G.B., Vol. 2 1972, pp 12-1, 12-50.

10. Jensen, P.S. and Felippa, C.A., "Variable Grid Finite Difference Element Solution of Elliptic Partial Differential Equations," LMSC Report for AFOSR, May 1974.

11. Felippa, C.A. and Clough, R.W., "The Finite Element Method in Solid Mechanics," ASM Symp. Numer. Solution Field Probl. Continuum Mech., Durham, N.C., 1968.

12. Gallagher, R.H., "Finite Element Analysis Fundamentals," Prentice Hall, Englewood Cliffs, N.J., 1975.

13. Clough, R.W. and Tocher, J.L., Finite Element Stiffness Matrices for Analysis of Plate Bending, Proceedings of 1st Conference on Matrix Methods in Structural Mechanics, AFFDL TR 66-80, Nov 1967.

14. Melosh, R.J., "A Stiffness Matrix for the Analysis of Thin Plates in Bending, JAS, Vol. 28, 1961.

15. Zienkiewicz, O.C., "The Finite Element Method in Engineering Science," McGraw Hill, New York, N.Y.

16. Bogner, F.K., Fox, R.L. and Schmit, L.A., "The Generation of Interelement, Compatible Stiffness and Mass Matrices by the Use of Interpolation Formulas," Proceedings of the 1st Conference on Matrix Methods in Structural Mechanics, AFFDL TR 66-80, Nov 1967.

17. Rand, T., An Approximative Method for the Calculation of the Stresses in Sweptback Wings, JAS, 1951.

18. Haggenmacher, G.W., "A New Four-Node Plate Element Using a Stress Field," Lockheed California Company, Report #LR98386, Oct 1977.

19. Pian, T.H.H., Element Stiffness Matrices for Boundary Compatibility and Prescribed Boundary Stresses," Proceedings of the 1st Conference on Matrix Methods in Structural Mechanics, AFFDL TR 66-80, Oct 1965.

20. Whetstone, W.D., "SPAR Structural Analysis System Reference Manual," NASA CR 145098-1, Feb 1977.

21. Strang, G., "Variational Crimes in the Finite Element Method," Math. Foundations of the Finite Element Method, Editor Aziz, A.K., Academic Press, p. 689, N.Y., 1972.

22. Irons, B.M. and Razzaque, A., "Experience with the Patch Test for Convergence of Finite Elements," Math. Foundations of the Finite Element Method, Editor Aziz, A.F., Academic Press, p. 557, N.Y., 1972.

23. Wilson, E.L., Taylor, W.P., Doherty, W.P., and Ghaboussi, J., Incompatible Displacement Models, University of Illinois Symposium, 1971.

24. Taylor, R.L., Beresford, P.J., and Wilson E.L., "A Non-conforming Element for Stress Analysis", Int. J. Num. Meth. Engrg., V.10, pp. 1211-1219, 1976.

25. Timoshenko, S., Elastic Stability, McGraw Hill, New York, N.Y.

26. Ahmad, S., Irons, B.M., and Ziekiewicz, O.C., "Analysis of Thick and Thin Shell Structures by Curved Elements," Int. J. Num. Meth. Eng., Vol. 2, pp 419-451, 1970.

27. Pawsey, S.F., "The Analysis of Moderately Thick to Thin Shells by the Finite Element Method," Struct. Eng. Lab. Rept. 7-12, Dept. of Civil Eng., U.C., Berkeley, Cal., 1970.

28. Haftka, R.T., Mallett, R.H. and Nachbar, W., "Adaption of Koiter's Method to Finite Element Analysis of Snap-Through Behavior," Int. J. Solids Structures, Vol. 7, 1971.

29. Mak, C.K., "Finite Element Analysis of Buckling and Post-Buckling Behaviors of Arches with Geometric Imperfections," J. Comp. Struct., 1972.

30. Hartung, R.F., "An Assessment of Current Capability for Computer Analysis of Shell Structures," Computers & Structures, Vol. 1, pp 3-32, 1971.

31. Almroth, B.O. and Holmes, A.M.C., "Buckling of Shells with Cutouts, Experiment and Analysis, Int. Journal Solids and Structures, Vol. 8, pp. 1057-1071, 1972.

32. Irons, B. M., "The Semiloof Shell Element", Chapter 11, Finite Elements for Thin Shells and Curved Membranes, Editors D. G. Ashwell and R. H. Gallagher, Wiley 1976.

33. Hughes, T. J. R. and Tezduyar, T. E., "Finite Elements Based Upon Mindlin Plate Theory with Particular Reference to the Four-Node Bilinear Isoparametric Element", AMD- Vol. 44, ASME N.Y., 1981.

34. Horrigmoe, G., Finite Element Instability Analysis of Free-Form Shells, Report 77-2, Division of Structural Mechanics, Norwegian Institute of Technology, University of Tronheim, Norway, May 1977.

Appendix

STIFFNESS MATRIX FOR THE QUAF ELEMENT

The degrees of freedom of the system are the displacement vectors u^s, v^s, and w^s on the shell (or plate) and the vector of rotation components γ_1^s, γ_2^s, β_1^s and β_2^s as shown in Figure A1. These vectors represent the components of displacements and rotations in a local coordinate x', y', z' system where the x' and y' axes are tangents to the coordinate lines, and z' is directed along the outward normal. The component of inplane rotation, γ_1^s or γ_2^s, through the node point. If a set of surface coordinates x, y are used for the grid generation, the notation γ_1^s refers to the rotation of a coordinate line corresponding to constant y and γ_2^s refers to the rotation of a line corresponding to constant x.

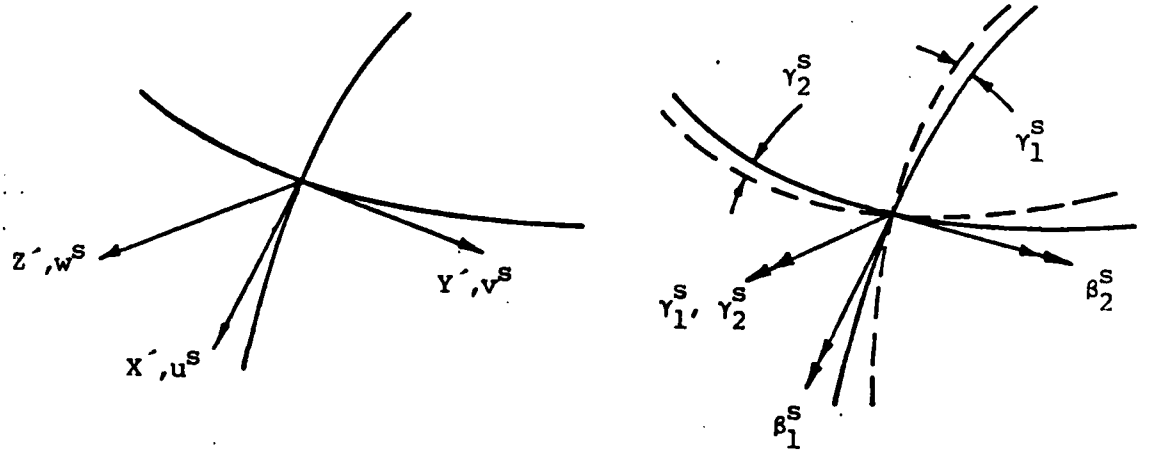

Fig. A1 The Degrees of Freedom

Next, a flat element is considered with the corners at four node points as shown in Figure A2. A total of eight nodes are defined on the element as shown in the figure. A Cartesian system x,y,z is introduced with x,y in the directions as shown, and z completing a right-handed system.

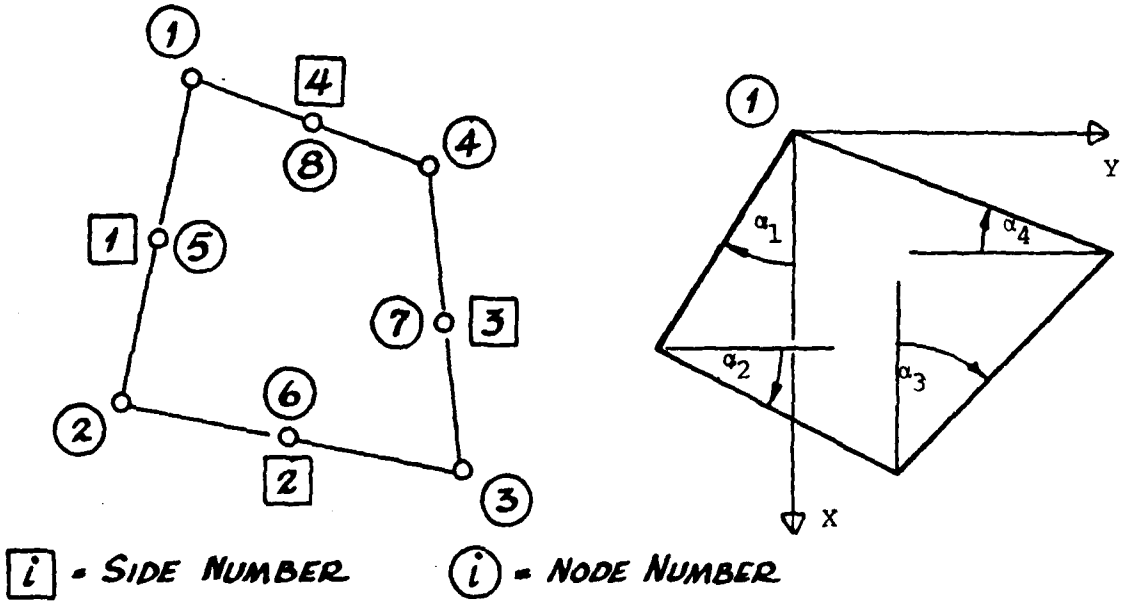

Fig. A2 The Flat Element

The 3x3 matrix $T^{(i)}$ transforms a vector in the system x', y', z' at corner i into a vector in the coordinate system x,y,z for the element. The displacement components at each of the corners are obtained from

$$\begin{Bmatrix} u \\ v \\ w \end{Bmatrix}^{(i)} = [T]^{(i)} \begin{Bmatrix} u^s \\ v^s \\ w^s \end{Bmatrix}^{(i)} \qquad \text{(A1)}$$

The vector $\{\beta\}^{(i,j)}$ corresponds to the rotation of side number i at corner number j. Thus

$$\begin{Bmatrix} \beta_1 \\ \beta_2 \\ \beta_3 \end{Bmatrix}^{(1,j)} = [T]^{(j)} \begin{Bmatrix} \beta_1^s \\ \beta_2^s \\ \gamma_1^s \end{Bmatrix}^{(j)} \qquad j = 1, 2$$

$$\begin{Bmatrix} \beta_1 \\ \beta_2 \\ \beta_3 \end{Bmatrix}^{(2,j)} = [T]^{(j)} \begin{Bmatrix} \beta_1^s \\ \beta_2^s \\ \gamma_2^s \end{Bmatrix}^{(j)} \qquad j = 2, 3$$

$$\begin{Bmatrix} \beta_1 \\ \beta_2 \\ \beta_3 \end{Bmatrix}^{(3,j)} = [T]^{(j)} \begin{Bmatrix} \beta_1^s \\ \beta_2^s \\ \gamma_1^s \end{Bmatrix}^{(j)} \qquad j = 3, 4 \qquad \text{(A2)}$$

$$\begin{Bmatrix} \beta_1 \\ \beta_2 \\ \beta_3 \end{Bmatrix}^{(4,j)} = [T]^{(j)} \begin{Bmatrix} \beta_1^s \\ \beta_2^s \\ \gamma_2^s \end{Bmatrix}^{(j)} \qquad j = 1, 4$$

The next step is to determine the derivatives of the displacement components with respect to the coordinates ξ and η which are defined so that $\xi = -1$ on side 4 and $+1$ for side 2 and $\eta = -1$ on side 1 and $+1$ for side 3.

That is,

$$x = \langle \phi^{(1)} \rangle \{x_i\}$$
$$y = \langle \phi^{1} \rangle \{y_i\} \qquad \text{(A3)}$$

where

$$\langle \phi^{(1)} \rangle = \langle 1/4(1-\xi)(1-\eta),\ 1/4(1+\xi)(1-\eta),$$
$$1/4(1+\xi)(1+\eta),\ 1/4(1-\xi)(1+\eta) \rangle$$

where x_i, y_i are the x and y coordinates of the four corners. First the derivatives are determined with respect to a parameter representing the distance along the side of the element, see Figure A3.

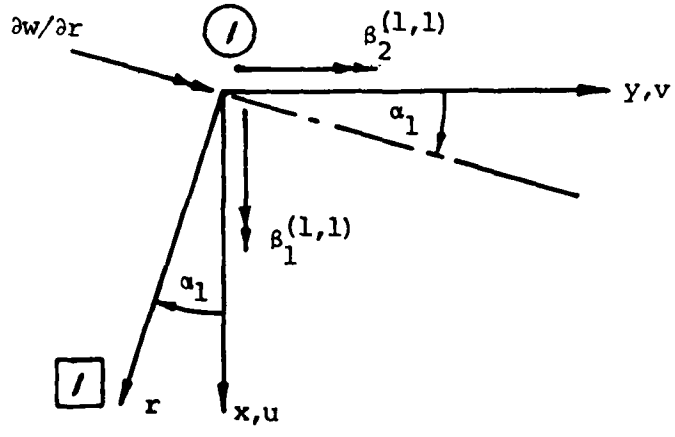

Fig. A3 Inplane Rotation of x-Coordinate Line

For example, for line 1 at corner 1

$$\frac{\partial w}{\partial r}^{(1)} = \beta_1^{(1,1)} \sin \alpha_1 + \beta_2^{(1,1)} \cos \alpha_1 \qquad \text{(A4)}$$

With the notations

$$c_{\alpha_i} = \cos(\alpha_i) \text{ and} \tag{A5}$$

$$s_{\alpha_i} = \sin(\alpha_i) \text{ at corner 1:}$$

$$\frac{\partial r^{(1)}}{\partial \xi} = 2(x_2 - x_1)/c_{\alpha 1} \text{ and consequently} \tag{A6}$$

$$\frac{\partial w^{(1)}}{\partial \xi} = \frac{2(x_2 - x_1)}{c_{\alpha 1}} \left[s_{\alpha_1} \beta_1^{(1,1)} + c_{\alpha_1} \beta_2^{(1,1)} \right] \tag{A7}$$

The derivatives with respect to η are determined in the same way (See Figure A4).

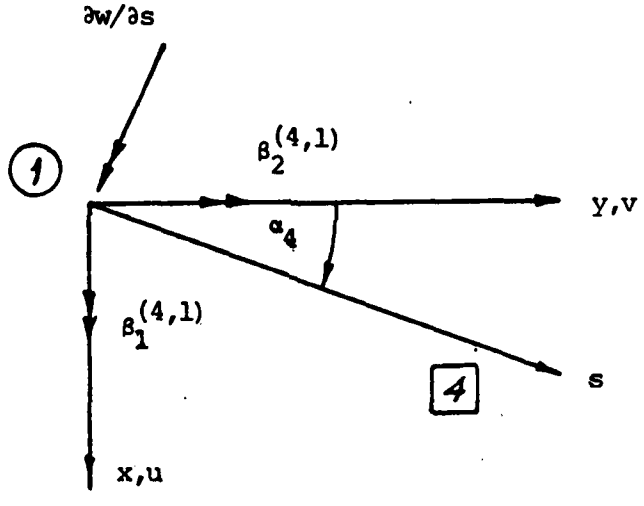

Fig. A4 Inplane Rotation of y-Coordinate Line

$$\frac{\partial w^{(1)}}{\partial s} = c_{\alpha_4} \beta_1^{(4,1)} - s_{\alpha_4} \beta_2^{(4,1)} \tag{A9}$$

$$\frac{\partial w^{(1)}}{\partial \eta} = \frac{2(y_4 - y_1)}{c_{\alpha_4}} \left(c_{\alpha_4} \beta_1^{(4,1)} - s_{\alpha_4} \beta_2^{(4,1)} \right) \tag{A10}$$

Corresponding derivatives at the remaining three corners are then determined in the same way.

The field of lateral displacement is determined from the lateral displacements and their derivatives with respect to the Cartesian coordinates x and y at the corner nodes. The chain rule of differentiation yields

$$\begin{Bmatrix} w,_x \\ w,_y \end{Bmatrix} = \begin{bmatrix} \frac{\partial \xi}{\partial x} & \frac{\partial \eta}{\partial x} \\ \frac{\partial \xi}{\partial y} & \frac{\partial \eta}{\partial y} \end{bmatrix} \begin{Bmatrix} w,_\xi \\ w,_\eta \end{Bmatrix} = [J^*] \begin{Bmatrix} w,_\xi \\ w,_\eta \end{Bmatrix} \tag{A11}$$

The transformation matrix J* is obtained as the transpose of the inverse of

$$[J] = \begin{bmatrix} \frac{\partial x}{\partial \xi} & \frac{\partial x}{\partial \eta} \\ \frac{\partial y}{\partial \xi} & \frac{\partial y}{\partial \eta} \end{bmatrix} \tag{A12}$$

$$[J]^{-1} = \begin{bmatrix} \frac{\partial y}{\partial \eta} & -\frac{\partial y}{\partial \xi} \\ -\frac{\partial x}{\partial \eta} & \frac{\partial x}{\partial \xi} \end{bmatrix} \Big/ \left(\frac{\partial y}{\partial \eta} \frac{\partial x}{\partial \xi} - \frac{\partial y}{\partial \xi} \frac{\partial x}{\partial \eta} \right) \tag{A13}$$

and

$$[J^*] = \begin{bmatrix} \frac{\partial y}{\partial \eta} & -\frac{\partial x}{\partial \eta} \\ -\frac{\partial y}{\partial \xi} & \frac{\partial x}{\partial \xi} \end{bmatrix} \Big/ \left(\frac{\partial y}{\partial \eta} \frac{\partial x}{\partial \xi} - \frac{\partial y}{\partial \xi} \frac{\partial x}{\partial \eta} \right) \tag{A14}$$

The derivatives of x and y with respect to ξ and η are readily obtained from Eqs. (A3). The freedoms of the flat element (in addition to w and its derivatives) are u and v displacements at the corner nodes, the correction to the inplane tangential displacements at nodes 5, 6, 7, and 8, and the corner node freedoms corresponding to the boundary line rotations about the normal to the plate (see Figure A1).

The displacement field that matches these freedoms will now be defined. A bilinear field is used to match the corner displacement. The biquadratic displacement field has zero displacements at corner nodes. It represents an addition to the tangential displacements at the midside nodes as determined from the bilinear field. The parameters γ^u and γ^v are the corrections to the displacement field that are necessary in order that the inplane rotations will match the rotations of boundary lines at the corners (as determined by β_3, see Eqs. A2).

Hence, we have

$$u = \langle \phi^{(1)} \rangle \{u_i\} + \langle \phi^{(2)} \rangle \{t_i^u\} + \langle \phi_u^{(3)} \rangle \{\gamma_i^u\} + \langle \phi_{vu}^{(3)} \rangle \{\gamma_i^v\}$$

$$v = \langle \phi^{(1)} \rangle \{v_i\} + \langle \phi^{(2)} \rangle \{t_i^v\} + \langle \phi_v^{(3)} \rangle \{\gamma_i^v\} + \langle \phi_{uv}^{(3)} \rangle \{\gamma_i^u\}$$

$$i = 1, 2, 3, 4 \qquad \text{(A15)}$$

Notice that each of the four components of the biquadratic field corresponds to displacements parallel to one of the sides. Likewise, the components of the bicubic field include only displacements in a direction normal to one of the sides. Consequently

$$\{t_i^u\} = \langle t_1 c_{\alpha_1}, t_2 s_{\alpha_2}, t_3 c_{\alpha}, t_4 s_{\alpha_4} \rangle$$
$$\{t_i^v\} = \langle -t_1 s_{\alpha_1}, t_2 c_{\alpha_2}, -t_3 s_{\alpha_3}, t_4 c_{\alpha_4} \rangle \quad \text{(A16)}$$

The form of the components in the bilinear field are given by $\langle \phi^{(1)} \rangle$ in Eqs. A3. That is,

$$\langle \phi^{(2)} \rangle = \langle 1/2(1-\xi^2)(1-\eta),\ 1/2(1+\xi)(1-\eta^2),\ 1/2(1-\xi^2)(1+\eta),\ 1/2(1-\xi)(1-\eta^2) \rangle \quad \text{(A17)}$$

and

$$\langle \phi_u^{(3)} \rangle = \langle 1/16\, c_{\alpha 4}(2-3\xi+\xi^3)(1-\eta-\eta^2+\eta^3),\ 1/16\, c_{\alpha 2}(2+3\xi-\xi^3)(1-\eta-\eta^2+\eta^3),$$
$$1/16\, c_{\alpha 2}(2+3\xi-\xi^3)(-1-\eta+\eta^2+\eta^3),\ 1/16\, c_{\alpha 4}(2-3\xi+\xi^3)(-1-\eta+\eta^2+\eta^3) \rangle$$
$$\langle \phi_{uv}^{(3)} \rangle = \langle -1/16\, s_{\alpha 4}(2-3\xi+\xi^3)(1-\eta-\eta^2+\eta^3),\ -1/16\, s_{\alpha 2}(2+3\xi-\xi^3)(1-\eta-\eta^2+\eta^3),$$
$$-1/16\, s_{\alpha 2}(2+3\xi-\xi^3)(-1-\eta+\eta^2+\eta^3),\ -1/16\, s_{\alpha 4}(2-3\xi+\xi^3)(-1-\eta+\eta^2+\eta^3) \rangle$$
$$\langle \phi_v^{(3)} \rangle = \langle 1/16\, c_{\alpha 1}(1-\xi+\xi^2+\xi^3)(2-3\eta+\eta^3),\ 1/16\, c_{\alpha 1}(-1-\xi+\xi^2+\xi^3)(2-3\eta+\eta^3),$$
$$1/16\, c_{\alpha 3}(-1-\xi+\xi^2+\xi^3)(2+3\eta-\eta^3),\ 1/16\, c_{\alpha 3}(1-\xi-\xi^2+\xi^3)(2+3\eta-\eta^3) \rangle$$
$$\langle \phi_{vu}^{(3)} \rangle = \langle 1/16\, s_{\alpha 1}(1-\xi+\xi^2+\xi^3)(2+3\eta-\eta^3),\ 1/16\, s_{\alpha 3}(1-\xi-\xi^2+\xi^3)(2+3\eta-\eta^2) \rangle \quad \text{(A18)}$$

Differentiating Eq. (A15) with respect to the normalized coordinate yields in matrix notation

$$\begin{Bmatrix} u,_{\xi i} \\ u,_{\eta i} \\ v,_{\xi i} \\ v,_{\eta i} \end{Bmatrix} = \begin{bmatrix} -T_{vv} & 0 \\ -T_{uu} & 0 \\ 0 & -T_{vv} \\ 0 & -T_{uu} \end{bmatrix} \begin{Bmatrix} u_i \\ v_i \end{Bmatrix} + \begin{bmatrix} T_{u\alpha_1} \\ T_{u\alpha_2} \\ T_{v\alpha_1} \\ T_{v\alpha_2} \end{bmatrix} \begin{Bmatrix} t_i^u \\ t_i^v \end{Bmatrix} + \begin{bmatrix} 0 & 0 \\ I & 0 \\ 0 & I \\ 0 & 0 \end{bmatrix} \begin{Bmatrix} \gamma_i^u \\ \gamma_i^v \end{Bmatrix} \quad \text{(A19)}$$

where

$$T_{vv} = 1/2 \begin{bmatrix} 1 & -1 & 0 & 0 \\ 1 & -1 & 0 & 0 \\ 0 & 0 & -1 & 1 \\ 0 & 0 & -1 & 1 \end{bmatrix}, \quad T_{uu} = 1/2 \begin{bmatrix} 1 & 0 & 0 & -1 \\ 0 & 1 & -1 & 0 \\ 0 & 1 & -1 & 0 \\ 1 & 0 & 0 & -1 \end{bmatrix} \tag{A20}$$

If the operations indicated by the second term on the right side of Eq. (A19) are carried out, this term is found to be identically equal to zero at all corner nodes. Consequently, the derivatives with respect to ξ and η of the displacement field corresponding to the midnode displacements will vanish and need not be given any further consideration.

Next the boundary line normal rotations corresponding to the linear polynomial. For this purpose the inplane displacements normal to the boundary are differentiated with respect to the distance along the element side.

From the figure, it is observed that

$$\begin{aligned} r &= \xi(x_2 - x_1)/2 \quad , \quad \frac{\partial}{\partial r} = \frac{2}{(x_2 - x_1)} \frac{\partial}{\partial \xi} \quad \text{on boundary 1} \\ s &= \eta(y_4 - y_1)/2 \quad , \quad \frac{\partial}{\partial s} = \frac{2}{(y_4 - y_1)} \frac{\partial}{\partial \eta} \quad \text{on boundary 4} \end{aligned} \tag{A21}$$

Also,

$$\begin{aligned} v_n &= v\, c_{\alpha_1} + u\, s_{\alpha_1} \quad \text{on boundary 1} \\ u_n &= v\, s_{\alpha_4} + u\, c_{\alpha_4} \quad \text{on boundary 4} \end{aligned} \tag{A22}$$

where

$$T_{\beta u} = \begin{bmatrix} \frac{y_4 - y_1}{2c_{\alpha_4}} & 0 & 0 & 0 \\ 0 & \frac{y_3 - y_2}{2c_{\alpha_2}} & 0 & 0 \\ 0 & 0 & \frac{y_3 - y_2}{2c_{\alpha_2}} & 0 \\ 0 & 0 & 0 & \frac{y_4 - y_1}{2c_{\alpha_4}} \end{bmatrix} \quad \text{(A26)}$$

$$T_{\beta v} = \begin{bmatrix} \frac{x_2 - x_1}{2c_{\alpha_1}} & 0 & 0 & 0 \\ 0 & \frac{x_2 - x_1}{2c_{\alpha_1}} & 0 & 0 \\ 0 & 0 & \frac{x_3 - x_4}{2c_{\alpha_3}} & 0 \\ 0 & 0 & 0 & \frac{x_3 - x_4}{2c_{\alpha_3}} \end{bmatrix} \quad \text{(A27)}$$

$$T_{\alpha u} = \begin{bmatrix} t_{\alpha_4} & 0 & 0 & 0 \\ 0 & t_{\alpha_2} & 0 & 0 \\ 0 & 0 & t_{\alpha_2} & 0 \\ 0 & 0 & 0 & t_{\alpha_4} \end{bmatrix} \quad \text{(A28)}$$

$$T_{\alpha v} = \begin{bmatrix} -t_{\alpha_1} & 0 & 0 & 0 \\ 0 & -t_{\alpha_1} & 0 & 0 \\ 0 & 0 & -t_{\alpha_3} & 0 \\ 0 & 0 & 0 & -t_{\alpha_3} \end{bmatrix} \quad \text{(A29)}$$

$$T_{\beta v} = \begin{bmatrix} \frac{x_2 - x_1}{2c_{\alpha_1}} & 0 & 0 & 0 \\ 0 & \frac{x_2 - x_1}{2c_{\alpha_1}} & 0 & 0 \\ 0 & 0 & \frac{x_3 - x_4}{2c_{\alpha_3}} & 0 \\ 0 & 0 & 0 & \frac{x_3 - x_4}{2c_{\alpha_3}} \end{bmatrix} \quad \text{(A27)}$$

$$T_{\alpha u} = \begin{bmatrix} t_{\alpha_4} & 0 & 0 & 0 \\ 0 & t_{\alpha_2} & 0 & 0 \\ 0 & 0 & t_{\alpha_2} & 0 \\ 0 & 0 & 0 & t_{\alpha_4} \end{bmatrix} \quad \text{(A28)}$$

$$T_{\alpha v} = \begin{bmatrix} -t_{\alpha_1} & 0 & 0 & 0 \\ 0 & -t_{\alpha_1} & 0 & 0 \\ 0 & 0 & -t_{\alpha_3} & 0 \\ 0 & 0 & 0 & -t_{\alpha_3} \end{bmatrix} \quad \text{(A29)}$$

and $t_{\alpha_i} = \tan(\alpha_i)$.

From comparison of the left-hand side of Eq. (A25) to similar terms in Eq. (A19) the expression for the correction terms γ^u and γ^v are determined, yielding

$$\begin{Bmatrix} \gamma_i^u \\ \gamma_i^v \end{Bmatrix} = \begin{bmatrix} T_{uu} & T_{vu} \\ T_{uv} & T_{vv} \end{bmatrix} \begin{Bmatrix} u_i \\ v_i \end{Bmatrix} + \begin{bmatrix} T_{\beta u} & 0 \\ 0 & T_{\beta v} \end{bmatrix} \begin{Bmatrix} -\beta_3^{(j,i)} \\ \beta_3^{(k,i)} \end{Bmatrix} \quad \text{(A30)}$$

where j = 1, if i = 1 or 2, j = 3 if i = 3or 4, and k = 4 if i = 1 or 4, k = 2 if i = 2 or 3.

T_{uu}, T_{vv}, $T_{\beta u}$, $T_{\beta v}$ are defined in Eqs. (A20), (A26), (A27); the $\beta_3^{(i,j)}$ are defined in Eqs. (A2). Notice also that $u_{,s_i} = -\beta_3^{(2 \text{ or } 4, i)}$ and $v_{,r_i} = \beta_3^{(1 \text{ or } 3, i)}$.

$$T_{uv} = 1/2 \begin{bmatrix} t_{\alpha_1} & -t_{\alpha_1} & 0 & 0 \\ t_{\alpha_1} & -t_{\alpha_1} & 0 & 0 \\ 0 & 0 & -t_{\alpha_3} & t_{\alpha_3} \\ 0 & 0 & -t_{\alpha_3} & t_{\alpha_3} \end{bmatrix}, \quad T_{vu} = 1/2 \begin{bmatrix} -t_{\alpha_4} & 0 & 0 & t_{\alpha_4} \\ 0 & -t_{\alpha_2} & t_{\alpha_2} & 0 \\ 0 & -t_{\alpha_2} & t_{\alpha_2} & 0 \\ -t_{\alpha_4} & 0 & 0 & t_{\alpha_4} \end{bmatrix} \quad \text{(A31)}$$

By substituting Eq. (A30) into Eq. (A15), the correction terms γ^u and γ^v are eliminated and the expression for u and v is obtained in terms of the selected flat plate freedoms.

$$
\begin{aligned}
u &= \langle \phi^{(1)} \rangle \{ u_i \} + \langle \phi^{(2)} \rangle \{ t_i^u \} \\
&\quad + \langle \phi^{(3)} \rangle \left(T_{uu} \{ u_i \} + T_{vu} \{ v_i \} + T_{\beta u} \{ u, s_i \} \right) \\
&\quad + \langle \phi^{(3)}_{vu} \rangle \left(T_{uv} \{ u_i \} + T_{vv} \{ v_i \} + T_{\beta v} \{ v, r_i \} \right)
\end{aligned}
\tag{A32}
$$

$$
\begin{aligned}
v &= \langle \phi^{(1)} \rangle \{ v_i \} + \langle \phi^{(2)} \rangle \{ t_i^v \} \\
&\quad + \langle \phi^{(3)}_{v} \rangle \left(T_{uv} \{ u_i \} + T_{vv} \{ v_i \} + T_{\beta v} \{ v, r_i \} \right) \\
&\quad + \langle \phi^{(3)}_{v} \rangle \left(T_{uv} \{ u_i \} + T_{vv} \{ v_i \} + T_{\beta v} \{ v, r_i \} \right)
\end{aligned}
$$

The derivatives of u and v with respect to x and y are needed at the integration points inside the element. The chain rule of differentiation yields

$$
\begin{Bmatrix} u,_x \\ u,_y \\ v,_x \\ v,_y \end{Bmatrix}
\begin{bmatrix} J^* & 0 \\ 0 & J^* \end{bmatrix}
\begin{Bmatrix} u,_\xi \\ u,_\eta \\ v,_\xi \\ v,_\eta \end{Bmatrix}
\tag{A33}
$$

where J* is defined by Eq. (A14).

Hence,

$$
J = (1/K) \begin{bmatrix} \langle \phi^{(1)} \rangle,_\eta \{ y_i \} & - \langle \phi^{(1)} \rangle,_\xi \{ y_i \} \\ - \langle \phi^{(1)} \rangle,_\eta \{ x_i \} & \langle \phi^{(1)} \rangle,_\xi \{ x_i \} \end{bmatrix}
\tag{A34}
$$

where

$$K = (<\phi^{(1)}>_{,\eta}\{y_i\})\quad(<\phi^{(1)}>_{,\xi}\{x_i\})$$

$$-(<\phi^{(1)}>_{,\xi}\{y_i\})\quad(<\phi^{(1)}>_{,\eta}\{x_i\}) \tag{A35}$$

The values of the shape functions $\phi^{(1)}$, $\phi^{(2)}$, and $\phi^{(3)}$ at the eight nodes (four corners and four mid nodes) are shown in Table A1.

Table A1

SHAPE FUNCTIONS AND DERIVATIVES EVALUATED AT NODES AND MID NODES

a) Bilinear Functions

$$\langle \phi^{(1)} \rangle_{,\xi} = \langle -1/4(1-\eta),\ 1/4(1-\eta),\ 1/4(1+\eta),\ -1/4(1+\eta) \rangle$$

$$\langle \phi^{(1)} \rangle_{,\eta} = \langle -1/4(1-\xi),\ -1/4(1+\xi),\ 1/4(1+\xi),\ 1/4(1-\xi) \rangle$$

Node	ξ	η	$\phi^{(1)}$	$\phi^{(1)}_{,\xi}$	$\phi^{(1)}_{,\eta}$
1	-1	-1	1, 0, 0, 0	-1/2, 1/2, 0, 0	-1/2, 0, 0, 1/2
2	1	-1	0, 1, 0, 0	-1/2, 1/2, 0, 0	0, -1/2, 1/2. 0
3	1	1	0, 0, 1, 0	0, 0, 1/2, -1/2	0, -1/2, 1/2, 0
4	-1	1	0, 0, 0, 1	0, 0, 1/2, -1/2	-1/2, 0, 0, 1/2
5	0	-1	1/2, 1/2, 0, 0	-1/2, 1/2, 0, 0	-1/4, -1/4, 1/4, 1/4
6	1	0	0, 1/2, 1/2, 0	-1/4, 1/4, 1/4, -1/4	0, -1/2, 1/2, 0
7	0	1	0, 0, 1/2, 1/2	0, 0, 1/2-1/2	-1/4, -1/4, 1/4, 1/4
8	-1	0	1/2, 0, 0, 1/2	-1/4, 1/4, 1/4, -1/4	-1/2, 0, 0, 1/2

b) Biquadratic Function

$$\langle \phi^{(2)} \rangle_{,\xi} = \langle -\xi(1-\eta),\ 1/2(1-\eta^2),\ -\xi(1+\eta),\ -1/2(1-\eta^2) \rangle$$

$$\langle \phi^{(2)} \rangle_{,\eta} = \langle -1/2(1-\xi^2),\ -(1+\xi)\eta,\ 1/2(1-\xi^2),\ -(1-\xi)\eta \rangle$$

Node	ξ	η	$\phi^{(2)}$	$\phi^{(2)}_{,\xi}$	$\phi^{(2)}_{,\eta}$
1	-1	-1	0, 0, 0, 0	2, 0, 0, 0	0, 0, 0, 2
2	1	-1	0, 0, 0, 0	-2, 0, 0, 0	0, 2, 0, 0
3	1	1	0, 0, 0, 0	0, 0, -2, 0	0, -2, 0, 0
4	-1	1	0, 0, 0, 0	0, 0, 2, 0	0, 0, 0, -2
5	0	-1	1, 0, 0, 0	0, 0, 0, 0	-1/2, 1, 1/2, 1
6	1	0	0, 1, 0, 0	-1, 1/2, -1, -1/2	0, 0, 0, 0
7	0	1	0, 0, 1, 0	0, 0, 0, 0	-1/2, -1, 1/2, -1
8	-1	0	0, 0, 0, 1	1, 1/2, 1, -1/2	0, 0, 0, 0

c) Bicubic Functions

$$\langle \phi_u^{(3)} \rangle_{,\xi} = \langle 1/16\, c_{\alpha_4}(-3+3\xi^2)(1-\eta-\eta^2+\eta^3),\ 1/16\, c_{\alpha_2}(3-3\xi^2)(1-\eta-\eta^2+\eta^3),$$
$$1/16\, c_{\alpha_2}(3-3\xi^2)(-1-\eta+\eta^2+\eta^3),\ 1/16\, c_{\alpha_4}(-3+3\xi^2)(-1-\eta+\eta^2+\eta^3) \rangle$$

$$\langle \phi_u^{(3)} \rangle_{,\eta} = \langle 1/16\, c_{\alpha_4}(2-3\xi+\xi^3)(-1-2\eta+3\eta^2),\ 1/16\, c_{\alpha_2}(2+3\xi-\xi^3)(-1-2\eta+3\eta^2),$$
$$1/16\, c_{\alpha_2}(2+3\xi-\xi^3)(-1+2\eta+3\eta^2),\ 1/16\, c_{\alpha_4}(2-3\xi+\xi^3)(-1+2\eta+3\eta^2) \rangle$$

$$\langle \phi_v^{(3)} \rangle_{,\xi} = \langle 1/16\, c_{\alpha_1}(-1-2\xi+3\xi^2)(2-3\eta+\eta^3),\ 1/16\, c_{\alpha_1}(-1+2\xi+3\xi^2)(2-3\eta+\eta^3)$$
$$1/16\, c_{\alpha_3}(-1+2\xi+3\xi^2)(2+3\eta-\eta^3),\ 1/16\, c_{\alpha_3}(-1-2\xi+3\xi^2)(2+3\eta-\eta^3) \rangle$$

$$\langle \phi_v^{(3)} \rangle_{,\eta} = \langle 1/16\, c_{\alpha_1}(1-\xi-\xi^2+\xi^3)(-3+3\eta^2),\ 1/16\, c_{\alpha_1}(-1-\xi+\xi^2+\xi^3)(-3+3\eta^2),$$
$$1/16\, c_{\alpha_3}(-1-\xi+\xi^2+\xi^3)(3-3\eta^2),\ 1/16\, c_{\alpha_3}(1-\xi-\xi^2+\xi^3)(3-3\eta^2) \rangle$$

$$\langle \phi_{uv}^{(3)} \rangle_{,\xi} = \langle 1/16\, s_{\alpha_4}(-3+3\xi^2)(1-\eta-\eta^2+\eta^3),\ -1/16\, s_{\alpha_2}(3-3\xi^2)(1-\eta-\eta^2+\eta^3),$$
$$-1/16\, s_{\alpha_2}(3-3\xi^2)(-1-\eta+\eta^2+\eta^3),\ -1/16\, s_{\alpha_4}(-3+\xi^2)(-1-\eta+\eta^2+\eta^3) \rangle$$

$$\langle \phi_{uv}^{(3)} \rangle_{,\eta} = \langle 1/16\, s_{\alpha_4}(2-3\xi+\xi^3)(-1-2\eta+3\eta^2),\ -1/16\, s_{\alpha_2}(2+3\xi-\xi^3)(-1-2\eta+3\eta^2),$$
$$-1/16\, s_{\alpha_2}(2+3\xi-\xi^3)(-1+2\eta+3\eta^2),\ -1/16\, s_{\alpha_2}(2-3\xi+\xi^3)(-1+2\eta+3\eta^2) \rangle$$

$$\langle \phi_{vu}^{(3)} \rangle_{,\xi} = \langle 1/16\, s_{\alpha_1}(-1-2\xi+3\xi^2)(2-3\eta+\eta^3),\ 1/16\, s_{\alpha_1}(-1+2\xi+3\xi^2)(2-3\eta+\eta^3),$$
$$1/16\, s_{\alpha^3}(-1+2\xi+3\xi^2)(2+3\eta-\eta^3),\ 1/16\, s_{\alpha_3}(-1-2\xi+3\xi^2)(2+3\eta-\eta^3) \rangle$$

$$\langle \phi_{vu}^{(3)} \rangle_{,\eta} = \langle 1/16\, s_{\alpha_1}(1-\xi-\xi^2+\xi^3)(-3+3\eta^2),\ 1/16\, s_{\alpha_1}(-1-\xi+\xi^2+\xi^3)(-3+3\eta^2),$$
$$1/16\, s_{\alpha_3}(-1-\xi+\xi^2+\xi^3)(3-3\eta^2),\ 1/16\, s_{\alpha_3}(1-\xi-\xi^2+\xi^3)(3-3\eta^2) \rangle$$

The changes of curvature in the element are determined from the lateral displacements and the rotation components $w_{,x}$ and $w_{,y}$ as given by Eq. (A11). The cubic interpolating functions defined for the membrane element could be used if the analysis were restricted to rectangular elements. However, for the bending part the isoparametric mapping to the ξ,η coordinates produces strain energy under rigid body displacement if the element is nonrectangular. Therefore the Taylor series approach was used. The two-dimensional Taylor series includes all terms through the third-order and two fourth-order terms $w_{13}x^3y$ and $w_{31}xy^3$. A penalty function is applied to the freedoms w_{13} and w_{31}. This constraint is found to reduce significantly the effect of rotational nonconformity.

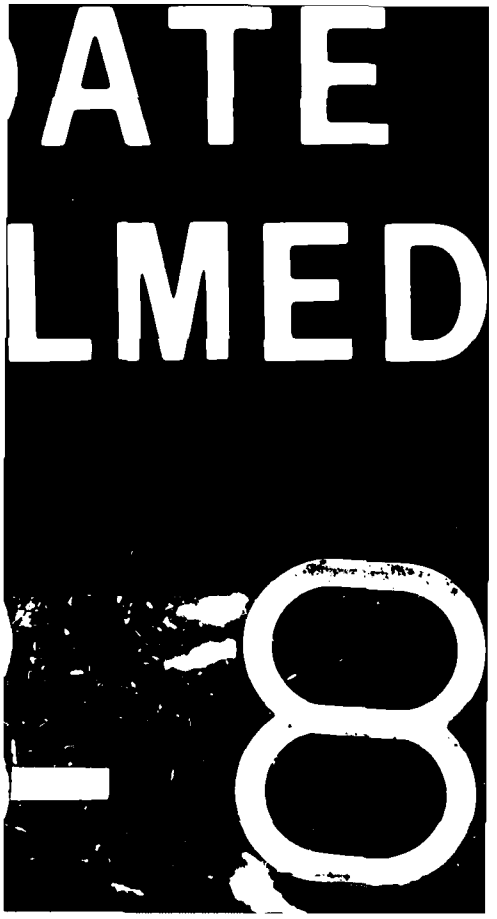
ATE
LMED
8